博士論文

# Probabilistic information processing via quantum fluctuation
(量子揺らぎを用いた確率的情報処理)

大坪　洋介

*“ That’s where quantum computing comes in. We actually think quantum machine learning may provide the most creative problem-solving process under the known laws of physics.”*

H. Neven

*“ I think of my lifetime in physics as divided into three periods.*

*In the first period, I was in the grip of the idea that everything is particles.*

*I call my second period everything is fields.*

*Now I am in the grip of a new vision, that everything is information. ”*

John A. Wheeler

# Abstract

This thesis provides theoretical studies on a probabilistic information processing incorporated quantum fluctuations through statistical mechanical approaches.

Quantum fluctuations cause transitions between states, which play same role as thermal fluctuations. Such an idea has been used in optimization problems for searching a ground state of a cost function. The algorithm is called *quantum annealing* (QA) in a manner analogous to *simulated annealing*. Simulated annealing is the conventional algorithm for finding the ground state by using the thermal fluctuations. QA has been applied to various optimization problems by solving the Schrödinger equation or carrying out Quantum Monte Carlo simulations on classical computers. However, what we call a *quantum annealer* with current superconducting devices has been launched by D-wave systems. For this situation, the algorithms by using the quantum fluctuations have received a lot of attention in recent years.

With the developments in the research fields of the algorithms by making use of the quantum fluctuations, it is also interesting for us to consider the possible application of the quantum fluctuations to *probabilistic information processing*. Main problem of the probabilistic information processing in the context of this thesis is to recover the original information from damaged information, e.g., image restoration, error correcting codes, and CDMA multiuser demodulation. Such problems can be denoted as the infinite-range spin glass model, adopting the framework of Bayesian statistics. Then, we can apply statistical mechanical approaches to it in order to figure out the average-case performance of those systems.

We examine the average-case performance of the probabilistic information processing in which quantum fluctuations is utilized to recover the original information in the context of the Bayesian inference. The quantum fluctuations are built into the system as transverse fields put in the infinite-range Ising spin glass model. We evaluate the performance measurement by using statistical mechanics which mean mean-field theory. Accordingly, we find the following properties on the quantum fluctuations in the probabilistic information processing:

1. The quantum fluctuations controlled by the transverse field is available for the decoding process in place of the thermal fluctuations. This statement mean that the quantum fluctuations can complement the effects of the thermal fluctuations.

2. The quantum fluctuations cannot improve the optimal performance of the conventional algorithm although it roughly approaches to the conventional optimal one.

3. In the low temperature region, the improvable region exists due to the quantum fluctuations. Thus, the transverse field actually improves the average-case performance for some choices of non- optimal parameters although the optimal performance with the transverse field cannot be improved.

Figuring out the relationships between the thermal fluctuations and the quantum fluctuations in terms of probabilistic information processing, the quantum annealer may have anew potentiality that it can perform Bayes inference by only controlling the quantum fluctuations.

# Acknowledgment

The works summarized in this thesis were done during Ph. D. course of the Department of Complexity science and Engineering, Graduate School of Frontier Sciences, The University of Tokyo. My works are conducted with aid of many people.

First of all, I would like to thank my supervisor, Professor Masato Okada, not only for his technical supports but also for his instructive advice. His words in some comments and even his preachy tale have helped my growth. I owe my successful achievements in this five years to his supports.

Special thanks also goes to Professor Jun-ichi Inoue (Hokkaido University) for giving me interesting subjects and expertise in the quantum information processing. When I went to his laboratory, he gave me wonderful hospitality and a huge inspiration through stimulating discussion. I also would like to thank Dr. Kenji Nagata for encouragement and technical lecture. He has been supported me from my first year of the master's program, when I faced some difficulties and got depressed.

I would like to thank the all members of my Ph D committee, Professor Koichiro Saiki, Professor Takashi Mizokawa, and Professor Akira Ejiri, for providing valuable comments on my draft of this thesis and my presentation.

The all members in our laboratory always give me exciting ideas and amusing conversations. I would like to thank my peers as good rivals, Mr. Yasuhiko Igarashi, Mr. Hiroki Terashima, and Mr. Hiroshi Saito for useful comments and friendliness. Dr. Masafumi Oizumi and Dr. Munenori Iida, and Dr. Jun Kitazono who are senior staff also give me intellectual advice and exhortation. My junior fellows, Mr. Yoshinori Ohno, Mr. Akira Manda, Mr. Ryo Karakida, Mr. Satoru Tokuda, Mr. Shin Murata, Mr. Shinpei Yotsukura, Mr. Kensuke Wakasugi, Mr. Hikaru Takenaka, Mr. Yuya Takemura, and Mr. Kenji Tanaka groove my college life. Especially, I have been making a certain argument about the research of the associative memory model with Mr. Shin Murata as a research collaborator. I would also like to thank the members of Inoue laboratory in Hokkaido university for their hospitality. I enjoy myself through college life for their interesting characters and intellectual atmosphere.

I would like to express my appreciation to my fiancée, Natsuko Okamura, for her encouragement, much-valued advice, and special affection. I have shared a lot of time with her since I entered the university and have developed through friendly competition. I am sure that I can write this thesis through grace of her supports. I will be counting on you.

In the last part of this section, I would like to thank my family. My mother, Noriko, gave lots of special advice in my life and encourage me when I were going well and I also got negative. Without her supports, I could not enjoy myself during a difficult period. My father, Masato, gave me technical guidance sometimes and taught me mathematics with enthusiasm when I was growing up. My brother, Kyosuke, is good conversational partner and then give some comments from interesting view points. I am lucky to have you as my family.

This work was partially supported by Research Fellow of the Japan Society for the Promotion of Science.

This was a great fun to do. Thank you to everyone.

# List of Publications

**Papers**

1. Igarashi, Y., Oizumi, M., Otsubo, Y., Nagata, K., and Okada, M. (2009). Influence of synaptic depression on memory storage capacity. *Journal of Physics: Conference Series*, **197**, 012018.

2. Otsubo, Y., Nagata, K., Oizumi, M., and Okada, M. (2010). Instabilities in associative memory model with synaptic depression and switching phenomena among attractors. *Journal of the Physical Society of Japan*, **79**(8), 084002.

3. Otsubo, Y., Nagata, K., Oizumi, M., and Okada, M. (2011). Influence of synaptic depression on memory storage capacity. *Journal of the Physical Society of Japan*, **80**(8), 084004.

4. Otsubo, Y., Inoue, J., Nagata, K., and Okada, M. (2012). Effect of quantum fluctuation in error-correcting codes. *Physical Review E*, **86**, 051138.

5. Katori,Y., Otsubo, Y., Okada, M., and Aihara, K. (2013). Stability analysis of associative memory network composed of stochastic neurons and dynamic synapses. *Frontiers in Computational Neuroscience*, **7**, 6.

6. Otsubo, Y., Inoue, J., Nagata, K., and Okada, M. CDMA multiuser demodulator by using quantum fluctuation. *in preparation.*

**Technical Reports in Japanese**

1. Otsubo, Y., Nagata, K., Oizumi, M., and Okada, M. (2011). Storage Capacity of Hopfield Model with Synaptic Depression. *Technical Report of IEICE*, NC**66**, 292.

2. Otsubo, Y., Inoue, J., Nagata, K., and Okada, M. (2012). Decoding Performace of quantum fluctuation for Sourlas code, *Technical Report of IEICE*, NC**111**, 95.

**International Conferences**

1. Otsubo, Y., Inoue, J., Nagata, K., and Okada, M. (2013). The effect of quantum fluctuation in information processing. *International Conference on the Diverse Applications of Statistical Physics (Diversity and Complexity: Realm of today's Statistical Physics), SINP*, Kolkata, India, January.

2. Otsubo, Y., Inoue, J., Nagata, K., and Okada, M. (2013). Decoding algorithm with transverse field in information processing. *ELC International Meeting on "Inference, Computation, and Spin Glasses" (A satellite meeting of STATPHYS 25, Seoul, Korea)*, Sapporo, Japan, July.

3. Otsubo, Y., Inoue, J., Nagata, K., and Okada, M. (2014). Statistical mechanical studies on the information processing with quantum fluctuation. *APS March Meeting 2014*, Denver, Colorado, USA, March.

# List of Awards

1. Otsubo, Y. (2009).
   Japanese Neural Network Society Young Researcher Award.

2. Otsubo, Y. (2012).
   IEEE Computational Intelligence Society Japan Chapter Young Researcher Award.

3. Otsubo, Y. (2012).
   The 4th IEEE Career Development Essay Contest for Young Professionals and Women Engineers, 1st Prize.

# Contents

# Chapter 1

# Introduction

Our works provide a theoretical studies on a probabilistic information processing incorporating quantum effects, which hold the potential to discover a new possibilities of quantum fluctuations in information processing and may contribute to a new standpoints in quantum devices.

## 1.1 Quantum annealing

Basic ideas that quantum effects utilize for computation have been proposed since 1950's. Feynmen thought that the quantized energy levels and quantized spins may be widely used in various fields beyond original field (Feynman's talk, entitled "There's Plenty of Room at the Bottom"). From this time, in some sense, the quantum theory make a connection with information bit by bit. Concepts of quantum computer have been occurred since Benioff present quantum computing which can be done without consumption of energy through a computation (Benioff 1980). Then, what the quantum computing can do is hot subject for many physicists, mathematicians, and information engineer. Shor proposed an algorithms for integer factorization, which runs in polynomial time and then can break RSA which is one of the first practicable public-key cryptosystems (Shor 1994). NMR quantum computing is one of successful technology for implementing quantum computation. Vandersypen et al. reported the implementation of Shor's algorithm in NMR quantum computer and then solved the integer factorization of fifteen (Vendersypen et al. 2001). However, the subsequent growth of quantum computer has been unfavorable because of difficulty of the implementation of many qubits. After that, the quantum computing has been developed as futural technologies step by step.

*Quantum annealing* (QA) is an algorithm for finding a ground state in a complicated energy landscape by using a quantum fluctuations which induces tunneling between states. It has been proposed in an analogous to *simulated annealing* (SA) (Geman and Geman 1984) and has been said to bring an optimal solution in combinatorial optimization problems through adiabatic Schrödinger evolution (Finnila et al. 1994; Kadowaki and Nishimori 1998; Farhi et al. 2001). The detailed formulation will be described in the next chapter. It is most interesting developments that QA come with quantum devices by using superconducting quantum bits (qubits) more than hundreds. In other words, The hardware to realize a physical implementation for QA (Quantum

annealer, i.e., a realistic adiabatic quantum processor) has been launched.

Nevertheless, QA has the long history since it was proposed. In order to solve combinatorial optimization problems by using QA, we need to solve Schrödinger equation in which the Hamiltonian is described as $2^N \times 2^N$ matrix, where $N$ corresponds to the system size. Farhi et al investigated Max-cut problem, one of the combinatorial optimization problem, in $N = 20$ by using QA through solving Schrödinger equation numerically. The results suggest that QA works well and then it may be able to outperform ordinary computers (Farhi et al. 2001). Hogg also solved random 3-SAT for $N \leq 24$ by using such an adiabatic evolution (Hogg 2004). We, however, cannot approach the large size system for computing capacity. Then, the *quantum Monte Carlo* (QMC) simulation for demonstrating QA instead of the solver of the Schödinger equation is effective tool. The QMC make it possible to perform the QA in the large size spin system by transforming the quantum system to corresponding classical system by using Suzuki-Trotter (S-T) decomposition. The algorithm is usually called the *path-integral Monte Carlo* (PIMC). [1] Elaborating it a little more, we perform standard Monte Carlo algorithm in the classical system mapped on the $d + 1$-dimensions which corresponds to $d$-dimensional quantum system. In such an algorithm, the strength of the transverse field reduces from some high initial value to zero finally through appropriate schedule. Below, we call the algorithm the *quantum Monte Carlo annealing* (QMCA) in order to distinguish from true quantum computing which means it with Schrödinger dynamics. Kadowaki performed QMCA in TSP for $N = 51$ and then compare the performance of QA and SA. Numerical results in the investigation showed that QA has a better performance than SA in the probability to find the minimum-length of the closed tour and the average of the tour length at the same Monte Carlo step (Kadowaki 1998). In two-dimensional *Edward-Anderson* (E-A) model which is the general formulated spin glass model, the residual energy decreases faster than it of SA (Santoro et al. 2002) and then such a behavior is also confirmed in TSP for $N = 1002$ (Martonak et al. 2002). In random 3-SAT for $\alpha = N/M \sim 4.24$ which is more difficult case than the above instances, where $M$ means the number of the constraints of the problem, the residual energy between the final state and optimal state which is known is worse than it of SA (Battaglia et al. 2005). Suzuki and Okada show that the residual energy in QA decreases in proportion to $1/\tau^2$ in terms of adiabatic theorem and then checked it in the tight-binding model and the two-dimensional E-A model in the case of small size by solving Schrödinger equation (Suzuki and Okada 2007). Young et al. approach Max-cut problem in which the complexity shows exponential behavior in classical computer for $N \leq 128$ in terms of QMCA and then show that it has polynomial median complexity (Young et al. 2008). The problem in lager size ($N \leq 256$) however shows that the first-order transition occurs and then QMCA does not work well (Young et al. 2010). The other approach is the *Density matrix renormalization group* (DMRG), in which we rule out a small eigenvalue of the density matrix. Although this technique can be applied to one-dimensional quantum system, the large system can be treated trough it (White 1992; Verstraete et al. 2006; Schuch et al. 2008).

The mathematical formulations of the combinatorial optimization problems and the quantum annealing will be given in the next chapter. We below introduce to

[1] There are various algorithms in QMC which simulate a quantum system, e.g., Green's function Monte Carlo. In the context of QA, PIMC described here is usually used.

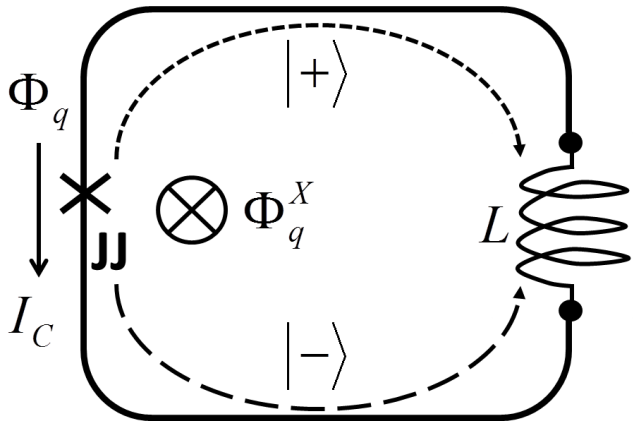


Figure 1.1: rf-SQUID Flux qubit.

the developments of the device technologies briefly and then will focus on the quantum annealer which can demonstrate the quantum annealing as realistic quantum processor.

Since the concepts of quantum computing was contrived, the manufactured quantum computers such as quantum communication systems (Scarani et al. 2009), quantum random number generators (Jennewein et al. 2000) and quantum simulators (Bloch et al. 2012) have been proposed in various ways, the devices however with realistic size scale off from practical use. The Quantum annealer which may find out solutions of a optimization problem in particular is a few device which is applied to large-scale problems. In order to demonstrate the QA physically, we need to consider how the quantum bits (qubits) which induce tunneling effect are built. One possible possible implementation of an artificial Ising spin system involves superconducting flux qubits (e.g., Lupascu et al. 2007; Berns et al. 2008). The Josephson device which contain Josephson junction (JJ) allows us to measure macroscopic quantum tunneling (Josephson 1962). For example, the simple circuit (Rf-SQUID: Radio Frequency Superconducting Quantum Interference Device) which is base of the quantum annealer is drawn in Fig. 1.1, where loop is subjected to an external flux bias $\Phi_q^X$ and JJ of critical current $I_c$ is introduced to a superconducting loop of inductance $L$. In this case, we observe the persistent current $I_q^p$ proportional to phase drop: $I_q^p \propto \Phi_q - \Phi_a^X$. Regarding this circuit as a single spin system, the Hamiltonian can be denoted as $H \sim -\frac{1}{2}(\epsilon_q \hat{\sigma}^z + \Delta_q \hat{\sigma}^x)$. We can catch a state of such the artificial spin by observing the current $I_q^p$. To control the strength of tunneling energy term $\Delta_q$ strictly, Harris et al. proposed compound-compound Josephson junction (CCJJ) rf-SQUID and investigated the quantum mechanical properties (Harris et al. 2010). Johnson et al. proposed a programmable artificial spin system manufactured as an integrated circuit by extending CCSJ rf-SQUID, and then report on an experiment that demonstrates a signature of quantum annealing in a coupled set of eight artificial Ising spins (Johnson et al. 2011). As a result, the annealing to find the low-energy configuration can be realized and then the field of the quantum computer makes advance. The type coupler between manufactured spins has been designed well after these studies, and the QA with one hundred qubits has been realized. [2] The

[2]D-wave Systems, Inc. which is a quantum computing company based on British Columbia is

applications for various combinatorial optimization problems are beginning with developments of number qubits (e.g., Perdomo-Ortiz et al. 2012; Boixio et al. 2013). For example, Naven et al. use the quantum annealing hardware in machine learning and then successfully build a classifier for the detection of cars in digital images (Neven et al. 2009). In 2014, the performance of quantum annealing on random Ising problems implemented using the D-Wave Two which is quantum annealer with 512 qubit will be reported (Wang et al. 2014). Whether the quantum speed up can be achieved or not comparing it with a classical computer is not clarified at the present stage. The future developments of the quantum annealer is expected.

## 1.2 Statistical physics of probabilistic information processing

The introduction of the QA which is an algorithm for finding the ground state of the complicated energy landscape by using the quantum fluctuations was given in the previous section. We expect that such a character of the quantum fluctuation can be effective tool for probabilistic information processing.

Although the combinatorial optimization problems is the one of information processing in a sense, there are many problems of an information processing around the world. For example, in the case of image restorations, we should restore the degraded image which has many pixels, as clean as possible. However, it is usually difficult to restore an original image because we do not know the kind of the noise. Even if we have the information of a noise, we may not restore the original one perfectly due to the stochastic fluctuations of the noise. Such a problem remain in the other fields. The error correcting codes is also important issue in the situation that someone transmit some information through a noisy channel. Neural networks which is consisted of many neurons is one of famous example of the information processing. Code-division multiple access (CDMA) which is modern telecommunication system has been also researched as the information processing problem. Although the above instances are apparently-unrelated, the restore (decode, retrieve, or demodulate) processes can be formulated in a similar way trough Bayes inference. The Bayes inference give an probabilistic distribution of the estimated sequence as posterior distribution through prior information. Thus, by describing a noise as the probability distribution and setting how an original information generate a priori, Bayes inference provide an formulation to recover the original information. Such a formulation of the information processing is called the probabilistic information processing, which is closely related to the spin glass model, amazingly (Nishimori 2001; Mézard and Montanari 2008). The spin glass is the glassy system described as spin models which have random interactions among each spin. It is because the information bit, in a lot of cases, is regarded as binary bits and there is correlation among many bits when they are sent through channel that the formulation in a recovery process from noisy message can be Ising spin model with disorder inter-

contributing to a series of developments of quantum devices. D-wave One which is quantum computer with 128-qubit processor and is the world's first commercially available quantum computer system was announced on May , 2011. D-wave system revealed 512-qubit quantum computer in 2013 and the collaboration among Google, NASA and USRA by using it was announced in 2013 (D-wave Systems, Inc.).

actions. In the statistical mechanical point of view, the spin configuration follows the Boltzman distribution which positively corresponds to the posterior distribution in the probabilistic distribution.

The simplest spin glass model is the Sherrington-Kirkpatrick (SK) model which is the infinite range model with Gaussian distributed interactions (Sherrington and Kirkpatrick 1975), which is regarded as the Edwards-Anderson model in the limit of the spatial dimension (Edwards and Anderson 1975). The mean field theory of this model give exact solutions phase transition between glassy phase and ferromagnetic phase. Because this model can be expanded to various fields beyond the physics, various problems of information processing have been analyzed through the statistical mechanical approaches. Hopfield analyzed the neural network described as spin glass model and then reveal memory storage conceptually (Hopfield 1982). After that, the field of neural network through statistical physics has been developed. The restoration performance of the image restoration which has Markov random field prior was analyzed through mean field theory by Nishimori and Wong based on previous studies (Nishimori and Wong 1999; Geman and Geman 1984). The error correcting codes and the CDMA are also related to spin glass models, and then they were analyzed by spin glass theory (Sourlas 1989; Tanaka 2001).

For these previous studies, in order to optimal performance in the recovery process of the probabilistic information processing, the maximizer of the posterior marginal (MPM) estimate is effective. In this algorithm, we need to control the temperature corresponding to estimated noise power. This is natural consequence. If the temperature is equal to true noise power, the estimation will be successful. Because the temperature is controlled in this process, such an estimated algorithm is also *finite temperature decoding*. Such an optimal temperature is called Nishimori temperature in which the performance behavior can be peaked. The MPM estimate is also regarded as consideration of minimum of free energy which is different from the energy, cost function, in the finite temperature case. Therefore, we derive the macroscopic parameter which make minimum of the free energy in the MPM estimate.

Then, we find that it is similar to searching process in the complicated energy landscape by using SA. In both cases, we seek the appropriate state by controlling the temperature, thermal fluctuation which induces jump between energy hills. Hence, the MPM estimate in the probabilistic information processing is similar to SA in terms of the algorithm for finding a state by using thermal fluctuations. The mathematical formulation of the probabilistic information processing and statistical mechanical analysis including the concrete problems will be given in the next chapter.

## 1.3 Our concepts

How does the quantum fluctuations affects the probabilistic information processing? This is key concept of this thesis. As we mentioned above, the QA has been proposed inspired by the SA. In this algorithm, the quantum fluctuations are used for finding a ground state instead of thermal fluctuations. On the other hands, the MPM estimate, finite temperature decoding, is supposed to be effective in the probabilistic information processing in which the temperature control is important to realize the appropriate state. Because of this context, we can consider the decoding process including the

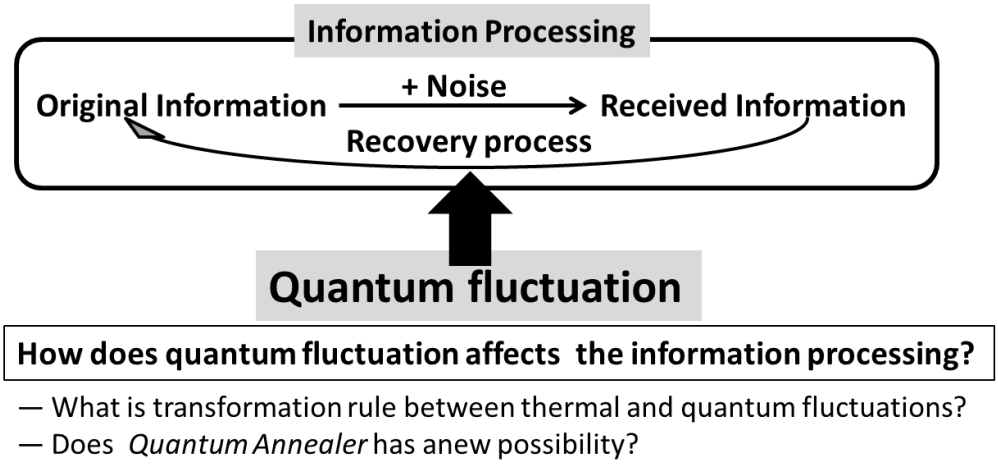


Figure 1.2: Concepts of this thesis.

quantum fluctuation and compare the performance with it by using the conventional MPM estimate. With the help of state transition due to the quantum fluctuation, the state may close in the appropriate state which represents the original information. Then, our investigation will unveil the transformation rule between the thermal fluctuations and the quantum fluctuations. With such achievements, the quantum annealer will have anew possibility of the probabilistic estimation.

The concrete goals including the mathematical discussion will be given in the las part of the next chapter.

# Chapter 2

# Previous studies on quantum annealing and statistical physics of information processing

In this chapter, we review the previous studies on the quantum annealing and the probabilistic information processing including the mathematical formulation. The spin glass theory and the necessary techniques for reading this thesis are also remarked. In the last part, the concrete goals of this thesis is given.

## 2.1 Background of applications for quantum fluctuation

The optimization problem is usually to find a minimum or maximum of a function which is called the cost function or the energy. The energy landscape represents a complexity of the problem and often has many solutions. Then, it is sometimes difficult to find an optimal solution through an algorithm. One can separated the problems into some classes which is the measure of difficulty. When $N$, the system size of the problem, increase, the kind of the problems that the complexity of the calculations increase exponentially and goes over the limit of the computational power are called *Nondeterministic Polynomial-time solvable hard or complete* (NP-hard or NP-complete). Roughly speaking, the NP is the subclass that we can check either "yes" or "no" according with a given solution of the problem. In the *Polynomial-time solvable* (P), one can find an algorithm to solve a problem within a time of the polynomial time order, and then it can be seen as easy problem in NP. In NP-complete, the problems of NP-hard are contained in NP. The rough sketch of each class if $P \neq NP$ is given in Fig. 2.1. In the combinatorial optimization problem which is the special case, the variable take discrete values and then it closely related to Ising spin models or spin glass models.

### 2.1.1 Combinatorial optimization problems

The combinatorial optimization problem is formulated in terms of spin models and peculiarly is related to the problem for searching the ground state. In this subsection, we give a brief introduction for the combinatorial optimization problems providing some instances.

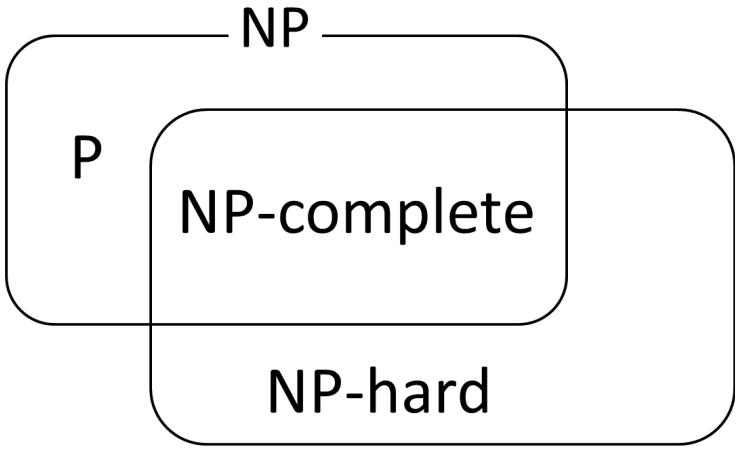


Figure 2.1: Class of NP problems in the case that $P \neq NP$.

**Random $K$-satisfiability problem**

Let us consider a set of $N$ logical variables (Boolean variables) $(x_1, ..., x_N)$, each of which takes "true" or "false". First, we randomly choose $K$ literals $z_i^{(l)}$ corresponding to $x_i$ or its negations $\bar{x}_i$ with equal probability $\frac{1}{2}$. A clause $C_l$ is the logical OR of these $K$ variables. Next, we repeat this process to $M$ independently and ask for them to be true at the same time. Thus, we take the logical AND of these $M$ clauses

$$F = \bigwedge_{l=1}^{M} C_l = \bigwedge_{l=1}^{M} \left( \bigvee_{i=1}^{K} z_i^{(l)} \right), \tag{2.1}$$

where $\wedge$ and $\vee$ represent AND and OR operations, respectively. If an assignment of $x_i$ satisfying all clauses, $F$ is " true", and then the logical assignment is satisfiable. If there is no such assignment, $F$ is said to be unsatisfiable. For example, we consider the case that $N = 5$, $M = 4$ and $K = 2$ representing as following clauses:

$$C_1 = x_1 \vee x_3,\ C_2 = \bar{x}_2 \vee x_3,\ C_3 = \bar{x_3} \vee \bar{x}_4,\ C_4 = x_1 \vee \bar{x}_5, \tag{2.2}$$

and $F = C_1 \wedge C_2 \wedge C_3 \wedge C_4 \wedge C_5$. One of the condition to satisfy $F$ is $x_1$ ="true", $x_2$ ="true or false", $x_3$ ="true", $x_4$ ="false" and $x_5$ ="true or false".

Here, we consider $K$-SAT in terms of Ising system. We represent anew the logical variables as Ising spins $\boldsymbol{\sigma}$ which take 1 or $-1$ corresponding to "true" or "false". The Hamiltonian of the above instance can be described as

$$H = \frac{1}{4}\left\{(1-\sigma_1)(1-\sigma_3) + (1+\sigma_2)(1-\sigma_3) + (1+\sigma_3)(1+\sigma_4) + (1-\sigma_1)(1+\sigma_5)\right\} \tag{2.3}$$

which corresponds to the cost function of the problem. If $F$ is satisfied, $H = 0$, and otherwise $H > 0$. We can extend the above instance to general $K$-SAT case as follows,

$$H = \sum_{l=1}^{M} (1 - \zeta_{i1,l}\sigma_{i1}^{(l)})(1 - \zeta_{i1,l}\sigma_{i2}^{(l)}), \tag{2.4}$$

where $\zeta_{ik}^{(l)}$ is random variables which takes $+1$ or $-1$ according to the condition in $C_l$.

On the basis of above discussion, the generalized Hamiltonian of random $K$-SAT can be obtained as follows:

$$H^{\mathrm{K-SAT}} = \frac{1}{2^K} \sum_{l=1}^{M} \prod_{k=1}^{K} \left(1 - \zeta_{i1,l} \sigma_{i1}^{(l)}\right). \tag{2.5}$$

The random $K$-SAT problem corresponds to investigating the ground state of the random Ising model. Because of this, the random $K$-SAT has been studied in terms of the statistical mechanics as $M,\ N \to \infty$ with $\alpha = M/N$ fixed. (Monasson and Zecchina 1997; Monasson et al. 2000).

**Traveling salesman problem**

The *Traveling salesman problem* (TSP) is also typical example of a optimization problem. Let us consider $N$ cities randomly and the situation that a salesman has to make a tour to cover every city and then finally returns to the starting point. The problem of the TSP is to find the shortest or lowest-cost route to visit given cities and paths among cities. Such a problem has been investigated by using various techniques because it happens in various situations, e.g., path definition of an aircraft. First, we give a set $\{d_{ij}; i, j = 1, ..., N\}$, where $d_{ij}$ indicates the distance between $i$th city and $j$th city or is regarded as a cost for going from the former to later. A tour matrix can be represented as $N \times N$ matrix $\boldsymbol{T} = \{T_{ij}\}$ with elements either 1 or 0. If a salesman visit $j$th city immediately after visiting $i$th city, $T_{ij} = 1$ and $T_{ji} = 0$. Note that the TSP give the constraint that the cities have to be visited only once. Therefore, the row and column of the matrix $\boldsymbol{T}$ has one and only one element, which mean the following conditions are satisfied,

$$\sum_{i=1}^{N} T_{ij} = 1,\ \sum_{j=1}^{N} T_{ij} = 1. \tag{2.6}$$

Because $\boldsymbol{T}$ is not symmetry, we define the symmetric matrix $\boldsymbol{U}$ as follows,

$$\boldsymbol{U} = \boldsymbol{T} + \boldsymbol{T}^T, \tag{2.7}$$

where $\boldsymbol{T}^T$ is the transpose of $\boldsymbol{T}$. The matrix $\boldsymbol{U}$ must be a symmetric matrix having only two distinct entries equal to 1 with every row and every column. Using the matrix $\boldsymbol{U}$, we can define the cost function as follows,

$$H = \frac{1}{2} \sum_{<i,j>} d_{ij} U_{ij}, \tag{2.8}$$

where $< i, j >$ means "all links" which correspond to all paths between a city and another city. Introducing the expression of the Ising spin $\sigma_i = 2U_{ij} - 1$, we refine the above cost function in terms of Ising spin model as follows:

$$H^{TSP} = \frac{1}{2} \sum_{<i,j>} d_{ij} \frac{1 + \sigma_{ij}}{2}. \tag{2.9}$$

Although we here give two instances, random $K$-SAT and TSP, above, the problem for searching the ground state of spin glass model is also famous example of the combinatorial optimization problems. Then, we can see that a strategy of such a problem closely relate to statistical mechanics.

### 2.1.2 Simulated annealing

As we see above, the combinatorial problems can be described as Ising spin models. The combinatorial problems are general NP-complete or NP-hard problems. The difficulty of these problems comes from complicated energy landscape of the system, and then there are many local minima. The *simulated annealing* (SA) is the general method to solve these problems by using the "thermal fluctuation" in terms of statistical mechanics, which allows a system to escape the local minimum of the problem Hamiltonian (cost function) under an appropriate annealing schedule.

Once a problem Hamiltonian $H(\boldsymbol{\sigma})$ is given, the probability of the spin configuration can be described as the *Maxwell Boltzman distribution*:

$$P(\boldsymbol{\sigma}) = \frac{\exp(-\beta(t)H(\boldsymbol{\sigma}))}{Z}. \tag{2.10}$$

The key idea of SA is "annealing" with changing the temperature $T(t) = 1/\beta(t)$ which depends on time $t$. If the system is at high temperature, a state frequently moves in the configuration space because the strength to drive other stats is intensive. On the other hand, a state stay in the neighborhood of a minimum at low temperature. For these reasons, decreasing the temperature sufficiently slowly, we will obtain the equivalent a ground state in the low temperature limit. The important problem in SA is how to schedule the annealing process. If the process is not slow, the state does not remain in equivalent state and then SA fail in deriving the ground state. It is known that the algorithm works well if the temperature decreases according to the following schedule (Geman-Geman 1984):

$$T(t) \propto \frac{N}{\log(t+2)} \tag{2.11}$$

Here, $N$ corresponds to system size. The Huse-Fisher showed that the residual energy which means the difference of energies between ground state and present state depends on annealing time $\tau$ as follows:

$$E_{res} \simeq \frac{1}{(\log \tau)^{\zeta}}, \quad \zeta \leq 2. \tag{2.12}$$

The simulated annealing thus gives good solution, if we can choose the appropriate schedule and annealing time.

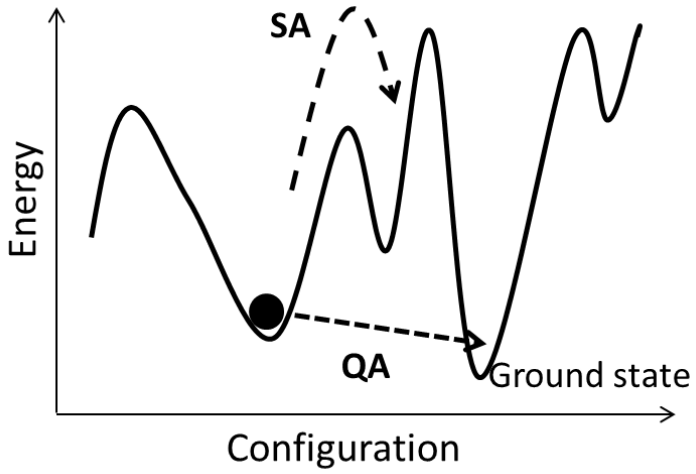


Figure 2.2: Simulated annealing (SA) and quantum annealing (QA) in an optimization problem.

## 2.2 Basic formulation for quantum annealing

The *Quantum Annealing* (QA) is an algorithm for solving optimization problems with the aid of quantum adiabatic evolution (Finnila et al. 1994; Kadowaki 1998). [1] While SA is the algorithm by using thermal fluctuation, the quantum fluctuation is used in QA.

Let us consider the $H_0(\boldsymbol{\sigma})$, which corresponds to a problem (potential) Hamiltonian in an optimization problem. The optimization problem, as we state above, is to find the minimum of this function and to find the set of Ising spins. In QA, we redefine the problem as Hilbert space as follows,

$$\sigma_i \rightarrow \hat{\sigma}_i^z \tag{2.13}$$

$$\hat{\sigma}_i^z = \begin{pmatrix} 1 & 0 \\ 0 & -1 \end{pmatrix}, \tag{2.14}$$

where $\sigma_i^z$ is the $z$ component of the Pauli matrix, and then the diagonal components, (1 or $-1$), of the matrix correspond to the value of Ising spin. In other words, denoting the eigenstate of $\sigma_i^z$ as $|+\rangle = (1\ 0)^T$ and $|-\rangle = (0\ 1)^T$, we have

$$\hat{\sigma}_i^z |+\rangle = |+\rangle\,, \quad \hat{\sigma}_i^z |-\rangle = -|-\rangle\,. \tag{2.15}$$

For this simple transformation, we regard the problem Hamiltonian as $H(\hat{\boldsymbol{\sigma}}^z)_0 (\equiv \hat{H}_0)$ and write a state as $|\sigma_1, ...., \sigma_N\rangle$ which mean spin configuration.

Now we introduce the "kinetic energy" term $\hat{H}_{\rm kin}$ which drive a state to an other state in a problem Hamiltonian as follows:

$$\hat{H}(t) = f(t)\hat{H}_{\rm kin} + g(t)\hat{H}_0, \tag{2.16}$$

[1] For this reason, QA is also called the *quantum adiabatic algorithm* (Farhi 2001).

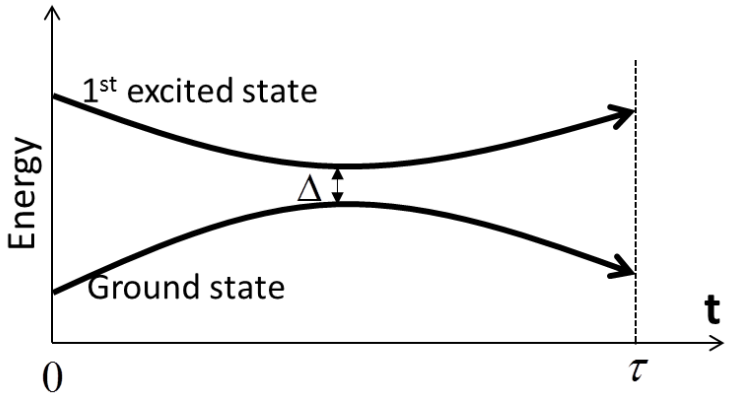


Figure 2.3: Adiabatic evolution of the stats. Here, $\Delta$ is the energy gap between the 1st excited state and a ground state.

where $\hat{H}$ depends on time, and $f(t)$ and $g(t)$ represent a wight for $\hat{H}_{\text{kin}}$ and $\hat{H}_0$ respectively. In standard formulation of QA, the state vector $|\Psi(t)\rangle$ follows the real-time Schrödinger equation:

$$i\frac{d}{dt}|\Psi(t)\rangle = \hat{H}(t)\,|\Psi(t)\rangle\,. \tag{2.17}$$

The adiabatic theorem of the quantum mechanics, which support QA, tell us that:

> a physical system will remain in its instantaneous eigenstate if a given dynamical parameter is slow enough and if there is a gap between the eigenstate and the rest of the Hamiltonian (Born and Fock 1928.).

Thus, if an initial state is ground state $|\Psi(0)\rangle_g$ and then the state evolve slowly enough following the Schrödinger equation, the state remain in a ground state $|\Psi(t)\rangle_g$. Following this behavior of the quantum quantum system, we can get the ground state of the problem Hamiltonian $\hat{H}_0(t)$ under the condition that $f(0)/g(0) \to \infty$ and $f(\infty)/g(\infty) \to 0$. This means that the initial state is set on the trivial ground state of the kinetic Hamiltonian $\hat{H}_{\text{kin}}$ and then a state goes to a ground state of $\hat{H}_0$ remaining the ground state. In QA, the kinetic Hamiltonian need to have two properties at least:

1. The ground state is trivially known to set the initial state.
2. A jump between stats occurs.

In the standard formulation of QA, we simply adopt the *transverse field* as kinetic term, [2] which can be written as

$$\hat{H}_{\text{kin}} = -\sum_i \hat{\sigma}_i^x, \;\; \hat{\sigma}_i^x \;\; = \;\; \begin{pmatrix} 0 & 1 \\ 1 & 0 \end{pmatrix}, \tag{2.18}$$

[2] If the system has spin glass state, it is known that QA with the transverse field may be not effective in an optimization problem. In recent years, to avoid the issue, the formulation introducing the anti-ferromagnetic term has been proposed (Seki et al. 2012).

where $\sigma_i^x$ is the $x$ component of the Pauli matrix. We know immediately the relations, $\hat{\sigma}_i^x |+\rangle = |-\rangle$ and $\hat{\sigma}_i^x |-\rangle = |+\rangle$. Thus, the kinetic term $\hat{H}_{\rm kin}$ can transform the up state to down state and vice versa. And then we can see the ground state of the above matrix as follows:

$$|\Psi\rangle_g^{\rm kin} = \sum_{k_1=\pm} \sum_{k_2=\pm} \cdots \sum_{k_N=\pm} |k_1\rangle \otimes |k_2\rangle \otimes \cdots \otimes |k_N\rangle \,. \tag{2.19}$$

Here, we reconsider the Hamiltonian (2.16) incorporated the transverse field as the kinetic term. For simplicity, we adopt the function form of $f(t)$ and $g(t)$ as

$$f(t) = 1 - \frac{t}{\tau}, \;\; g(t) = \frac{t}{\tau}, \tag{2.20}$$

where $\tau$ is called the annealing time. Because the total Hamiltonian is $\hat{H}_{\rm kin}$ at initial time, $t = 0$, and finally it will be $\hat{H}_0$ at $t = \tau$, the ground state of the problem Hamiltonian, $|\Psi(\tau)\rangle_g^0$, can be derived started from the ground state of the kinetic Hamiltonian, $|\Psi(0)\rangle_g^{kin}$, following the adiabatic evolution.

Although QA is supported by the adiabatic evolution, if the evolution is not slow, the state may be excited from a ground state to an excited state. In such a case, QA fail to catch the ground state at the final state. The probability of non-adiabatic excitation can be evaluated analytically as follows:

$$P_{\rm na} = e^{-2\pi\gamma} \tag{2.21}$$

$$\gamma = \frac{\Delta^2}{\frac{d}{dt}(E_0(t) - E_1(t))}, \tag{2.22}$$

where $\Delta$ is the minimum energy gap between the ground state and the 1st excited state. The above theorem is called *Landau-Zener theorem* (Landau and Lifshitz 1965). Whether QA works or not hinge on whether such a non-adiabatic excitation occurs or not in the course of the dynamics. Although classical computer may not demonstrate QA in large systems to a need for solving the Schrödinger equation, the quantum Monte Carlo simulation has been implemented. Below we mention the quantum Monte Carlo simulation to figure out the treatment of QA in the classical computer.

In order to demonstrate the QA by using the classical computer instead of the quantum computer, we consider the transformation from the Hamiltonian with the transverse field described in Hibert space to the corresponding classical Hamiltonian. It is well known that Suzuki-Trotter (S-T) decomposition allows us to perform such a transformation (Suzuki 1976):

$$H_d(\hat{\boldsymbol{\sigma}}) \;\; \rightarrow \;\; H_{d+1}(\boldsymbol{\sigma}), \tag{2.23}$$

where $H_d$ represents the d-dimensional Hamiltonian. The rigorous mathematical formulation is devoted in Appendix B. The extra dimension is called the *Trotter axis* or the *imaginary time*. We consider the case that $f(t) \equiv \Gamma$ and $g(t) \equiv \Lambda$ in an equilibrium state below. After such a treatment, the Hamiltonian can be formulated as follows:

$$H_{\rm eff}(\boldsymbol{\sigma}(t)) = \frac{\beta\Lambda}{P} \sum_{t=1}^{P} H_0(\boldsymbol{\sigma}(t)) - \frac{1}{2} \log \left( \coth \frac{\beta\Gamma}{P} \right) \sum_{i=1}^{N} \sum_{t=1}^{P} \sigma_i(t)\sigma_i(t+1), \;\; (P \rightarrow \infty) \tag{2.24}$$

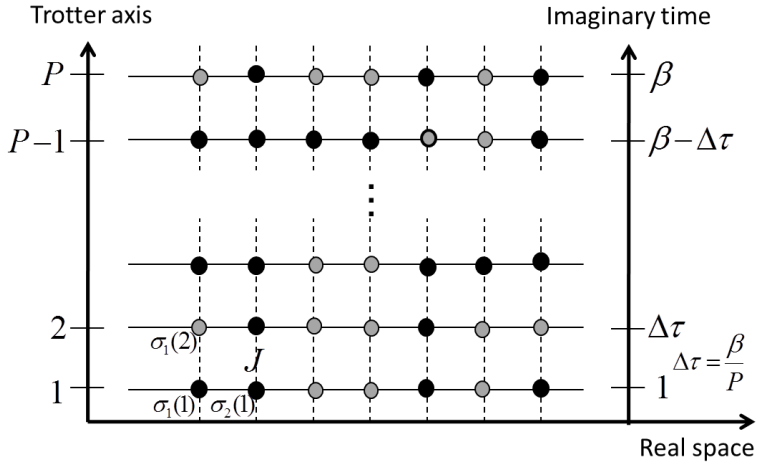


Figure 2.4: System after S-T decomposition in the case that $d = 1$, which is expanded the two dimensional space. Black and gray circles at each grate indicate spins which take 1 or $-1$. Horizontal axis corresponds to the real space while vertical axis is called Trotter axis or the imaginary time which corresponds to temperature space. Interaction strength $J$ between two spins along Trotter axis is $\frac{P}{2\beta}\log\left(\coth\frac{\beta\Gamma}{P}\right)$.

where the effective Hamiltonian is the one incorporating the inverse temperature and the the Bolzman factor can be described as $P_B \propto \exp(-H_{\text{eff}})$ for $H_{eff} = \beta H$. The number of $P$ is called Trotter number and $t$ is the index along Trotter axis and $\sigma_i(t)$ mean the $t$-th extra dimensional variable on $i$-the space. We can see that the Hamiltonian with the transverse field corresponds to the classical Hamiltonian with the ferromagnetic interaction ($J = \frac{P}{2\beta}\log\left(\coth\frac{\beta\Gamma}{P}\right)$) along the Trotter axis (Fig. 2.4). In this formulation, we notice that the temperature exist. In QA through S-T decomposition, taking the value $\beta/P(\equiv \Delta\tau)$ to be sufficiently small and $\Gamma/\Lambda$ to be sufficiently large, we perform the Monte Carlo simulation and obtain an equilibrium sate. Next, we decrease $\Gamma/\Lambda$ to zero sufficiently slowly with equilibrium state. If the temperature is sufficiently low the final state at $\Gamma/\Lambda = 0$ can be a ground state of $H_0$. The above approach is strictly difference from QA by solving the Schrödinger equation with developing the quantum dynamics. The QA through the quantum Monte Carlo simulation, however, is known to work well and then the system approaches to the ground state of the problem Hamiltonian $H_0$ in the condition that the inverse temperature is sufficiently large (Morita and Nishimori 2008).

## 2.3 Formulation for information processing based on Bayes inference

Below, we give an introduction to the information processing based on Bayes inference and the statistical mechanical techniques for deriving the macroscopic properties of the system.

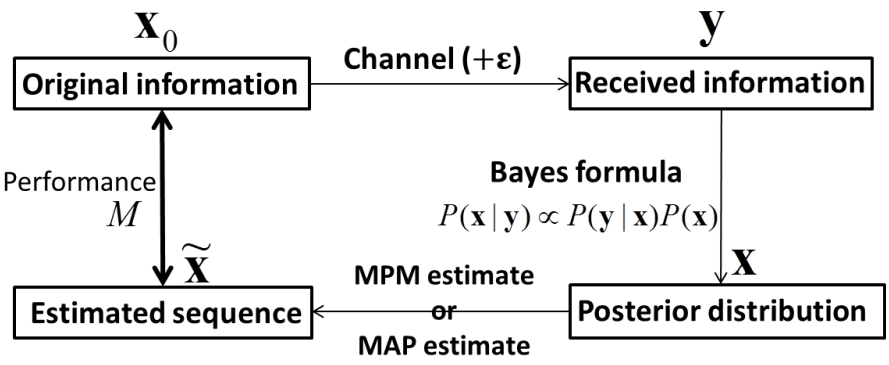


Figure 2.5: Basic picture of information processing through Bayes inference.

We first note that the original information is $\boldsymbol{x}_0 \equiv \{x_{0i}\}, (x_{0i} = \pm 1, i = 1, ..., N)$, which $\boldsymbol{x}_0$ sometimes corresponds to "pixels" or "message"according to a problem. Such a binary variable is called *Ising spins* in terms of the statistical mechanics. [3] As set up common to many problems of information processing, the original information is damaged through noisy channel as follows,

$$\boldsymbol{y} = \boldsymbol{x}_0 + \boldsymbol{\epsilon}, \tag{2.25}$$

where $\boldsymbol{y} \equiv \{y_i\}, (i = 1, ..., N)$ represents the received information and $\boldsymbol{\epsilon}$ represents a channel noise. It is relevant we focus on here how the original information recover from damaged information $\boldsymbol{y}$. Then, we consider the estimated sequence $\boldsymbol{x} \equiv \{x_i\}, (x_i = \pm 1, i = 1, ..., N)$ which is generally difference from $\boldsymbol{x}_0$. It goes without saying that the condition that $\boldsymbol{x} = \boldsymbol{x}_0$ means best restoration. [4] The probabilistic distribution of a channel noise is described as $P(\boldsymbol{y}|\boldsymbol{x})$ which is conditional probability for $\boldsymbol{y}$ under the condition that $\boldsymbol{x}$ occurred. If the channel noise is, for example, memoryless Gaussian channel with $\boldsymbol{x}$ mean and $\sigma^2$ variance in which each bit is affected by noise independently, the probability distribution is

$$P(\boldsymbol{y}|\boldsymbol{x}) = \prod_{i=1}^{N} P(y_i|x_i) \tag{2.26}$$

$$P(y_i|x_i) = \frac{1}{\sqrt{2\pi}\sigma} \exp\left(-\frac{1}{2\sigma^2}(y_i - x_i)^2\right). \tag{2.27}$$

The above probability is called the *likelihood function* of $\boldsymbol{x}$. As a matter of course, because the form of $P(\boldsymbol{y}|\boldsymbol{x})$ is unknown, we should assume the some kind of type of it. We also consider the *prior distribution* $P(\boldsymbol{x})$, which means how an original information

[3] Here, we assume the *Ising type* ($x_i = \pm 1$) for applying the statistical mechanics later. It can reduces to $\{0, 1\}$ code by using simple operation (Nishimori 2001).

[4] Equation (2.25) should be denoted as $\boldsymbol{y} = f(\boldsymbol{x}_0) + \boldsymbol{\epsilon}$ because the original information is sent by processing it in the standard information processing problem as we see below. However, we here consider the situation that the original information is sent without change for easy formulation.

is generated. This is powerful assumption about an original information to use the Bayes formula as described below. By using the basic formula of the joint probability,

$$P(\boldsymbol{x},\boldsymbol{y}) = P(\boldsymbol{x}|\boldsymbol{y})P(\boldsymbol{y}) = P(\boldsymbol{y}|\boldsymbol{x})P(\boldsymbol{x}) \tag{2.28}$$

and then we obtain immediately the following formula:

$$P(\boldsymbol{x}|\boldsymbol{y}) = \frac{P(\boldsymbol{y}|\boldsymbol{x})P(\boldsymbol{x})}{P(\boldsymbol{y})} = \frac{P(\boldsymbol{y}|\boldsymbol{x})P(\boldsymbol{x})}{\sum_{\boldsymbol{x}} P(\boldsymbol{y}|\boldsymbol{x})P(\boldsymbol{x})}. \tag{2.29}$$

The formula is called *Bayes formula* and $P(\boldsymbol{x}|\boldsymbol{y})$ is called the *posterior distribution*, which mean the probability distribution of $\boldsymbol{x}$ under the condition that $\boldsymbol{y}$ occurred. In Bayes inference, we can find that the causation is switched and then evaluate an original information through $P(\boldsymbol{x}|\boldsymbol{y})$, assuming the likelihood function and the prior. Here, we introduce two basic strategy by using the Bayes formula below to extract the estimated bit sequence $\tilde{\boldsymbol{x}}$.

First, the *maximum a posteriori probability* (MAP) estimate which is conventional method of the Bayes inference is

$$\tilde{\boldsymbol{x}}^{\mathrm{MAP}} = \arg\max_{\boldsymbol{x}} P(\boldsymbol{x}|\boldsymbol{y}). \tag{2.30}$$

Second, the *maximizer of the posterior marginals* (MPM) estimate is defined by

$$\tilde{x}_i^{\mathrm{MPM}} = \arg\max_{x_i} P(x_i|\boldsymbol{y}) \tag{2.31}$$

$$= \mathrm{sgn}\left[\sum_{x_i \pm 1} x_i P(x_i|\boldsymbol{y})\right] \tag{2.32}$$

$$P(x_i|\boldsymbol{y}) = \sum_{\boldsymbol{x} \neq x_i} P(\boldsymbol{x}|\boldsymbol{y}), \tag{2.33}$$

where we focus on a single bit $x_i$, and then comparing $P(x_i = 1|\boldsymbol{y})$ and $P(x_i = -1|\boldsymbol{y})$ we adopt $x_i = 1$ or $-1$ which enlarge $P(x_i|\boldsymbol{y})$. The transformation from Eq. (2.31) to (2.32) can be possible for the condition that $x_i = \pm 1$. [5] The MPM estimate has important mean in terms of statistical mechanics. Seeing the posterior $P(\boldsymbol{x}|\boldsymbol{y})$ as Boltzman distribution, it may be denotes as follows,

$$P(\boldsymbol{x}|\boldsymbol{y}) = \frac{\exp(-\beta H(\boldsymbol{x}))}{Z}, \tag{2.34}$$

where $Z$ is the partition function and $\beta(\equiv 1/T)$ means the inverse temperature. [6] And then, $H(\boldsymbol{x})$ corresponds to the Hamiltonian of the system in the context of the statistical mechanics. Here, the Hamiltonian $H(\boldsymbol{x})$ in this case corresponds to *Ising spin system*. From this view point, Eq. (2.31) may be rewritten as follows:

$$\tilde{x}_i^{\mathrm{MPM}} = \mathrm{sgn}\left(\frac{\sum_{\boldsymbol{x}} x_i P(\boldsymbol{x}|\boldsymbol{y})}{\sum_{\boldsymbol{x}} P(\boldsymbol{x}|\boldsymbol{y})}\right) = \mathrm{sgn}\left(\frac{\sum_{\boldsymbol{x}} x_i e^{-\beta H(\boldsymbol{x})}}{\sum_{\boldsymbol{x}} e^{-\beta H(\boldsymbol{x})}}\right) = \mathrm{sgn}\langle x_i \rangle_\beta, \tag{2.35}$$

[5] We will often use the expression "Tr" instead of "$\sum_{\boldsymbol{x}}$" in the following arguments.

[6] We below use the unit system that Boltzman factor is one, i.e., $k_B = 1$.

where $\langle\cdot\rangle_\beta$ represents the local magnetization, which means the thermal average of $x_i$. For this reason, the MPM estimate is sometimes called *Finite temperature decoding*. We can also see that the MAP estimate is the specific case of the MPM estimate for Eqs. (2.30) and (2.35). The MAP estimate corresponds to the problem for finding the ground state of a Hamiltonian $H(\boldsymbol{x})$, and then it is consideration for the low temperature limit ($\beta = 1/T \to \infty$). On the other hand, in the finite temperature case ($\beta << 1$), the solution of MPM estimate is better than it of MAP estimate because the posterior distribution is formed with a narrow or wide width and then the mean is supposed to give a different value from the mode in the posterior distribution (Fig. 2.6). [7] Below, $\tilde{\boldsymbol{x}}$ indicate $\{\tilde{x}_i^{\mathrm{MPM}}\}$ unless otherwise noted.

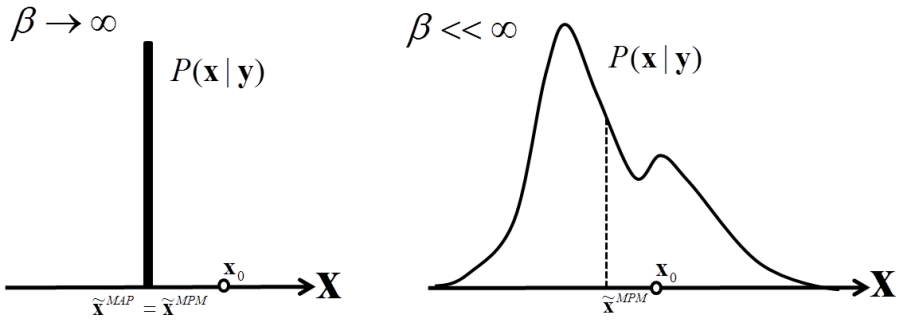


Figure 2.6: The schematic diagram of the posterior distribution on the configuration space in the cases of the low temperature limit ($\beta \to \infty$) (left panel) and finite temperature ($\beta << \infty$) (right panel).

Another perspective can be given below. We can see that the thermal average, ensemble average, corresponds to consideration of the minimum of the free energy, $F = -\frac{1}{\beta}\log Z$ instead of energy which mean cost function. In the case that $\beta \to \infty$, the free energy goes to the energy. Because the the system including the temperature goes to the minimum of the free energy, the MPM estimate can be performed by calculating the order parameter minimizing the free energy. The schematic picture of such the interpretation is given in Fig. 2.7.

The above discussion is the procedure to influence the original information from received information which is damaged through noisy channel. We here consider the decoding performance of the estimated sequence $\tilde{\boldsymbol{x}}$, comparing with the original information. In this context, we should assume that the original information and "true" channel is known, which mean that $P(\boldsymbol{x}_0)$ and $P(\boldsymbol{y}|\boldsymbol{x}_0)$ are given. Under such a assumption, the Hamming distance between the original sequence and estimated sequence is defined as

$$D_H = ||\boldsymbol{x}_0 - \tilde{\boldsymbol{x}}||^2, \tag{2.36}$$

where smaller $D_H$ gives better the performance. Focusing on the condition that each bit takes 1 or $-1$, the other decoding measure can be represented as follows with the

[7] In these figures, the horizontal line $\boldsymbol{x}$ obviously represents not one dimension but high dimension, $N$-dimension.

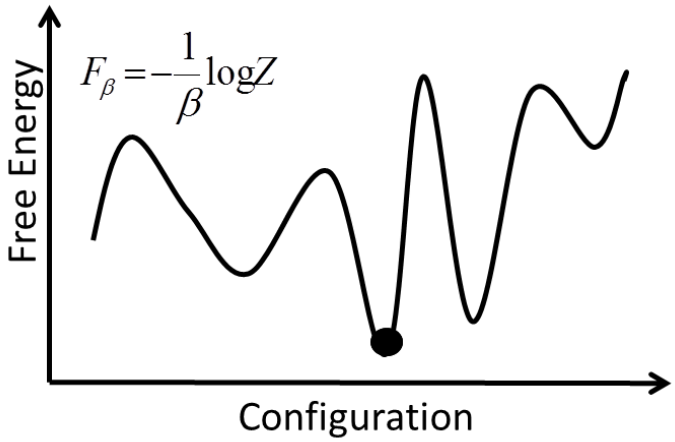


Figure 2.7: Free energy of the system.

normalized factor $N$,

$$M = \frac{1}{N}\boldsymbol{x}_0^T\tilde{\boldsymbol{x}} = \frac{1}{N}\sum_{i=1}^{N} x_{0i}\tilde{x}_i^{\mathrm{MPM}}, \tag{2.37}$$

which is called the overlap between the original bit sequence and the estimated bit sequence. Note that the condition that $M = 1$ gives the perfect restoration (decoding or demodulation). Because the $\boldsymbol{x}_0$ is generated from $P(\boldsymbol{x_0})$ and the channel noise fluctuate stochastically according to $P(\boldsymbol{y}|\boldsymbol{x}_0)$, the overlap incorporating the MPM estimate should be rewritten as follows:

$$\begin{aligned} M &= \frac{1}{N}\sum_{\boldsymbol{x}_0} P(\boldsymbol{x}_0)\int P(\boldsymbol{y}|\boldsymbol{x}_0)\boldsymbol{x}_0^T\tilde{\boldsymbol{x}} && (2.38)\\ &= \frac{1}{N}\sum_{\boldsymbol{x}_0} P(\boldsymbol{x}_0)\int P(\boldsymbol{y}|\boldsymbol{x}_0)\sum_i x_{0i}\mathrm{sgn}\langle x_i\rangle_\beta && (2.39)\\ &= \frac{1}{N}[\boldsymbol{x}_0^T\tilde{\boldsymbol{x}}], && (2.40) \end{aligned}$$

where the bracket $[\cdot]$ in above equation denote the averages over $\boldsymbol{x}_0$ and $\boldsymbol{y}$. Note that the overlap depends on $\beta$ through $\tilde{\boldsymbol{x}}$ and some parameters through $P(\boldsymbol{x}|\boldsymbol{y})$, $P(\boldsymbol{y}|\boldsymbol{x}_0)$ and $P(\boldsymbol{x}_0)$. Because we often fix the parameter in $P(\boldsymbol{y}|\boldsymbol{x}_0)$ and $P(\boldsymbol{x}_0)$, we describe $M$ as the function depending on the inverse temperature $\beta$ which can be seen to be the control parameter of noise.

To wrap up, the procedure to derive the estimated bit sequence $\tilde{\boldsymbol{x}}$ and to evaluate the decoding performance $M$ can be stated as follows:

**Procedure to derive the estimated bit sequence**

1. We consider how the original information is emerged, and then set the prior, $P(\boldsymbol{x})$.

2. We assume some kind of channel noise, e.g., Gaussian or Binary symmetric channel. Thus, we set the likelihood function of $\boldsymbol{x}$, $P(\boldsymbol{y}|\boldsymbol{x})$.

3. We calculate the posterior $P(\boldsymbol{x}|\boldsymbol{y})$ following the Bayes formula. Then, the MPM estimate gives the estimated bit as $\tilde{x}_i^{\mathrm{MPM}}$.

**Procedure to evaluate average-case performance**

1. In order to evaluate the average-case performance, we must preliminarily know the original information and true channel parameters. Consequently, we assume the probability distribution of "true" channel type $P(\boldsymbol{y}|\boldsymbol{x}_0)$ and of an original information $P(\boldsymbol{x}_0)$ as some types. [8]

2. We calculate the overlap $M$ between the original and estimated sequence. Note that here the overlap should be averaged over original data and true channel because they are represented as probabilistic form.

In this thesis, we particularly focus on the procedure to evaluate decoding performance and then will have the explicit expression for the overlap. In order to achieve this, we will discuss the very large system, i.e., the condition that $N \to \infty$. For this treatment, we can use the statistical mechanics which is powerful tool in an analysis of physical systems.

## 2.4 Statistical mechanical analysis for basic mean-field models

As already discussed in previously, the information processing closely relate to "Ising spin systems" through Bayes formula. For such a treatments, the statistical mechanical approach can be powerful and effective tool to understand the macroscopic property of the information processing models, i.e., average-case performance. Considering the $N$ Ising spin system with Hamiltonian $H(\boldsymbol{\sigma})$, the probability of the spin configuration follows as *Maxwell Boltzman distribution*;

$$P(\boldsymbol{\sigma}) = \frac{\exp(-\beta H(\boldsymbol{\sigma}))}{Z} \tag{2.41}$$

$$Z = \operatorname*{Tr}_{\boldsymbol{\sigma}} \exp(-\beta H(\boldsymbol{\sigma})), \tag{2.42}$$

where $Z$ in terms of the statistical mechanics is called the partition function which corresponds to the normalization term and $\beta \equiv 1/T$ corresponds to inverse temperature. Free energy in the system can be written by [9]

$$F = -\beta^{-1} \log Z. \tag{2.43}$$

[8] We here these probability distributions, $P(\boldsymbol{y}|\boldsymbol{x}_0)$ and $P(\boldsymbol{x}_0)$, are assumed to be same type of $P(\boldsymbol{y}|\boldsymbol{x})$ and $P(\boldsymbol{x})$ because we consider only the difference of parameters, e.g., variance in channel or smoothness. That is, if $P(\boldsymbol{y}|\boldsymbol{x})$ is Gaussian channel with $\sigma^2$ variance, $P(\boldsymbol{y}|\boldsymbol{x}_0)$ is Gaussian channel with $\sigma_0^2 (\neq \sigma^2)$.

[9] Here, we use the term *free energy* as Helmholtz type. Although the other types of free energies, of course, exist, e.g., Gibbs type, we omit those introduction in this paper.

Because the system evolves with decreasing free energy, an investigation of the form of free energy leads to understanding an equilibrium state of the system. The Hamiltonian form can be changed depending on systems and has complicated form generally. By calculating free energy through the sense of statistical mechanical analysis, we can obtain the macroscopic parameters (order parameters) as the saddle point conditions of the free energy (Yeomans 1992; Stanley 1987). In this section, we give the statistical mechanical analysis in thermodynamic limit $N \to \infty$ for two basic models, *Hushimi-Temperly* (H-T) model and *Sherington-Kirkpatrick* (S-K) model. The both are described as infinite range (mean-field) model in which all spins in the network are interacting with all others.

### 2.4.1 Hushimi-Temperly model

First, we consider the simplest model called *Hushimi-Tempely* (H-T) model which can be described by

$$H = -\frac{J}{2N}\sum_{i\neq j}\sigma_i\sigma_j - h\sum_{i=1}^{N}\sigma_i, \tag{2.44}$$

where $\sigma_i$ takes 1 or $-1$ and $\frac{J}{N}$ represents the strength of connection between spins. Each site has a own energy $-h\sigma_i$. And $\sum_{i\neq j}$ means that the spins connect the all other spins, which is called the infinite range model or mean field model. [10] The partition function of this system can be written as

$$Z = \mathop{\mathrm{Tr}}_{\boldsymbol{\sigma}} \exp\left(\frac{J\beta}{2N}\left(\sum_i \sigma_i\right)^2 - \frac{\beta J}{2} + \beta h\sum_i \sigma_i\right). \tag{2.45}$$

Introducing the following transformation to the partition function,

$$e^{ax^2} = \left(\frac{Na}{\pi}\right)\int_{-\infty}^{\infty} dm \exp\left(-Nam^2 + 2\sqrt{N}amx\right), \tag{2.46}$$

which is called *Hubbard-Stratonovich transformation*, we can perform $\mathrm{Tr}_{\boldsymbol{\sigma}}$ in Eq. (2.45) because the square of $\sum_i \sigma_i$ is disappear and then it transform to simple integral. Thus, the partition function can be rewritten as the following form:

$$\begin{aligned}
Z &= \mathop{\mathrm{Tr}}_{\boldsymbol{\sigma}} \int dm \exp\left(-\frac{N\beta Jm^2}{2} - \frac{\beta J}{2} + N\beta Jm\sum_i \sigma_i + \beta h\sum_i \sigma_i\right) && (2.47)\\
&= \int dm e^{-\frac{N\beta Jm^2}{2} - \frac{\beta J}{2}} \mathop{\mathrm{Tr}}_{\boldsymbol{\sigma}} \exp\left\{(\beta Jm + \beta h)\sum_i \sigma_i\right\} && (2.48)\\
&= \int dm e^{-\frac{N\beta Jm^2}{2} - \frac{\beta J}{2}} \left[\mathop{\mathrm{Tr}}_{\sigma} \exp\left\{(\beta Jm + \beta h)\sigma_i\right\}\right]^N && (2.49)\\
&= \int dm \exp\left(-\frac{N\beta Jm^2}{2} - \frac{\beta J}{2} + N\log 2\cosh\beta(Jm + h)\right). && (2.50)
\end{aligned}$$

[10] The mean field theory give the exact solution in the infinite range model. For this reason, the infinite range model is also called the infinite range model (Nishimori 2001).

The physical meaning of $m$ corresponds to the *magnetization* because of the relation that $m = \frac{1}{N}\sum_{i=1}^{N}\sigma_i$. Considering the thermodynamic limit $N \to \infty$, $-\frac{\beta J}{2}$ goes to zero and then the free energy per spin $f \equiv \frac{F}{N}$ is

$$-\beta f = -\frac{\beta J m^2}{2} + \log 2\cosh\beta(Jm + h). \tag{2.51}$$

Here, we use the saddle point approximation (see AppendixA), so that $m$ satisfies the saddle point condition as follows:

$$\frac{\partial}{\partial m}\left(-\frac{\beta J m^2}{2} + \log 2\cosh\beta(Jm + h)\right) = 0. \tag{2.52}$$

By calculating the above derivation, we derive the self consistent equation of $m$ as follows:

$$m = \tanh\beta(Jm + h). \tag{2.53}$$

By solving the above equation with respect to $m$ numerically, we can understand the macroscopic property of the system. Before we see these solutions, we sketch the relations among $y = 2x$, $y = x/2$ and $y = \tanh x$ in Fig. 2.8(a) conceptually. While there are two solutions in the case that $y = x/2$, one solution in the case that $y = 2x$ occurs. Therefore, while $m$ has unique solution that $m = 0$ for $\frac{1}{\beta} \equiv T > 1$, there are two solutions $m > 0$ except for $m = 0$ which is a trivial solution in other case that $T < 1$. Figure 2.8(b) denotes the dependence of $m$ on $T$which is the numerical solutions of Eq. (2.53). We see that $m$ decreases from 1 (or $-1$) to 0 gradually and $m$ becomes 0 at $T = 1$. In other words, there is the phase transition from the *ferromagnetic* phase to *paramagnetic* phase. Here, the boundary point between phases is called the *critical temperature*.

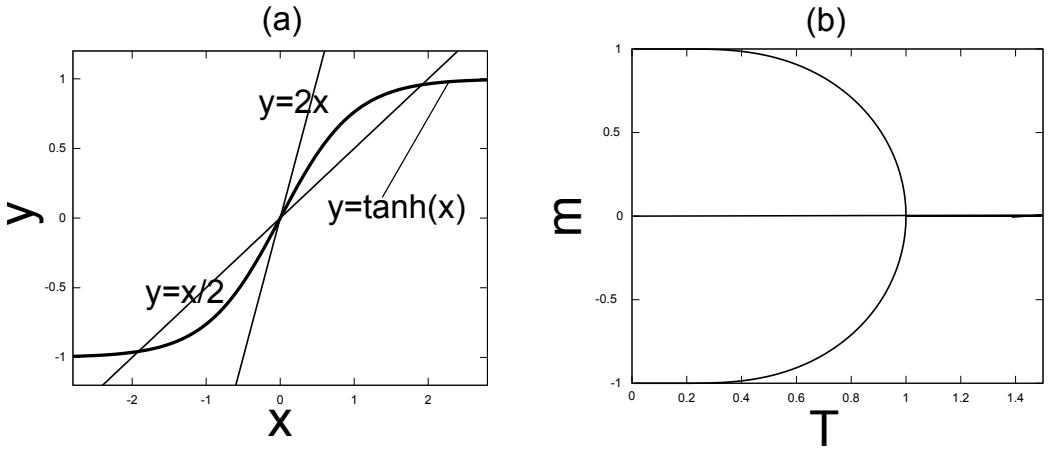


Figure 2.8: (a): Schematic solutions of state equation. (b): Temperature $T$ dependence of magnetization $m$.

### 2.4.2 Sherrington-Kirkpatrick model

Next we present the analysis of the *Sherrington-Kirkpatrick* (S-K) model which is the simple mean-field spin glass model (Edwards and Anderson 1975; Sherrington and Kirkpatrick 1975; Mezard et al. 1987). While the H-T model where the interactions between spins are uniform, we consider the random interactions between spins in the spin glass model. The basic technique for analyzing the mean-field spin glass models is given in this section.

In spin glass models, the interaction between the spins usually generate from a probabilistic distribution $P(\boldsymbol{J})$. In this context, we need to consider the average of free energy with respect to random interaction $J_{ij}$. Thus, we consider the following partition function:

$$[F] = -\beta^{-1}[\log Z] = -\beta^{-1}\int d\boldsymbol{J}P(\boldsymbol{J})\log Z = -\beta^{-1}\int d\boldsymbol{J}P(\boldsymbol{J})\log \mathop{\mathrm{Tr}}_{\boldsymbol{\sigma}} e^{-\beta H(\boldsymbol{\sigma})}, \quad (2.54)$$

where the bracket $[\cdot] = \int d\boldsymbol{J}P(\boldsymbol{J})(\cdot)$ means the average over the distribution of $\boldsymbol{J}$, which is called the *configurational average* or the *data average*. [11] Because the time scale of thermal fluctuation is rapid comparing that of $\boldsymbol{J}$, we trace over $\boldsymbol{\sigma}$ first, and after the operation we calculate the average over $\boldsymbol{J}$. It is not easy to calculate the above equation (2.54) for the complicated dependence of the $\log Z$ on $\boldsymbol{J}$. Then, we use the following formula, viz., *Replica trick*, to calculate it:

$$[\log Z] = \lim_{n\to 0}\frac{[Z^n]-1}{n}. \quad (2.55)$$

Here, the logarithm of $Z$ transform to the polynomial form considering $n$ "replicas" of the system and then the problem becomes much easier. Although the mathematical proof still is not exists, it is known that the formula gives correct solutions empirically. This technique is called the *Replica trick* or *Replica method*. Below, by using this strategy, we evaluate the free energy averaged over $\boldsymbol{J}$.

In S-K model, We consider the following Hamiltonian,

$$H = -\sum_{i<j} J_{ij}\sigma_i\sigma_j \quad (2.56)$$

$$P(J_{ij}) = \sqrt{\frac{N}{2\pi J^2}}\exp\left\{-\frac{N}{2J^2}\left(J_{ij}-\frac{J_0}{N}\right)^2\right\}. \quad (2.57)$$

Note that the interaction here is Gaussian distribution and then fluctuate stochastically. The sum on the right hand side of the Hamiltonian runs over all distinct pairs of spins, ${}_NC_2 = N(N-1)/2$. Following the replica method (2.55), we calculate the following integration,

$$[Z^n] = \int\prod_{i<j} dJ_{ij}P(J_{ij})Z^n \quad (2.58)$$

$$= \int\prod_{i<j} dJ_{ij}P(J_{ij})\mathop{\mathrm{Tr}}_{\boldsymbol{\sigma}^\mu}\exp\left\{\beta\sum_{\mu=1}^{n}\sum_{i<j}J_{ij}\sigma_i^\mu\sigma_j^\mu\right\}, \quad (2.59)$$

[11] We may not understand why $[\cdot]$ is also called the "data" average at this point. In the context of the probabilistic information processing, $\boldsymbol{J}$ usually corresponds to a received information and then we call it so (see the later sections).

where $\mu$ is the replica index. In order to understand the macroscopic behavior, introducing the following two order parameters,

$$m_\mu = \frac{1}{N}\sum_{i=1}^{N}\sigma_i^\mu \tag{2.60}$$

$$q_{\mu\nu} = \frac{1}{N}\sum_{i=1}^{N}\sigma_i^\mu\sigma_i^\nu, \tag{2.61}$$

and then the configuration average of $Z^n$ can be represented as

$$\begin{aligned}[Z^n] &= \int\prod_{\mu=1}^{n}dm_\mu\delta\left(\sum_i\sigma_i^\mu - Nm_\mu\right)\int\prod_{\mu<\nu}dq_{\mu\nu}\delta\left(\sum_i\sigma_i^\mu\sigma_i^\nu - Nq_{\mu\nu}\right)\\ &\times \operatorname*{Tr}_{\boldsymbol{\sigma}^\mu}\int\prod_{i<j}dJ_{ij}P(J_{ij})\exp\left\{\beta\sum_{\mu=1}^{n}\sum_{i<j}J_{ij}\sigma_i^\mu\sigma_j^\mu\right\}.\end{aligned} \tag{2.62}$$

Performing the integral over $J_{ij}$ by using Gaussian integral

$$\int dx e^{-\alpha x^2} = \sqrt{\frac{\pi}{\alpha}}, \tag{2.63}$$

the part concerning $J_{ij}$ is[12]

$$\exp\left\{\frac{J^2\beta^2}{2N}\sum_{i<j}\left(\sum_{\mu=1}^{n}\sigma_i^\mu\sigma_j^\mu\right)^2 + \frac{J_0\beta}{N}\sum_{\mu=1}^{n}\sum_{i<j}\sigma_i^\mu\sigma_j^\mu\right\} \tag{2.64}$$

$$\simeq \exp\left\{\frac{J^2\beta^2N}{2}\left(\frac{n}{2}+\sum_{\mu<\nu}q_{\mu\nu}^2\right) + \frac{\beta J_0N}{2}\sum_{\mu=1}^{n}m_\mu^2\right\}, \tag{2.65}$$

where we use the relation, $(\sum_i X_i)^2 = \sum_i X_i^2 + 2\sum_{i<j}X_iX_j$ and consider the condition that $n$ is sufficiently small. We define the exponent proportional to $N$ as

$$e_n(m_\mu, q_{\mu\nu}) \equiv \frac{\beta J_0}{2}\sum_{\mu=1}^{n}m_\mu^2 + \frac{\beta^2J^2}{2}\left(\frac{n}{2}+\sum_{\mu<\nu}q_{\mu\nu}^2\right), \tag{2.66}$$

and then Eq. (2.62) can be described as the following:

$$[Z^n] = \operatorname*{Tr}_{\boldsymbol{\sigma}^\mu}\int\prod_{\mu=1}^{n}dm_\mu\delta\left(\sum_i\sigma_i^\mu - Nm_\mu\right)\prod_{\mu<\nu}dq_{\mu\nu}\delta\left(\sum_i\sigma_i^\mu\sigma_i^\nu - Nq_{\mu\nu}\right)e^{Ne_n(m_\mu,q_{\mu\nu})}. \tag{2.67}$$

[12]This part can be denoted as $[\exp(-\beta\sum_\mu H(\boldsymbol{\sigma}^\mu))]$.

Representing the delta function as the Fourier integral, we have:

$$\mathop{\mathrm{Tr}}_{\boldsymbol{\sigma}^\mu}\prod_{\mu=1}^{n}\delta\left(\sum_i\sigma_i^\mu-Nm_\mu\right)\prod_{\mu<\nu}\delta\left(\sum_i\sigma_i^\mu\sigma_i^\nu-Nq_{\mu\nu}\right) \tag{2.68}$$

$$= \mathop{\mathrm{Tr}}_{\boldsymbol{\sigma}^\mu}\int\prod_\mu\frac{d\hat{m}_\mu}{2\pi}\exp\left\{\sum_{\mu=1}^{n}\hat{m}_\mu(\sum_i\sigma_i^\mu-Nm_\mu)\right\}\prod_{\mu<\nu}\frac{d\hat{q}_{\mu\nu}}{2\pi}\exp\left\{\sum_{\mu<\nu}^{n}\hat{q}_{\mu\nu}\left(\sum_i\sigma_i^\mu\sigma_i^\nu-Nq_{\mu\nu}\right)\right\} \tag{2.69}$$

$$= \int\prod_\mu\frac{d\hat{m}_\mu}{2\pi}\int\prod_{\mu<\nu}\frac{d\hat{q}_{\mu\nu}}{2\pi}\exp\left[\log\mathop{\mathrm{Tr}}_{\boldsymbol{\sigma}^\mu}\exp\left\{\sum_\mu\hat{m}_\mu\sum_i\sigma_i^\mu+\sum_{\mu<\nu}\hat{q}_{\mu\nu}\sum_i\sigma_i^\mu\sigma_i^\nu\right\}\right.$$
$$\left.-N\sum_{\mu=1}^{n}\hat{m}_\mu m_\mu-N\sum_{\mu<\nu}^{n}\hat{q}_{\mu\nu}q_{\mu\nu}\right]. \tag{2.70}$$

Carrying out the trace over $\boldsymbol{\sigma}^\mu$ independently in the above equation as follows

$$\mathop{\mathrm{Tr}}_{\boldsymbol{\sigma}^\mu}\exp\left\{\sum_\mu\hat{m}_\mu\sum_i\sigma_i^\mu+\sum_{\mu<\nu}\hat{q}_{\mu\nu}\sum_i\sigma_i^\mu\sigma_j^\nu\right\} \tag{2.71}$$

$$= \mathop{\mathrm{Tr}}_{\boldsymbol{\sigma}^\mu}\prod_{i=1}^{N}\exp\left\{\sum_\mu\hat{m}_\mu\sigma_i^\mu+\hat{q}_{\mu\nu}\sigma_i^\mu\sigma_i^\nu\right\} \tag{2.72}$$

$$= \left(\mathop{\mathrm{Tr}}_{\boldsymbol{\sigma}}\exp\left\{\sum_\mu\hat{m}_\mu\sigma^\mu+\hat{q}_{\mu\nu}\sigma^\mu\sigma^\nu\right\}\right)^N, \tag{2.73}$$

Eq.(2.70) is

$$[Z^n] = \int\prod_\mu m_\mu\int\prod_{\mu<\nu}dq_{\mu\nu}\prod_\mu d\hat{m}_\mu\int\prod_{\mu<\nu}d\hat{q}_{\mu\nu}$$
$$\exp\left\{N(e_n(m_\mu,q_{\mu\nu})+s_n(m_\mu,q_{\mu\nu},\hat{m}_\mu,\hat{q}_{\mu\nu})\right\} \tag{2.74}$$

$$s_n(m_\mu,q_{\mu\nu},\hat{m}_\mu,\hat{q}_{\mu\nu}) = \log\mathop{\mathrm{Tr}}_{\boldsymbol{\sigma}}\exp\left\{\sum_{\mu=1}^{n}\hat{m}_\mu\sigma^\mu+\sum_{\mu<\nu}\hat{q}_{\mu\nu}\sigma^\mu\sigma^\nu\right\}-\sum_\mu\hat{m}_\mu m_\mu-\sum_{\mu<\nu}\hat{q}_{\mu\nu}q_{\mu\nu}. \tag{2.75}$$

Considering the limit $n\to 0$ taken with $N$ kept very large but finite, we find the following expression:

$$[Z^n] \simeq \exp\left\{Nn\left(\frac{e_n(m_\mu,q_{\mu\nu})}{n}+\frac{s_n(m_\mu,q_{\mu\nu},\hat{m}_\mu,\hat{q}_{\mu\nu})}{n}\right)\right\} \tag{2.76}$$

$$\simeq 1+Nn\left(\frac{e_n(m_\mu,q_{\mu\nu})}{n}+\frac{s_n(m_\mu,q_{\mu\nu},\hat{m}_\mu,\hat{q}_{\mu\nu})}{n}\right). \tag{2.77}$$

By using the formula (2.43), we find the free energy per spin is represented as follows:

$$-\beta[f] = \lim_{n\to0}\frac{[Z^n]-1}{nN} \tag{2.78}$$

$$= \lim_{n\to0}\left(\frac{e_n(m_\mu,q_{\mu\nu})}{n}+\frac{s_n(m_\mu,q_{\mu\nu},\hat{m}_\mu,\hat{q}_{\mu\nu})}{n}\right). \tag{2.79}$$

We assume the following relations to calculate the trace over $\boldsymbol{\sigma}$ for deriving a explicit form of free energy,

$$m = m_\mu, \quad \hat{m} = \hat{m}_\mu \tag{2.80}$$

$$q = q_{\mu\nu}, \quad \hat{q} = \hat{q}_{\mu\nu}, \tag{2.81}$$

which is called *Replica Symmetry*(RS) solutions. The RS means that the dependence of order parameters on the replica indices should not affect the physics of the system. Although we of course should also consider the asymmetry of the replicas, we adopt RS condition below. For these conditions, (2.80) and (2.81), we have:

$$s_n^{\mathrm{RS}} = \frac{n\hat{q}(q-1)}{2} - n\hat{m}m + n\int Dw \log 2\cosh(\hat{m} + w\sqrt{\hat{q}}) \tag{2.82}$$

$$e_n^{\mathrm{RS}} = \frac{n\beta J_0 m^2}{2} + \frac{n\beta J^2}{4}(1-q^2). \tag{2.83}$$

where $\int Dw(\cdot) = \frac{1}{\sqrt{2\pi}}\int dw e^{-w^2/2}$ and we use the formula of the Gauss integral. Thus, the integral is inspired the relation between the replica indices, whose source is the randomness of the interaction between spins. The integral in the right hand side of the above equation emerges from the following calculation

$$\exp\left(\hat{q}\sum_{\mu<\nu}\sigma^\mu\sigma^\nu\right) = \int Dw \exp\left\{\left(\sqrt{\hat{q}}\sum_{\mu=1}^{n}\sigma^\mu\right)w - \frac{n\hat{q}}{2}\right\}, \tag{2.84}$$

The final form of the free energy of the S-K model is

$$-\beta[f] = \frac{\beta J_0 m^2}{2} + \frac{\beta J^2}{4}(1-q^2) + \frac{\hat{q}(q-1)}{2} - \hat{m}m + \int Dw \log 2\cosh(\hat{m} + w\sqrt{q}) \tag{2.85}$$

The order parameters satisfies the following closed relations for the saddle point condition of the free energy (2.85):

$$\hat{m} = \beta J_0 m \tag{2.86}$$

$$\hat{q} = \beta^2 J^2 q \tag{2.87}$$

$$m = \int Dw \tanh(w\sqrt{\hat{q}} + \hat{m}) \tag{2.88}$$

$$q = \int Dw \tanh^2(w\sqrt{\hat{q}} + \hat{m}). \tag{2.89}$$

In the H-T model which is the mean-field model has constant interaction, we saw the ferromagnetic phase ($m > 0$) at low temperature region and the paramagnetic phase ($m = 0$) at high temperature region. On the other hand, in S-K model which is mean-field spin glass model, we can see three phases according to the value of the order parameters as listed in the table 2.1. Here, spin glass phase ($m = 0,\ q > 0$) emerge, which does not emerge in H-T model. Spin glass phase is the specific behavior of the mean-field spin glass models. The detailed discussion of their phases is given in Sec. 2.6 where we discuss an error correcting code model which can be modeled as general spin glass model with many body interactions. We here omit the discussion of *replica symmetry breaking* (RSB) and the condition that RSB occurs. It is well-known that the free energy of S-K model under the RS condition induce the problem of negative entropy at low temperature, and then the RSB condition should be considered (Mézard et al. 1987; Binder and Young 1986; Fischer and Hertz 1991).

Table 2.1: Phases in S-K model.

| Ferromagnetic | Paramagnetic | Spin glass |
|---|---|---|
| $m > 0,\ q > 0$ | $m = 0,\ q = 0$ | $m = 0,\ q > 0$ |

### 2.4.3 Notes of Replica method

The replica method is powerful tool to understand the spin glass system, and then it has been thought of correct results although a mathematical validity is disputable. While it is widely-accepted for many researchers, controversial points remain in fact. In this section, we roughly comment on the back ground and problems of the replica method. Because the mathematical and rigorous arguments of these problems are complicated and have not much to do with our studies explicitly, we will leave a brief introduction to them.

We first give the different representation of replica method from Eq. (2.55). Using the well known approximation

$$nx \simeq \log(1 + nx) \tag{2.90}$$

for $nx << 1$, we obtain the following relation:

$$n[\log Z] \simeq \log(1 + n[\log Z]) \tag{2.91}$$

for $n \to 0$. By using this, we can obtain the following representations:

$$[\log Z] \simeq \lim_{n\to 0} \frac{1}{n} \log \left\{ 1 + n \left( \frac{[Z^n] - 1}{n} \right) \right\} \tag{2.92}$$

$$= \lim_{n\to 0} \frac{1}{n} \log[Z^n]. \tag{2.93}$$

and

$$-\beta[f] = \frac{1}{N} \lim_{n\to 0} \frac{1}{n} \log[Z^n]. \tag{2.94}$$

As we mentioned in Sec. 2.4.2, for this trick, we have the logarithm of an averaged quantity instead of the mean of logarithm. The computation is then much easier.

#### Analytic continuation

The replica method logically requests the following procedure:

1. Assuming $n$ to be integer, we calculate $[Z]^n$.
2. Assuming $n$ to be real number, we take the limit of $n$, $n \to 0$.

The above treatments may be unnatural. If $n$ is integer, we can evaluate $[Z^n]$ by regarding as the $n$-th replicated discrete system and then can define the order parameters in each replicated system. If $n$ is real number, however, there are a discrepancy when we evaluate configuration average of the free energy analytically.

**Thermodynamic limit**

The problem here is the order of the limit operation. Rewriting $Z$ as $Z_N$, which means that the partition function before $N \to \infty$ depends on the system size $N$ explicitly, the replica method leads to

$$\lim_{N\to\infty} \frac{1}{N}[\log Z_N] = \lim_{N\to\infty} \frac{1}{N} \lim_{n\to 0} \frac{1}{n} \log[Z_N^n] \tag{2.95}$$

$$= \lim_{n\to 0} \frac{1}{n} \lim_{N\to\infty} \frac{1}{N} \log[Z_N^n]. \tag{2.96}$$

The above procedures where we counter-change the limitation of $n$ and $N$ may be inadequacy mathematically.

The above arguments have been serious problems in the replica method. It is difficult to justify the replica method generally in conclusion. Although there are negative perceptions in the replica method for these problems (Talagrand 2003), it has actually given correct and valid answer empirically as we still mentioned. The detailed reviews of them were given in the report by Tanaka (Tanaka 2007). In the field of physics, it often happen that the empirical argument has been performed primarily before the rigorous mathematical discussion. We expect that the mathematical treatments of the replica method would be done.

## 2.5 Image restoration

The purpose of the image restoration is to restore the original image as clean as possible. The original studies of image restoration through stochastic approaches owe to the papers by Geman and Geman (1984) and Derin et al. (1984). Average-case performance behavior for the mean-field model introduced here has been investigated by Nishimori and wong (1999). The recent topics in such the image restoration model are for example hyper parameter estimation (Tanaka and Inoue 2000) and the cluster variation method which improve the naive mean-field approximation (Tanaka and Morita 1995). In this section, we will see that the model can be described as Ising spin model with *Markov random field* (MRF) and then the statistical mechanical approach can be effective strategy in the analysis of the model for extracting the macroscopic properties and evaluating average-case restoration performance.

### 2.5.1 Model

We consider the white and black image which mean that each pixel takes binary value. The original image (pixels) $\boldsymbol{\xi} = \{\xi_i\}$ , $(\xi_i = \pm 1, i = 1, ..., N)$ is damaged as follows

$$\boldsymbol{\tau} = \boldsymbol{\xi} + \boldsymbol{\epsilon}, \tag{2.97}$$

where $\boldsymbol{\tau}$ is the degraded image and $\epsilon$ is some noise. In this context, the black and white correspond to 1 and $-1$, respectively. First, in order to consider the prior of the image, we introduce the *smoothness* into the image as a natural assumption. The smoothness means that neighboring pixels is likely to take a same value. That is, if a pixel take black ($\xi_i = 1$) the marginal pixels is likely to be black ($\xi_{j\sim i} = 1$) (see Fig. 2.9(b)),

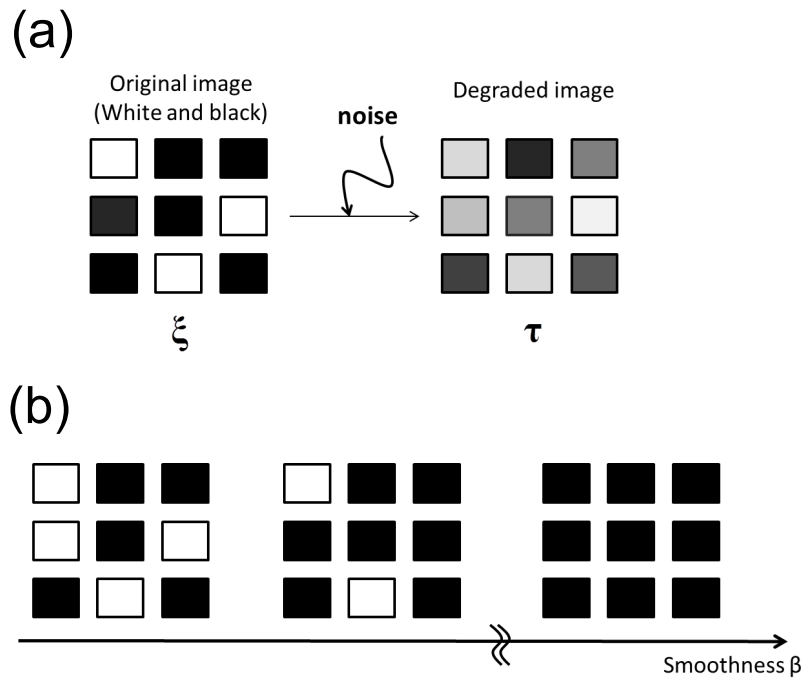


Figure 2.9: (a):Conceptual diagrams for the image restoration. The black and white squares correspond to binary pixels, respectively, i.e., $+1$ and $-1$. In these cases, we consider the case that $N = 9$ $(3 \times 3)$ and Gaussian noise. (b):Schematic concept of the smoothness $\beta$. Increasing $\beta$, neighboring pixels become same states.

where $j \sim i$ means the neighboring $j$-th pixels around $i$-th pixel. In order to express such a condition, we consider the following prior distribution,

$$P(\boldsymbol{\sigma}) = \frac{\exp(\beta \sum_{<i,j>} \sigma_i \sigma_j)}{Z(\beta)}, \tag{2.98}$$

where $< i, j >$ means the neighboring pixels, $\beta$ corresponds to the strength of the smoothness and $Z(\beta)$ is the partition function, normalization factor. We can immediately see that the above expression corresponds to the system with ferro-magnetic interaction, $H = -\sum \sigma_i \sigma_j$. As we saw in the H-T model, the configuration changes according with temperature and then the all spins are "up" or "down" in the low temperature limit. Thus, in the case of image restoration, $\beta = \frac{1}{T}$ controls the smoothness.

We adopt the Gaussian noise

$$P(\boldsymbol{\tau}|\boldsymbol{\sigma}) = \frac{1}{(\sqrt{2}\pi a_{e\tau})^N} \exp\left\{ -\sum_{i=1}^{N} \frac{(\tau_i - \tau_{e0}\sigma_i)^2}{2a_{e\tau}^2} \right\}, \tag{2.99}$$

under the assumption of independent noise at each pixels. Here, $a_{e\tau}^2$ is the variance and $\tau_{e0}$ represents the strength of the signal. Because we are interested in the $P(\boldsymbol{\tau}|\boldsymbol{\sigma})$ as a function of $\sigma$, we extract the $\boldsymbol{\sigma}$ term from the above expression and then we can

describe the likelihood as

$$P(\boldsymbol{\tau}|\boldsymbol{\sigma}) = \frac{\exp(h\sum_{i=1}^{N}\tau_i\sigma_i)}{Z(h)}, \tag{2.100}$$

where $h \equiv \frac{\tau_{e0}}{a_\tau^2}$ and $Z(h)$ corresponds to the redefined partition function. Although there many noise type besides the Gaussian type, we use the Gaussian type below as the simple case.

For these formulation, the posterior distribution can be represented as

$$\begin{aligned} P(\boldsymbol{\sigma}|\boldsymbol{\tau}) &= \frac{P(\boldsymbol{\tau}|\boldsymbol{\sigma})}{\mathrm{Tr}_{\boldsymbol{\sigma}} P(\boldsymbol{\tau}|\boldsymbol{\sigma})} && (2.101)\\ &= \frac{\exp(-H_{\mathrm{eff}})}{Z} && (2.102)\\ Z &= \mathop{\mathrm{Tr}}_{\boldsymbol{\sigma}} \exp(-H_{\mathrm{eff}}) && (2.103)\\ H_{\mathrm{eff}} &= -\beta \sum_{<i,j>} \sigma_i\sigma_j - h\sum_{i=1}^{N}\tau_i\sigma_i, && (2.104) \end{aligned}$$

where $Z(= Z(\beta)Z(h))$ is the partition function defined as $\mathrm{Tr}_{\boldsymbol{\sigma}} e^{-H_{\mathrm{eff}}}$ and $H_{\mathrm{eff}}$ is the effective Hamiltonian of the model. We can see that the Hamiltonian corresponds to the ferro-magnetic model with random field. The estimated pixel can be expressed as

$$\tilde{\sigma}_i = \mathrm{sgn}\langle\sigma_i\rangle_{\beta,h}, \tag{2.105}$$

following the MPM estimate(2.35).

We provide the procedure to evaluate the restoration performance below. We assume that the original image is generated from the following probability:

$$P(\boldsymbol{\xi}) = \frac{\exp\left(\beta_s \sum_{<i,j>}\xi_i\xi_j\right)}{Z(\beta_s)}, \tag{2.106}$$

where $\beta_s$ is the "true" smoothness parameter. Although the original image obviously is not generated from such a probability, we replace $\beta$ to $\beta_s$ in Eq. (2.98) to investigate the restoration property by using theoretical analysis. Indeed, when we evaluate the restoration performance, we fix the true parameter $\beta_s$, and then we investigate how the performance behave controlling $\beta$. The "true" noise follows

$$P(\boldsymbol{\tau}|\boldsymbol{\xi}) = \frac{1}{(\sqrt{2}\pi a_\tau)^N}\exp\left\{-\sum_{i=1}^{N}\frac{(\tau_i-\tau_0\xi_i)^2}{2a_\tau^2}\right\}, \tag{2.107}$$

where $a_\tau$ is the" true" variance and the $\tau_0$ is "true" the signal. The overlap between the original and estimated image with averaging over the original image can be defined as

$$M(\beta,h) = \mathop{\mathrm{Tr}}_{\boldsymbol{\xi}} \int d\boldsymbol{\tau} P(\boldsymbol{\xi})P(\boldsymbol{\tau}|\boldsymbol{\xi})\xi_i \mathrm{sgn}\langle\sigma_i\rangle_{\beta,h}. \tag{2.108}$$

Definitely, the overlap is maximized in the condition that $\beta = \beta_s, h/\beta = \frac{\tau}{\beta_s a_\tau^2}$, i.e., [13]

$$M(\beta, h) \leq M(\beta_s, \frac{\beta\tau}{\beta_s a_{\tau^2}}). \tag{2.109}$$

### 2.5.2 Analysis and result

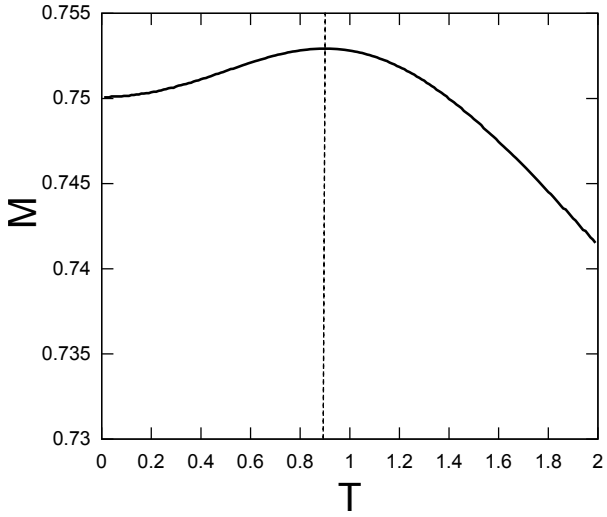


Figure 2.10: Restoration performance for $\tau_0 = 1.0, a_\tau = 1.0$ and $T_s = 0.9$ with $, h = T_s\tau_0/Ta_\tau^2$. Dashed line indicate the line for the Nisimori condition that $T = T_s$.

In this section, we present the analysis for deriving the explicit expression of order parameters and the overlap in the thermodynamic limit $N \to \infty$ of the image restoration model. And then, we give a numerical solutions of these equations and discuss the *Nishimori condition* which maximize the overlap. Our interesting is to have an information that the overlap depends on the parameters near the optimal point. The mean-field model is useful to attack this problem as we saw the above sections. Therefore, let us consider the mean-field version of the above model as follows:

$$\sum_{<i,j>} \to \frac{1}{2N} \sum_{i \neq j}. \tag{2.110}$$

Under this formulation which should be applied to the prior $P(\boldsymbol{\sigma})$ and $P(\boldsymbol{\xi})$, we can analyze the model by using the method similar to it stated in Sec. 2.4.

The free energy in the system is given in the following,

$$-\beta[F] = \operatorname*{Tr}_{\boldsymbol{\xi}} \int d\boldsymbol{\tau} P(\boldsymbol{\xi}) P(\boldsymbol{\tau}|\boldsymbol{\xi}) \log Z, \tag{2.111}$$

[13] We can easily understand this as follows. In this case, we have $H = -\sum_{<i,j>} \sigma_i\sigma_j - h/\beta \sum_i \tau_i\sigma_i$ as Hamiltonian, and then comparing the coefficient of the second term in the right hand side with $\frac{\tau_0}{\beta_s a_\tau^2}$, we can obtain the relation.

where $[\cdot]$ mean $\mathrm{Tr}_{\boldsymbol{\xi}} \int d\boldsymbol{\tau} P(\boldsymbol{\xi}) P(\boldsymbol{\tau}|\boldsymbol{\xi})(\cdot)$ which is "data" average. The partition function can be represented as

$$
\begin{aligned}
Z &= \mathop{\mathrm{Tr}}_{\boldsymbol{\sigma}} \exp(-H_{\mathrm{eff}}) && (2.112)\\
&= \mathop{\mathrm{Tr}}_{\boldsymbol{\sigma}} \exp\left\{ h \sum_i \tau_i + \frac{\beta}{2N} \sum_{j=1}^{N} (\sigma_j)^2 - \frac{\beta}{2} \right\}, && (2.113)
\end{aligned}
$$

where we use the condition that $\sum_{i \neq j} \sigma_i \sigma_j = (\sum_j \sigma_j)^2 - \sum_i \sigma_i^2$. By using the Hubbard-Stratonovich transformation,

$$
\exp\left\{ \frac{\beta}{N} (\sum_j \sigma_j)^2 \right\} = \left( \frac{N\beta}{2\pi} \right)^{\frac{1}{2}} \int \exp\left( -\frac{N\beta}{2} m^2 + \beta m \sum_j \sigma_j \right), \tag{2.114}
$$

we obtain the following relation

$$
\begin{aligned}
Z &= \left( \frac{N\beta}{2\pi} \right)^{\frac{1}{2}} \int dm \exp\left( -\frac{N\beta}{2} m^2 + N \log \mathop{\mathrm{Tr}}_{\sigma} e^L \right) && (2.115)\\
L &= \beta m \sigma + h\tau\sigma, && (2.116)
\end{aligned}
$$

where $\sigma$ and $\tau$ stands for the one pixel because we can calculate the trace over $\boldsymbol{\sigma}$ independently on each $\sigma_i$, i,e., $\mathrm{Tr}_{\boldsymbol{\sigma}} \prod_i \exp(\sigma_i) = (\mathrm{Tr}_{\sigma} \exp(\sigma))^N$. And we omit the trivial constant in the above equation. After the easy calculation of $\mathrm{Tr}_{\sigma} e^L$, we derive the following expression:

$$
\log Z = -\frac{N\beta}{2} m^2 + N \log 2\cosh(\beta m + h\tau). \tag{2.117}
$$

Following Eq. (2.111), we consider the data average of the above quantity. By performing easy calculation, we derive the data average term as follows from Eqs. (2.106) and (2.107) through the saddle point condition in $N \to \infty$:

$$
[\cdot] \to \prod_i \int Du \frac{\mathrm{Tr}_{\boldsymbol{\xi}} e^{\beta_s m_0 \xi}}{2\cosh \beta_s m_0}, \quad \left( Du = \frac{1}{\sqrt{2\pi}} e^{-\frac{u^2}{2}},\ u = \frac{\tau - \tau_0 \xi}{a_\tau} \right). \tag{2.118}
$$

Here, $m_0$ is the order parameter magnetization and it satisfied the saddle point condition of the following free energy of the original image:

$$
f_0 = -\frac{N\beta_s}{2} m_0^2 + N \log 2\cosh \beta_s m_0, \tag{2.119}
$$

which can be derived naturally from $\beta f_0 = \log Z_0, , Z_0 = \mathrm{Tr}_{\boldsymbol{\xi}} e^{\beta_s \sum_{i \neq j} \xi_i \xi_j / N}$. The final form of the free energy per spin of the system is expressed as

$$
-\beta[f] = -\frac{\beta[F]}{N} = -\frac{-\beta m^2}{2} + \mathop{\mathrm{Tr}}_{\xi} \int Du e^{\beta_s m_0 \xi} \tanh(\beta m + a_\tau h u + \tau_0 \xi). \tag{2.120}
$$

From the saddle point condition, the order parameters determine the macroscopic properties are obtained as follows:

$$
\begin{aligned}
m_0 &= \tanh \beta_s m_0 && (2.121)\\
m &= \frac{\mathrm{Tr}_{\boldsymbol{\sigma}} \int Du e^{\beta_s m_0 \xi} \tanh(\beta m + a_\tau h u + \tau_0 \xi).}{2\cosh \beta_s m_0}. && (2.122)
\end{aligned}
$$

Next, we consider the overlap defined by (2.108), which means the average-case performance measure. Because the overlap can be represented as $[\xi_i \mathrm{sgn}\langle\sigma_i\rangle_{\beta,h}]$, we can easily derive the following expression: [14]

$$M = \frac{\mathrm{Tr}_{\boldsymbol{\sigma}} \int Du e^{\beta_s m_0 \xi} \xi \mathrm{sgn}(\beta m + a_\tau h u + \tau_0 \xi).}{2\cosh \beta_s m_0}. \tag{2.123}$$

Calculating the above equations, we can understand the restoration property of the image restoration. In the last part of this section, we give the numerical result. Figure 2.10 is the dependence of the overlap $M$ on the temperature (smoothness parameter) $T$ for $T_s = \frac{1}{\beta_s} = 0.9, \tau_0 = \tau = 1.0$ and $h$ is kept to the optimum value $\frac{T_s \tau_0}{T a_\tau^2}$. We can see that $M$ is peaked at $T = T_s$, which is called *Nishimori temperature*. Because the MAP estimate corresponds to the consideration for $T \to 0$, we also explicitly see that the MPM estimate is better than the MAP estimate.

## 2.6 Error Correcting Codes

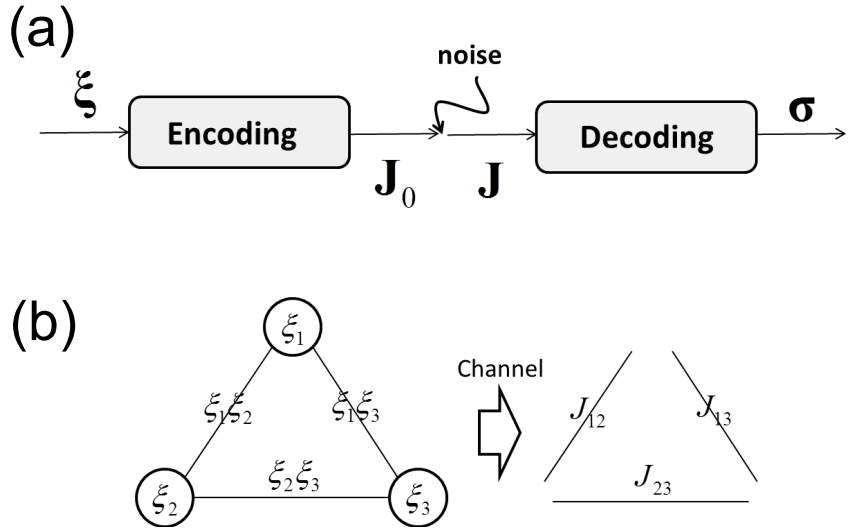


Figure 2.11: (a): Conceptual diagram for Sourlas code. (b):Encode and sending process in the case that $N = 3$ and $p = 2$.

The error correcting code is the system that the receiver can decode an original information by introducing redundancy. And then, the additional information help us to decode the original bit sequence although the original bit sequence is damaged trough noisy channel.

In this section, we give the mathematical formulation for *Error correcting codes* and then discuss particular reference to *Sourlas Code* which can be described as mean-field model (Sourlas 1989). It is well known that Sourlas code achieve the zero-error transmission asymptotically in a certain limit, which mean that it saturates Shannon bound.

[14] In this section, we derive the overlap in the intuitive manner. The mathematical derivation is given in Appendix in the quantum case explained later.

In the context of physics, the model is known as the *random energy model* (REM) in which the energy distribution of all spin configurations can be seen as independence (Derrida 1981). The Sourlas code can be extended to finite-connectivity and analyzed TAP-like decoding algorithm (Vicente et al. 1999; Thouless et al. 1977; Kabashima and Saad 2001). Although the statistical mechanical approaches of course bring us effective knowledge in the error correcting code e.g. Low density parity-check code (LDPC) or convolutional code (Kabashima et al. 2000; Montanari and Sourlas 2000), we treat here Sourlas code because it is basic and expandable solvable model.

### 2.6.1 Model

Sourlas code is the special case of the error correcting code. Introducing the following assumption, we apply the statistical mechanical approach to the analysis of the model because it corresponds to the infinite-range (mean field) $p$-body Ising model. In the Sourlas code, the original sequence (message) $\boldsymbol{\xi} = \{\xi_i\}\,; (i = 1, ..., \xi_N)$ is coded as the $p$-product spins,

$$J^0_{i1\ldots ip} = \xi_{i1} \cdots \xi_{ip}, \tag{2.124}$$

which is "encode" process.

Here, in Sourlas code, we assume that the all possible combinations of $p$ spins are chosen from $N$ spins, that is we consider ${}_NC_p$ encoded messages. For example, considering $N = 3$ and $p = 2$, the original bit sequence is denoted as $\boldsymbol{\xi} = (\xi_1, \xi_2, \xi_3)$ and the coded information can be ${}_3C_2 = 3$ possible sequence, $\boldsymbol{J^0} = (\xi_1\xi_2,\ \xi_2\xi_3,\ \xi_1\xi_3)$ (see Fig.2.11 (b)). The message sending process therefore can be represented as

$$\boldsymbol{J} = \boldsymbol{J}^0 + \boldsymbol{\epsilon}, \tag{2.125}$$

where $\boldsymbol{\epsilon}$ corresponds to channel noise.

The coded bit sequences $\boldsymbol{J^0}$ is transmitted trough a noisy channel, and then the received bit sequences $\boldsymbol{J}$ come to be damaged. In order to decode the original bit sequence from the corrupted received sequence, we set the type of noisy channel (see Fig.2.11 (a)). Using the notation as an estimated bit sequence $\boldsymbol{\sigma}$ instead of $\boldsymbol{\xi}$, we assume the following Gaussian channel as the specific case,

$$P(\boldsymbol{J}|\boldsymbol{\sigma}) \propto \exp\left\{-\frac{D_{Np}}{J_e^2}\sum_{i1<\cdots<ip}\left(J_{i1\ldots ip} - \frac{J_{e0}}{D_{Np}}\sigma_{i1}\cdots\sigma_{ip}\right)^2\right\} \tag{2.126}$$

$$= \exp\left\{-\frac{D_{Np}}{J_e^2}\sum_{i1<\cdots<ip}\left(J^2_{i1\ldots ip} + \frac{J^2_{e0}}{D_{Np}}\right) + \frac{2J_{e0}}{J_e^2}\sum_{i1<\cdots<ip} J_{i1\ldots ip}\sigma_{i1}\cdots\sigma_{ip}\right\} \tag{2.127}$$

$$\propto \exp(\beta \sum_{i1<\cdots<ip} J_{i1\ldots ip}\sigma_{i1}\cdots\sigma_{ip}) \tag{2.128}$$

where the equation runs over all possible combination of $p$ spins out of $N$ spins, and $D_{Np}(= N^{p-1}/p!)$ is appropriately scaled factor to derive the finite order parameters

below in the limit of $N \to \infty$. [15] The number of the terms $(\sum_{i1<\cdots<ip})$ is ${}_NC_p$. Thus, we assume the received information fluctuate around $\frac{J_{e0}}{D_{Np}}\sigma_{i1}\cdots\sigma_{ip}$ with variance $\frac{J_e^2}{D_{Np}}$ according to Gaussian distribution, and then $\beta = 1/T \equiv \frac{2J_{e0}}{J_e^2}$. Note that we also set the prior $P(\boldsymbol{\sigma})$ to use the Bayes formula (2.29) as follows

$$P(\boldsymbol{\sigma}) = \prod_{i=1}^{N} P(\sigma_i) \tag{2.129}$$

$$= \frac{1}{2^N}, \tag{2.130}$$

which mean that the original information is assumed to be generated from the uniform distribution $P(\boldsymbol{\sigma})$ independently. Accordingly, we can obtain the posterior distribution of $\boldsymbol{\sigma}$ as follows,

$$P(\boldsymbol{\sigma}|\boldsymbol{J}) = \frac{\exp(\beta \sum J_{i1\ldots ip}\sigma_{i1}\cdots\sigma_{ip})}{Z} \tag{2.131}$$

$$Z = \mathop{\mathrm{Tr}}_{\boldsymbol{\sigma}} \exp(\beta \sum J_{i1\ldots ip}\sigma_{i1}\cdots\sigma_{ip}). \tag{2.132}$$

Inspired the statistical mechanics, because the above distribution can be regarded as Boltzman distribution, the Hamiltonian of the Sourlas code is

$$H = -\sum_{i1<\cdots<ip} J_{i1\ldots ip}\sigma_{i1}\cdots\sigma_{ip}, \tag{2.133}$$

and $\beta = \frac{1}{T}$ is the inverse temperature. And then, the normalized factor $Z$ can be regarded as the partition function in the context of the statistical mechanics. We also have known the above Hamiltonian as $p$-body interaction Ising model. In the MPM estimate, the estimated bit can be denoted as

$$\tilde{\sigma}_i = \mathrm{sgn}\langle\sigma_i\rangle_\beta \tag{2.134}$$

$$\langle\sigma_i\rangle_\beta = \frac{\mathrm{Tr}_{\boldsymbol{\sigma}}\sigma_i e^{-\beta H}}{\mathrm{Tr}_{\boldsymbol{\sigma}} e^{-\beta H}}. \tag{2.135}$$

Here, in order to evaluate the decoding performance, we define the overlap between the original message and the estimated message as follows:

$$M(\beta) = \mathrm{Tr}_\xi \int d\boldsymbol{J} P(\boldsymbol{J}|\boldsymbol{\xi})P(\boldsymbol{\xi})\xi_i\hat{\sigma}_i \tag{2.136}$$

$$= [\xi_i \mathrm{sgn}\langle\sigma_i\rangle_\beta]. \tag{2.137}$$

Here, $[\cdot] \equiv \mathrm{Tr}_\xi \int d\boldsymbol{J} P(\boldsymbol{J}|\boldsymbol{\xi})P(\boldsymbol{\xi})(\cdot)$ means the average over the distribution of an original bit sequence (data average). From the above representation, we need to set the distribution of the original sequence $P(\boldsymbol{\xi})$ and the channel $P(\boldsymbol{J}|\boldsymbol{\Xi})$, although we usually do not know the true original message and the type of the channel in the nature of the

[15] Using Stirling formula, ${}_NC_p \sim N^p/p!$ for $N >> p$. Because the exponent term should be $O(N)$, $D_{Np}$ corresponds to $N^{p-1}/p!$.

things. We set the following assumptions about the "true" original bit sequence and the "true" channel:

$$P(\boldsymbol{\xi}) = \prod_{i=1}^{N} P(\xi_i) \tag{2.138}$$

$$= \frac{1}{2^N} \tag{2.139}$$

$$P(\boldsymbol{J}|\boldsymbol{\xi}) \propto \exp\left\{-\frac{D_{Np}}{J^2}\sum_{i1<\cdots<ip}\left(J_{i1\ldots ip}-\frac{J_0}{D_{Np}}\xi_{i1}\cdots\xi_{ip}\right)^2\right\}. \tag{2.140}$$

Here, the original bit is uniform as Eq. (2.130) and the channel is assumed to be Gaussian type with $J^2/D_{Np}$ variance and $J_0\xi_{i1}\cdots\xi_{ip}/D_{Np}$ mean. Because $J^2/D_{Np}$ is the "true" variance and $J_0$ is the "true" signal level, the overlap may be maximum at $\beta = \frac{2J_0}{J^2}$ where the inverse temperature corresponds to true effective noise level. That is, the following inequality is satisfied:

$$M(\beta) \leq \left(\frac{2J_0}{J^2}\right). \tag{2.141}$$

When we focus on Eqs. (2.133) with (2.140), the Sourlas code can be seen as spin glass model with $p$-body interaction.

### 2.6.2 Analysis and results

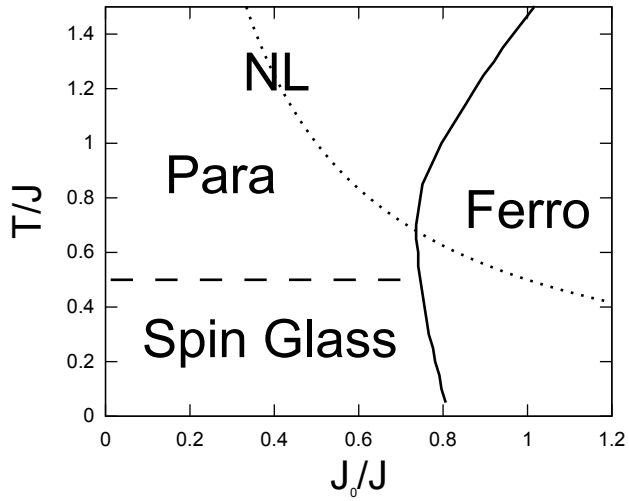


Figure 2.12: Phase diagram for $p = 3$ under Replica symmetry (RS). The ferromagnetic phase (Ferro), the paramagnetic phase (Para) and the spin glass phase (Spin Glass), are defined by Tab. 1.1. The dotted line stands for Nishimori Line (NL) which satisfy the condition that $T/J = J/2J_0$.

In this section, we derive the explicit form of the order parameters to understand the macroscopic behavior and investigate the average-case decoding performance in Sourlas code, considering the thermodynamic limit $N \to \infty$.

Following the replica calculations, we consider the configuration average of $n$th power of the partition function:

$$[Z^n] = \mathop{\mathrm{Tr}}_{\boldsymbol{\xi}} \int \prod_{i1<\cdots<ip} dJ_{i1\ldots ip} P(\boldsymbol{\xi}) P(\boldsymbol{J}|\boldsymbol{\xi}) Z^n \tag{2.142}$$

$$= \mathop{\mathrm{Tr}}_{\boldsymbol{\xi}} \frac{1}{2^N} \int \prod_{i_i<\cdots<ip} dJ_{i1\ldots ip} \left(\frac{N^{p-1}}{\pi J^2 p!}\right)^{\frac{1}{2}} \exp\left\{-\frac{N^{p-1}}{J^2 p!} \sum_{i_1<\cdots<i_p} \left(J_{i1\ldots ip} - \frac{J_0 p!}{N^{p-1}} \xi_{i1}\cdots\xi_{ip}\right)^2\right\} Z^n, \tag{2.143}$$

where $Z^n = \mathrm{Tr}_{\{\boldsymbol{\sigma}^\mu\}} \exp(-\beta \sum_\mu H(\boldsymbol{\sigma}^\mu))$. The Gage transformation,

$$J_{i1\ldots ip} \to J_{i1\ldots ip}\xi_{1i}\cdots\xi_{ip}, \quad \sigma_i \to \xi_i\sigma_i, \tag{2.144}$$

is performed to remove $\boldsymbol{\xi}$ from the integrand. Note that under this transformation the Hamiltonian is transformed as

$$H \to -\sum_{i1<\cdots<ip} J_{i1\ldots ip}\xi_{1i}\cdots\xi_{ip}\sigma_{i1}\xi_{i1}\cdots\sigma_{ip}\xi_{ip} = H, \tag{2.145}$$

which mean that the Hamiltonian is invariant for $\xi_i = \pm 1$. Thus, the problem is equivalent to the system of $\xi_i = 1, \forall i$, the ferromagnetic gage. By introducing the following order parameters

$$m_\mu = \frac{1}{N}\sum_{i=1}^N \sigma_i^\mu \tag{2.146}$$

$$q_{\mu\nu} = \sum_{i=1}^N \sigma_i^\mu \sigma_i^\nu, \tag{2.147}$$

and using the Fourier-transformation representation of the delta function, Eq. (2.143) under the replica symmetry condition can be denoted as

$$[Z^n] = \int \prod_{\mu<\nu} dq_{\mu\nu} d\hat{q}_{\mu\nu} \int \prod_\mu dm_\mu d\hat{m}_\mu \exp(-N\beta f) \tag{2.148}$$

$$-\beta[f] = -m\hat{m} + \beta J_0 m^p - \frac{1}{4}\beta^2 J^2 q^p + \frac{1}{2}q\hat{q} + \frac{1}{4}\beta^2 J^2 + \int Dw \log 2\cosh(\sqrt{\hat{q}}w + \hat{m}). \tag{2.149}$$

Here, the $[f]$ is the free energy per spin in this system under the replica symmetry condition. Although the detailed calculations are omitted here, the similar techniques given in the case of SK model stated in Sec. 2.4.2 can be performed for obtaining the free energy. For the saddle point condition, the order parameters are obtained as

follows:

$$m = \int Dw \tanh \Phi \tag{2.150}$$

$$q = \int Dw \tanh^2 \Phi \tag{2.151}$$

$$\hat{m} = \beta J_0 p m^{p-1} \tag{2.152}$$

$$\hat{q} = \frac{1}{2} p \beta^2 J^2 q^{p-1} \tag{2.153}$$

$$\Phi = \sqrt{\hat{q}} w + \hat{m}. \tag{2.154}$$

We can see that these equations correspond to the equations of state for conventional SK model when $p = 2$. The decoding performance measure, the overlap $M$, can be expressed as follows:

$$M = \int Dw \mathrm{sgn}(\Phi). \tag{2.155}$$

The expression can be derived from meaning of the overlap, $M = [\mathrm{sgn}\langle\sigma_i\rangle_\beta]$ under the ferromagnetic gage as we saw the case of the image restoration.

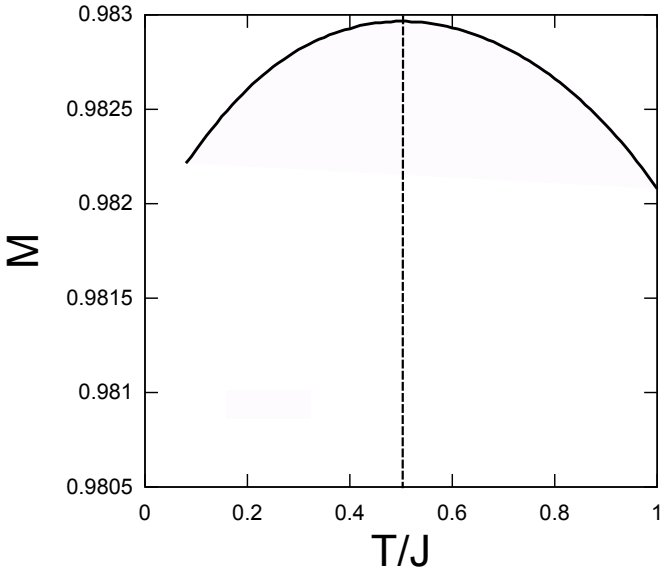


Figure 2.13: Decoding performance for $J = J_0 = 1.0$ and $p = 3$. Dashed line represents Nishimori condition, $T/J = J/2J_0 = 0.5$.

We here give some numerical results for Sourlas code by solving Eqs. (2.150)-(2.155). In the Sourlas code corresponding to $p$-body spin glass model, the phase transition occurs. Figure 2.12 is the phase diagram for $p = 3$, in which the spin glass phase and the paramagnetic phase occurs, where the signal strength $J_0/J$ is weak. In such phases, it is impossible to decode the message because $M = 0$, i.e., $\langle\sigma_i\rangle_\beta = 0$. And note that the phase diagram is given under the replica symmetry condition, and then the region for spin glass phase is actually not correct. It is known that the *replica*

*symmetry breaking* (RSB) occurs in Sourlas code (Nishimori 1999). [16] In this study, however, because we are interested in the region in which it is possible to decode the message, the ferromagnetic phase, we do not focus on the paramagnetic phase and spin glass phase and also RSB. In line with this, we investigate the decoding performance in the ferromagnetic phase. Figure 2.13 is the dependence of $M$ on $T/J$ for $J_0 = J = 1.0$ containing the Nishimori condition, $T/J = J/2J_0 = 0.5$. We can see that the overlap is peaked at Nishimori condition. In this case the Nishimori condition is also called Nishimori temperature.

In the last part of this subsection, we mention the case that $p \to \infty$. In this condition, the model corresponds to the REM and then the error-free decoding can be achieved because $M = 1$ in the ferromagnetic phase. We clarify this condition in a little more detail. The *transmission rate* is defined by

$$R \equiv \frac{N \text{ (number of bits in the original message)}}{N_B \text{ (number of bits in the encoded message)}} \tag{2.156}$$

and the capacity of the Gaussian channel is

$$C = \frac{1}{2}\log_2\left(1 + \frac{J_0^2}{J^2}\right), \tag{2.157}$$

which is derived from channel coding theorem. In the REM, the transmission rate and the capacity can be obtained by

$$R = \frac{N}{{}_N C_p} \simeq \frac{p!}{N^{p-1}} \tag{2.158}$$

and

$$C = \frac{J_0^2 p!}{J^2 D_{Np} \log 2}, \tag{2.159}$$

respectively, substituting $J_0 \to J_0/D_{Np}$ and $J^2 \to J^2/2D_{Np}$ for Eq. (2.140) in the limit $N >> 1$ with $p$ fixed. It is known that the error-free decoding is possible in the condition of satisfying the following inequality

$$R < C. \tag{2.160}$$

Thus, in the Sourlas code in the limit $p \to \infty$, the ferromagnetic phase in which the perfect decoding can be achieved is obtained by the following condition:

$$\sqrt{\log 2} < \frac{J_0}{J}. \tag{2.161}$$

The above condition corresponds to the boundary between the spin glass phase and ferromagnetic phase. Considering the spin glass phase simply, we cannot obtain the above condition under the RS condition because the free energy in the spin glass phase is

$$[f]_{\mathrm{SG}} = -T\sqrt{\frac{2\hat{q}}{\pi}} \to -\infty, \tag{2.162}$$

[16] In the RSB condition, the boundary between the paramagnetic phase and the spin glass phase in given at $T = 0.651J$ which is actually different from Fig. 2.12.

for the condition that $q = 1$ and $\hat{q} = \infty$ in the limit $p \to \infty$ for Eqs. (2.151) and (2.153) and then it not meant to be physics. In the REM, the RS solution does not give the exact solution (Derrida 1981; Gross and Mézard 1984). Under the RSB, the solutions is consistent with Eq. (2.161) in the boundary between the spin glass phase and the ferromagnetic phase.

## 2.7 CDMA multiuser demodulation

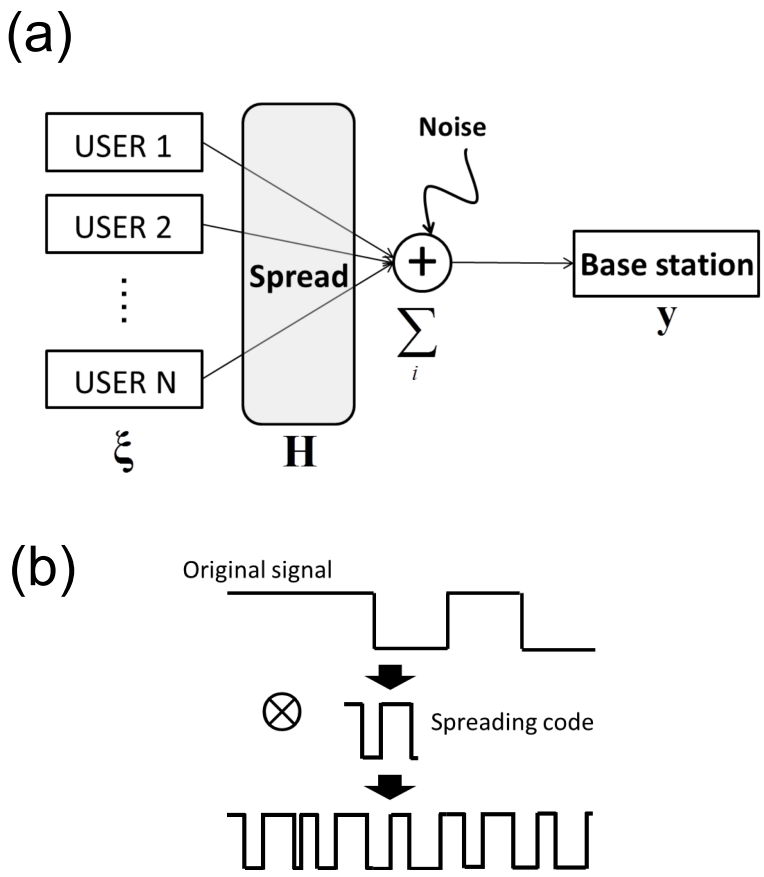


Figure 2.14: (a) Schematic picture of CDMA multiuser demodulation. (b) Basic concept of spreading code.

The topic in this section is the *Code-Division Multiple Access* (CDMA) multiuser demodulation which is an important modern wireless communication system, and then we present the statistical mechanics for it. The basic idea of CDMA is to demodulate the digital signal of users which is transmitted through channel that is shared by multiple users, assigning a spreading code sequence for each user (Simon et al. 1994; Viterbi 1995). The statistical mechanical approaches in the CDMA multiuser detectors has been proposed by Tanaka (Tanaka 2001), and then the average-case demodulation performance was clarified analytically. Because the model is closely related to Hopfield model which is typical neural network model described by mean-field spin glass model,

Tanaka and Okada discuss the demodulation dynamics in terms of statistical neurodynamics (Tanaka and Okada 2005). The formulation of CDMA multiuser detectors is also related to the *compressed sensing* (CS) which is the formulation to recover the original information from sparse received information. It is then expected that a deeper understanding of the behavior of CDMA model pay dividends for the various field e.g., functional magnetic resonance imaging (f-MRI) and photography.

### 2.7.1 Model

$N$-user send the signals $\boldsymbol{\xi} = \{\xi_i\}$, $(\xi_i = \pm 1, i = 1, ..., N)$ through the basic synchronous CDMA channel, and then the received signal $\boldsymbol{y} = \left\{y^k\right\}$, $(k = 1, ..., K)$ at the base station is

$$\boldsymbol{y} = \mathbf{H}\boldsymbol{\xi} + \boldsymbol{\epsilon} \tag{2.163}$$

where $\mathbf{H} = \left\{\eta_i^k\right\}$, $(\eta_i^k = \pm 1,\ i = 1, ..., N,\ k = 1, ..., K)$ is the spreading code sequence for user $i$ and $K$ corresponds to the number of chip of the spreading code sequence per symbol intervals. The channel noise $\boldsymbol{\epsilon}$ is assumed to be Gaussian noise (see Fig. 2.14 (a)). The problem is to demodulate the original information (sending bit sequence) from received signal $\boldsymbol{y}$. Let us here discuss the meaning of the spreading code $\mathbf{H}$. If one does not contrive any ways to demodulate the signals of users, the digital signals become mixed (interfere) with each signal, and then one cannot demodulate the original information at base station. We therefore divide the signal interval into $K$ *chip intervals*, where the interval is called *pitch*. This treatment is called the *modulation* and the coding is the spreading code. Assigning such a spreading code $\mathbf{H} = \left\{\eta_i^k\right\}$ to each users preliminarily, a base station catch the signal containing a noise at the chip interval $k$,

$$y^k = \frac{1}{\sqrt{N}} \sum_{i=1}^{N} \eta_i^k \xi_i + \epsilon^k, \tag{2.164}$$

which corresponds to $k$-th component of Eq. (2.163), and then can retrieve the original signal $\boldsymbol{\xi}$ from $\boldsymbol{y}$.

Before we state Bayesian estimation for this problem, let us consider the conventional demodulator and discuss the close relationship with other models, a neural network and a compressed sensing. Let us here consider the product of the received signal and the spreading code as follows:

$$h_i \equiv \frac{1}{\sqrt{N}} \sum_{k=1}^{K} \eta_i^k y^k = \frac{K}{N}\xi_i + \frac{1}{N} \sum_{k=1}^{K} \sum_{j \neq i} \eta_i^k \eta_j^k \xi_j + \frac{1}{\sqrt{N}} \sum_{k=1}^{K} \eta_i^k \epsilon^k. \tag{2.165}$$

The first term on the right hand side corresponds to the signal term and the second represents interference among users, multiple interference. The third is the channel noise. If user is much fewer than the number of chip, the first term, signal term, can be dominant. In other words, in the case that the chip ratio $\alpha \equiv \frac{K}{N}$ is much larger than 1, we then demodulate the signal by taking the sign of the quantity $h_i$ as follows:

$$\tilde{\xi}_i^{CD} = \mathrm{sgn}(h_i). \tag{2.166}$$

This conventional demodulation (CD) is called *matched filter* method or *single demodulator*, and thus the quantity $h_i$ corresponding to random field has a rich information for demodulation. The performance of the demodulation however is not good because the interference and channel noise is practically not negligible, .

We then introduce the *Bayesian demodulator* to improve the conventional demodulator. Let us denote the estimated variables by $\boldsymbol{\sigma} = \{\sigma_i\}, (i = 1, ..., N)$, and then the demodulation of MAP and MPM can be represented as

$$\tilde{\xi}_i^{\mathrm{MAP}} = \arg\max_{\boldsymbol{\sigma}} P(\boldsymbol{\sigma}|\boldsymbol{y}) \tag{2.167}$$

$$\tilde{\xi}_i^{\mathrm{MPM}} = \arg\max_{\sigma_i} \mathop{\mathrm{Tr}}_{\boldsymbol{\sigma}|\sigma_i} P(\boldsymbol{\sigma}|\boldsymbol{y}), \tag{2.168}$$

where $P(\boldsymbol{\sigma}|\boldsymbol{y})$ is the posterior distribution. Under the following prior,

$$P(\boldsymbol{\sigma}) = \frac{1}{2^N}, P(\mathbf{H}) = \frac{1}{2^{NK}}, \tag{2.169}$$

and the conventional distribution $P(\boldsymbol{y}|\boldsymbol{\sigma})$,

$$P(\boldsymbol{y}|\boldsymbol{\sigma}) = \left(\sqrt{\frac{\beta}{2\pi}}\right)^K \exp\left(-\frac{\beta}{2}||\boldsymbol{y} - \frac{\mathbf{H}\boldsymbol{\sigma}}{\sqrt{N}}||^2\right), \tag{2.170}$$

the posterior distribution can be represented as

$$P(\boldsymbol{\sigma}|\boldsymbol{y}) = \frac{\exp(-\beta H(\boldsymbol{\sigma}))}{Z} \tag{2.171}$$

$$Z = \mathop{\mathrm{Tr}}_{\boldsymbol{\sigma}} \exp(-\beta H(\boldsymbol{\sigma})) \tag{2.172}$$

$$H(\boldsymbol{\sigma}) = \frac{1}{2}\sum_{i,j} J_{ij}\sigma_i\sigma_j - \sum_{i=1}^N h_i^0\sigma_i, \tag{2.173}$$

$$J_{ij} = \frac{1}{N}\sum_{k=1}^K \eta_i^k\eta_j^k \tag{2.174}$$

$$h_i^0 = \frac{1}{\sqrt{N}}\sum_{k=1}^K \eta_i^k y^k. \tag{2.175}$$

Here, $\beta = 1/T = 1/\sigma^2$ corresponds to the inverse temperature, estimated noise power and then the Hamiltonian $H(\boldsymbol{\sigma})$ can be seen as the spin glass model with random field. Considering the relation between Eqs. (2.165) and (2.173), we can see that $h_i^0$ in Eq. (2.173) corresponds to $h_i$ in Eq. (2.165). Thus, it is the benefit of the Bayesian demodulation to potentially consider the interactions between spins. Let us consider the field corresponding to Eq. (2.165) in terms of the Bayesian demodulation as follows:

$$h_i = \sum_{j\neq i} J_{ij}\sigma_j - h_i^0 \tag{2.176}$$

$$= -\frac{K}{N}\xi_i + \frac{1}{N}\sum_{k=1}^K\sum_{j\neq i}\eta_i^k\eta_j^k(\sigma_j - \xi_j) + \frac{1}{\sqrt{N}}\sum_{k=1}^K \eta_i^k\epsilon^k. \tag{2.177}$$

We can see immediately that the second term contains $\sigma_j - \xi_j$ and thus the interference among users would be disappear in the case that the demodulation works well.

The MPM estimate (2.168) can be rewritten as

$$\tilde{\sigma}_i = \mathrm{sgn}\langle\sigma_i\rangle_\beta. \tag{2.178}$$

Focusing on the interaction between spins $J_{ij}$, we can see that it corresponds to it of anti-Hopfield model which is one of typical neural network model represented as mean-field model (Nokura 1998; Seung et al. 1992). Hopfield model is a famous neural network model which can be described as mean-field spin glass model, which implicates one of the property of a memory (Hopfield 1982). It is surprisingly fact that wireless communication can be formulated as similar model of neural network.

We here consider the average-case performance of the Bayesian demodulation, and then assume that the distribution of the original information follows,

$$P(\boldsymbol{\xi}) = \frac{1}{2^N}. \tag{2.179}$$

And the "true" channel noise is assumed to be described as

$$P(\boldsymbol{y}|\boldsymbol{\xi}) = \left(\frac{1}{\sqrt{2\pi\sigma_0^2}}\right)^K \exp\left(-\frac{1}{2\sigma_0^2}||\boldsymbol{y} - \frac{\mathbf{H}\boldsymbol{\xi}}{\sqrt{N}}||^2\right), \tag{2.180}$$

where $1/\sigma_0^2 = \beta_0 = 1/T_0$ is the "true" noise power. The measure of the demodulation performance can be represented as

$$\begin{aligned} M(\beta) &= \sum_{\mathbf{H}} \mathop{\mathrm{Tr}}_{\boldsymbol{\xi}} \int d\boldsymbol{y} P(\mathbf{H}) P(\boldsymbol{\xi}) P(\boldsymbol{y}|\boldsymbol{\eta}) \sum_{i=1}^N \xi_i \mathrm{sgn}\langle\sigma_i\rangle_\beta & (2.181)\\ &= [\xi_i \mathrm{sgn}\langle\sigma_i\rangle_\beta], & (2.182) \end{aligned}$$

the above quantity corresponds to the overlap between original and estimated signal averaged over the distribution of the spreading code, original signal and channel noise. Because of Eqs. (2.180) and (2.170), the following relation holds:

$$M(\beta) \leq M\left(\frac{1}{\sigma_0^2}\right). \tag{2.183}$$

Thus, Nishimori temperature, is $\beta = 1/T = 1/\sigma_0^2 = \beta_0 = 1/T_0$, which maximize the overlap.

### 2.7.2 Analysis and results

In this section, we derive the state equations and the explicit expression of the overlap by using the replica method in thermodynamic limit $N, K \to \infty$ with their ratio $\alpha = \frac{K}{N}$ fixed, and then give some results for CDMA multiuser demodulation.

We start with a explicit description of $[Z^n]$ following the replica method:

$$[Z^n] = \frac{1}{2^N}\frac{1}{2^{NK}} \sum_{\mathbf{H}} \mathop{\mathrm{Tr}}_{\boldsymbol{\xi}} \int \prod_{k=1}^K dy^k P(y^k|\boldsymbol{y}) \mathop{\mathrm{Tr}}_{\boldsymbol{\sigma}^\mu} \exp(-\beta \sum_{\mu=1}^n H(\boldsymbol{\sigma}^\mu)), \tag{2.184}$$

where $\mu$ indicates the replica index. Introducing the following order parameters, [17]

$$R_\mu = \frac{1}{N}\sum_{i=1}^{N}\xi_i\sigma_i^\mu \tag{2.185}$$

$$q_{\mu\nu} = \frac{1}{N}\sum_{i=1}^{N}\sigma_i^\mu\sigma_i^\nu, \tag{2.186}$$

Eq. (2.184) can be represented as

$$[Z^n] = \int\prod_{\mu<\nu}dq_{\mu\nu}d\hat{q}_{\mu\nu}\prod_\mu dR_\mu d\hat{R}_\mu\, e^{N(q_1+g_2+g_3)} \tag{2.187}$$

$$e^{Ng_1} = \int\prod_k\frac{du_0^k d\hat{u}_0^k}{2\pi}\int\prod_k\frac{du_\mu^k d\hat{u}_\mu^k}{2\pi}\sqrt{\frac{\beta_0}{2\pi}}\int dy^k\, e^{g_0} \tag{2.188}$$

$$\begin{aligned} g_0 &= i\hat{u}_0^k u_0^k + i\sum_\mu \hat{u}_\mu^k u_\mu^k - \frac{\beta_0}{2}(y^k-u_0^k)^2 - \frac{\beta}{2}\sum_\mu\left\{(u_\mu^k)^2 - 2y^k u_\mu^k\right\} \\ &\quad -\frac{1}{2}\sum_\mu(\hat{u}_\mu^k)^2 - \frac{1}{2}(\hat{u}_0^k)^2 - \sum_{\mu<\nu}\hat{u}_\mu^k\hat{u}_\nu^k q_{\mu\nu} - \hat{u}_0^\mu\sum_\mu\hat{u}_\mu^k R_\mu \end{aligned} \tag{2.189}$$

$$e^{Ng_2} = \frac{1}{2^N}\mathop{\mathrm{Tr}}_{\boldsymbol{\xi}}\exp\left\{\sum_{\mu<\nu}\hat{q}_{\mu\nu}\sum_i\sigma_i^\mu\sigma_i^\nu + \sum_\mu\hat{R}_\mu\sum_i\sigma_i^\mu\eta_i\right\} \tag{2.190}$$

$$e^{Ng_3} = \exp\left\{-N\sum_{\mu<\nu}q_{\mu\nu}\hat{q}_{\mu\nu} - N\sum_\mu\hat{R}_\mu R_\mu\right\}, \tag{2.191}$$

where we use the following notations,

$$u_0^k = \frac{1}{\sqrt{N}}\sum_{i=1}^{N}\eta_i^k\xi_i,\quad u_\mu^k = \frac{1}{\sqrt{N}}\sum_{i=1}\eta_i^\mu\sigma_i^\mu. \tag{2.192}$$

The free energy under the RS condition, $R_\mu = R, q_{\mu\nu} = q$, is given in the limit $n\to 0$ is

$$\begin{aligned} -\beta[f] &= \frac{\alpha}{2}\left\{-\log\left(1-\beta(q-\chi)\right) + \frac{\beta(1+\beta_0)}{\beta_0} + \frac{2R-q-(\beta_0^{-1})}{1+\beta^{-1}-q}\right\} \\ &\quad -\frac{\hat{q}}{2} + \frac{q\hat{q}}{2} - R\hat{R} + \int Dw\log 2\cosh(\sqrt{\hat{q}}w + \hat{R}). \end{aligned} \tag{2.193}$$

[17] Here, the order parameter $R_\mu$ corresponds to the overlap between original and current replicated spin and then it is slightly different from $m^\mu$, magnetization in the previous sections.

Extremization of the free energy yields the state equations for the order parameters as

$$R = \int Dw \tanh \Phi \tag{2.194}$$

$$q = \int Dw \tanh^2 \Phi \tag{2.195}$$

$$\hat{R} = \frac{\alpha\beta}{1+\beta(1-q)} \tag{2.196}$$

$$\hat{q} = \frac{\alpha\beta^2(1+q-2R+\beta_0^{-1})}{\{1+\beta(1-q)\}^2} \tag{2.197}$$

$$\Phi = \sqrt{\hat{q}}w + \hat{R}. \tag{2.198}$$

The overlap is determined from the state equations as follows:

$$M = \int Dw \, \mathrm{sgn}(\Phi). \tag{2.199}$$

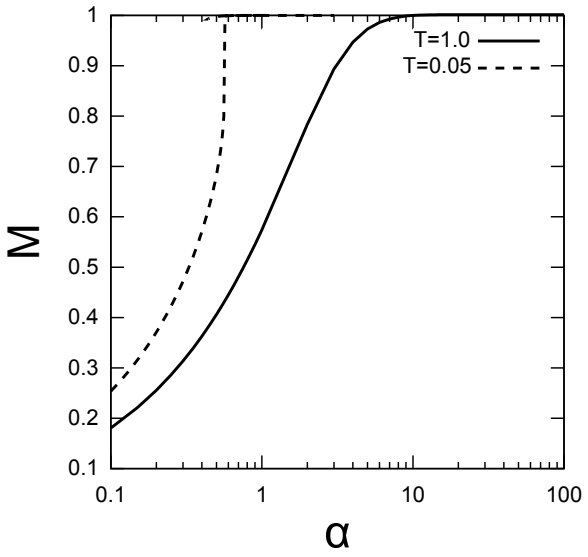


Figure 2.15: Dependence of the overlap $M$ on the chip ratio $\alpha$ for $T_0 = 1.0$, and $T_0 = 0.05$, and then we set $T_0 = T$ in both cases.

By solving Eqs. (2.194) - (2.199), we plot here the dependence of the overlap, average-case performance measure, on the temperature which means controlled parameter in Fig. 2.15 in the case that $T_0 = 1.0$ and $T_0 = 0.05$. In both cases, we can see that the perfect demodulation can be achieved in the limit, $\alpha \to \infty$. We can understand that naturally, because $\alpha$ is the chip ratio. While we can see that the performance drastically increase at about $T = 0.5$ in the case that $T = 1.0$, the performance in the that $T = 0.05$ gradually increases. In the last part of this section, we show the overlap as a function of the demodulation temperature. The overlap is seen to be a maximum at $T = T_0$, Nishimori temperature, and then MPM estimate better than MAP estimate.

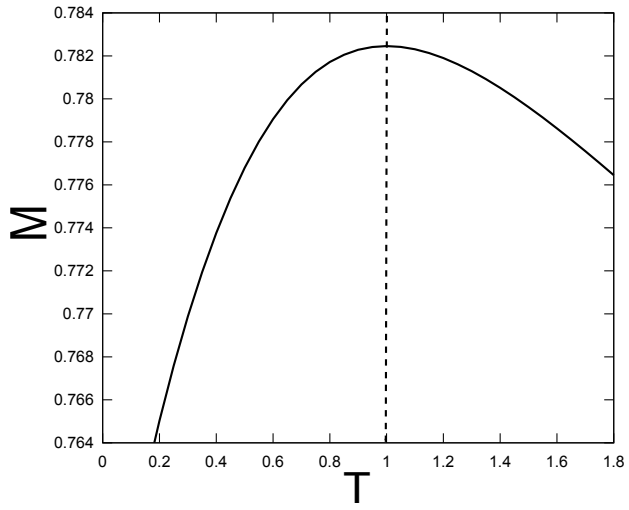


Figure 2.16: Demodulation performance for $\alpha = 2.0$ and $T_0 = 1.0$. Dashed line represents Nishimori condition, $T = T_0 = \sigma_0^2$.

In the last part of this section, we here summarize the notations used in the three models in Tab. 2.2. The notations were and will be used in this thesis consistently. We can see that each problem of information processing can be formulated with similar way through Bayes inference and the statistical physics.

Table 2.2: Notations of three models in this thesis.

| | Original information | Degraded process | Prior | Estimated process | Nishimori condition |
|---|---|---|---|---|---|
| Image Restoration | $\boldsymbol{\xi}$ | $\boldsymbol{\tau} = \boldsymbol{\xi} + \boldsymbol{\epsilon}$ | MRF | $\boldsymbol{\tau} \to \boldsymbol{\sigma}$ | $T = T_0$, $h = \frac{T_s \tau_0}{T a_\tau^2}$ |
| Sourlas Code | $\boldsymbol{\xi}$ | $\boldsymbol{J} = \boldsymbol{J}_0 + \boldsymbol{\epsilon}$ | uniform | $\boldsymbol{J} \to \boldsymbol{\sigma}$ | $T = J^2/2J_0$ |
| CDMA | $\boldsymbol{\xi}$ | $\boldsymbol{y} = \mathbf{H}\boldsymbol{\xi} + \boldsymbol{\epsilon}$ | uniform | $\boldsymbol{y} \to \boldsymbol{\sigma}$ | $T = \sigma_0^2$ |

## 2.8 Open questions and our goals

The transverse field which means quantum fluctuation may be expected to solve the optimization problems whose classes is in NP-hard or NP-complete. Simulated annealing (SA) has is the conventional algorithm for an optimization problems to search the global minimum by using the thermal fluctuation. In the case that the energy land scape is complicated, however, the thermal fluctuation may not jump the many hills of the energy and so the state may not reach the global minimum. On the other hand, the algorithm with the quantum fluctuation, the quantum annealing (QA), may pass through those due to the tunneling effect.

In this way, there has been conflict between the thermal and quantum fluctuations in terms of optimization problems. To investigate this problem is interesting and hot topic

even allowing for the increased technology in the quantum computer of implementing quantum annealing, i.e., Quantum Annealer.

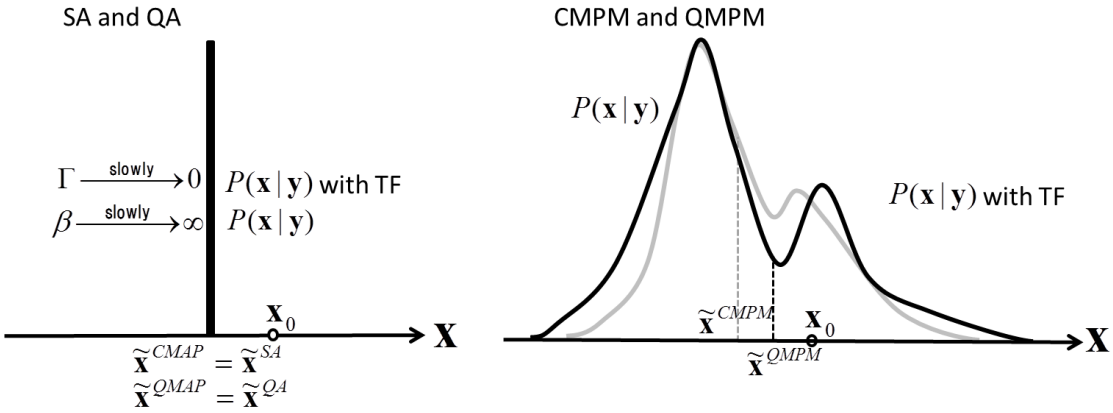


Figure 2.17: Left: Probability distribution with the conventional MAP estimate (the CMAP estimate) corresponding to the simulated annealing (SA) and MAP estimate incorporating the transverse field (the QMAP estimate) corresponding to the quantum annealing (QA). Right: Probability distributions with the conventional MPM estimate (the CMPM estimate) and MPM estimate incorporating the transverse field (the QMPM estimate). Gray line represents the probability distribution in the classical case and black line represents it in the quantum case. In this case, because the strength of the thermal and transverse field is finite, the distribution is broad form instead of delta-like function as the left figure.

From a slightly different viewpoints, we can notice that the retrieval process such an image restoration, error correcting code, CDMA multiuser detection has similar scheme with an optimization problems. When we interpret these issues in terms of the probabilistic distribution in the track of Fig. 2.6, the solutions of both QA and SA correspond to the ones of MAP estimate. In the left of Fig. 2.17, we draw the schematic posterior probabilistic distribution of a problem in the limit $\Gamma \to 0$ and $\beta \to \infty$. As previously mentioned, the QA and SA give the solutions corresponding to the mode of the distribution if the schedules of QA and SA are set appropriately. If these algorithms work well, although both solutions give same optimal solution, we here daringly distinguish these solutions in terms of the notations as the conventional MAP estimate (the CMAP estimate) corresponding to SA and the MAP estimate incorporating the transverse field (the QMAP estimate) corresponding to QA.

On the other hand the MPM estimate is the algorithm by controlling the temperature, which corresponds to data average. Then, we saw that there is a temperature called Nishimori temperature which give an optimal average-case performance. It is therefore important roll to control the temperature in the information processing based on Bayesian framework (see the right of Fig. 2.6).

The above discussion bring us a question: How does the quantum fluctuations affect the decoding process of the information processing in terms of MPM estimate?

The quantum fluctuations provide the tunneling effect between states, and then the state runs on the complicated energy landscape. In other words, the quantum fluctuations has a property for searching a state. If we catch the optimal configuration in the systems by controlling the thermal fluctuation, we may say the same for the quantum fluctuation. In order to treat this topic, we re-formulate the Hamiltonians of the information processing models simply as follows:

$$\hat{H} = H_0(\hat{\boldsymbol{\sigma}}^z) - \Gamma \sum_{i=1}^{N} \hat{\sigma}_i^x. \tag{2.200}$$

Here, $H_0(\hat{\boldsymbol{\sigma}}^z)$ corresponds to the problem Hamiltonian (the conventional model) which is transformed to the system illustrated by Pauli matrices. The second term on the right hand side in the above equation is the transverse field which mean the quantum fluctuation and induces the tunneling effect. The key point of our problems is to propose the MPM estimate incorporating the quantum fluctuation (the QMPM estimate ) and clear whether it can search the appropriate ensemble as is the case with conventional MPM estimate (the CMPM estimate). Discussing the problem from the aspect of probability distribution, we can describe our concepts as the right of Fig. 2.17. In this figure, because the posterior distribution is changed by introducing the transverse field, the solutions between the QMPM estimate and the CMPM estimate are supposed to have a gap. Here, we consider the picture of the free energy of such a discussion. The dashed line in Fig. 2.18 corresponds to the classical free energy. If the quantum effects affect the system, the form of the free energy may be changed like solid line in Fig. 2.18. Because of this, the configuration which make minimum of the free energy which depends on $T$ and $\Gamma$ is different from classical one.

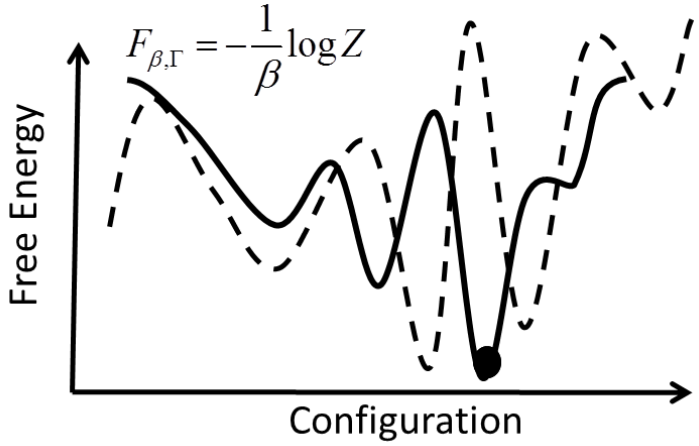


Figure 2.18: Free energy of the system incorporating the quantum fluctuation (solid line). Dashed line corresponds to the original free energy.

Which do the CMPM estimate and the QMPM estimate give the better solution which mean the solution close to the original information $\boldsymbol{x}_0$? As a matter of course,

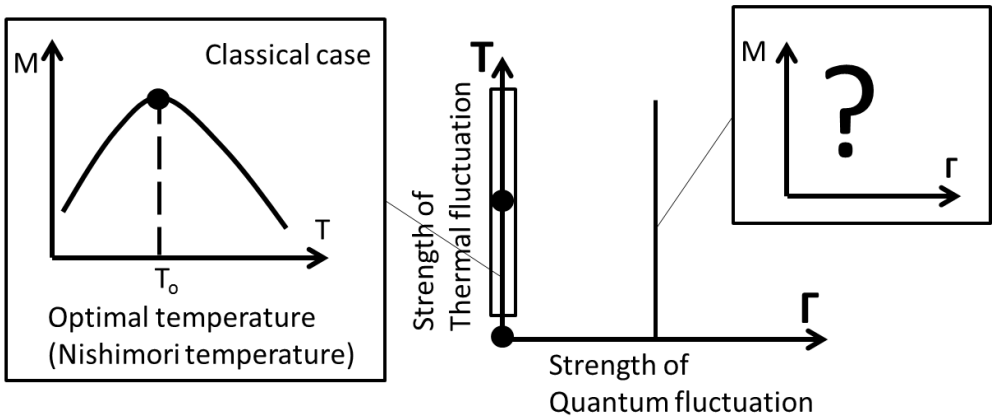


Figure 2.19: Our concrete interests in this thesis.

the answer is non-trivial. Note that the original information $\boldsymbol{x}_0$ is not changed with and without the transverse field in our formulation because the problem Hamiltonian is same one in the classical case with only rewriting the Ising spin as the $z$-th component of Pauli matrices.

By deriving the overlap which is the average-case performance measure in the system, we can consider the performance of the QMPM estimate. Thus, in our standpoint, we discuss the overlap in the space consisted by the thermal fluctuation $T(= 1/\beta)$ and the quantum fluctuation $\Gamma$ (see Fig. 2.19).

These topics bring out the influence of the quantum fluctuation on information processing, and also may give a benefit to improve the performance of the quantum annealing, because such the problem presentation may be intimately related to various problems that SA vs QA. For these reasons, it is worthy to investigate the information processing with the quantum fluctuation.

To wrap up, the main purposes of this paper are listed as follows:

1. Can an algorithm with the quantum fluctuation retrieve an original information? In other words, does the QMPM estimate works well?

2. Which does the performance through the QMPM estimate and CMPM estimate give better solution, if the answer of the above question is "yes"?

3. Does the behavior of solutions through the QMPM estimate change according with the problems?

To address these problems, we focus on three models, the image restoration model, the error correcting code model and the CDMA multiuser demodulation model which are described as spin models as previously mentioned, and analyze the average-case performance incorporating the quantum fluctuation of these models by using statistical mechanical approach and Monte Carlo simulation.

# Chapter 3

# Image restoration with transverse field

In this chapter, we investigate how the quantum fluctuation affects the performance of the image restoration formulated by mean-field Ising model. Although the restoration process in the image restoration incorporating the transverse field has been studied (Inoue 2001), we here present the expanded results. The results suggest that the restored performance incorporating the transverse field can achieve almost same performance of the conventional restoration, the MPM estimate. We also clarify that the improvable region for the transverse field exists in low temperature region.

## 3.1 Introduction

Recently, the statistical mechanics has been useful tool in an information processing scene, where the information is the data of the message, picture, neural signals and so on. The statistical mechanics give us the macroscopic property of the model in the thermodynamical limit. The information processing can be modeled as the spin model or spin glass model through Bayesian formulation, and then it can be formulated the network model which has many spins corresponding to bits, pixels or neurons. There are many models of the information processing as we stated in Chap. 2. One of the typical and simple problem in information processing is the image restoration. In such a problem, the nodes corresponds to pixels and then it can be formulated the *Markov random field* (MRF) which corresponds to the ferromagnetic term as the prior information (Geeman and Geeman 1984; Nishimori and Wong 1999). Hence, the Hamiltonian of the image restoration can be seen as the ferromagnetic Ising model with the random field. Conventionally, the restoration performance in the image restoration has been investigated via MPM estimate, *finite temperature restoration*, in terms of the statistical mechanics. As a result, the restoration can be optimized at Nishimori temperature and then the performance in the other parameter region is less than it at Nishimori temperature. Expanding the Ising model to the multi-state model, Tanaka investigated the performance of the gray scale image by using the technique of the statistical mechanics. The dynamics in such a model also analyzed. In these contexts, the temperature which is the control parameter is the important parameter when we restore an image.

On the other hands, the quantum fluctuation can be effective searching a state in the complicated energy landscape. The *quantum annealing* (QA) is the one of the example in such a context. The transverse field we use here is used in the standard QA and then the quantum device which is demonstrate QA has been launched (see Sec. **??**). Inoue proposed the formulation of the image restoration with the transverse field and analyze the restoration performance by using the strategy of the statistical mechanics. However, the formulation incorporated the transverse field may give slightly different results of the the image restoration model via the transverse field our use here. What does this mean? Inoue introduce the transverse field to the "effective" Hamiltonian which contain the inverse temperature intrinsically and not original Hamiltonian. The transverse field however should be introduced as independent parameter of the temperature, and then we can discuss the restoration performance in the competitive field with the temperature and the transverse field. We then need to reformulate the model proposed by Inoue and investigate the restoration incorporated the transverse field our mean. By investigating the restoration performance for further details, we clarify the improvable region via the transverse field.

This chapter is organized as follows. In the next section, we formulate the image restoration through the Bayesian formulation and introduce the transverse field where we contemplate the difference point proposed in the previous work. In Sec. 3.3, we give the analysis for the model and show the results of the mean-field model in Sec. 3.4. The final section is denoted to summary and discussions

## 3.2 Formulation

The purpose of an image restoration is to restore an original image from a degraded image. We denote the degraded image as $\boldsymbol{\tau} = \{\tau_i\}, (\tau_i = \pm 1, i = 1, ..., N)$, where $N$ indicates the number of pixels. The Ising system corresponds to black-and-white image which has binary pixels. We consider the noise as Gaussian distribution:

$$P(\boldsymbol{\tau}|\boldsymbol{\sigma}) \propto \exp\left\{-\frac{1}{2a_{e\tau}^2}\sum_{i=1}^{N}(\tau_i - \tau_0\sigma_i)^2\right\} \tag{3.1}$$

$$\propto \exp\left(-h\sum_{i=1}^{N}\tau_i\sigma_i\right), \tag{3.2}$$

where $\boldsymbol{\sigma} = \{\sigma_i\}, (\sigma_i = \pm 1, i = 1, ..., N)$ is the estimated image, $a_{e\tau}^2$ is variance and $\tau_{e0}$ corresponds to signal strength. In the above calculation, we extract the term according to $\sigma_i$ since $\boldsymbol{\sigma}$ and $\boldsymbol{\tau}$ are Ising type, and then we define $\frac{\tau_0}{a_{e\tau}^2}$ as $h$ which corresponds to hyper parameter. In order to use the Bayes formula, we introduce the local smoothness as prior

$$P(\boldsymbol{\sigma}) \propto \exp(\beta \sum_{<i,j>} \sigma_i\sigma_j) \tag{3.3}$$

where $\beta = 1/T$ determine the strength of the smoothness and the sum $< i, j >$ runs over neighboring pixels. Using Bayes formula, the posterior is

$$P(\boldsymbol{\sigma}|\boldsymbol{\tau}) = \frac{P(\boldsymbol{\tau}|\boldsymbol{\sigma})}{Z} \tag{3.4}$$

$$\propto \exp(-H_{\text{eff}}) \tag{3.5}$$

$$H_{\text{eff}} = -\beta \sum_{<i,j>} \sigma_i \sigma_j - h \sum_{i}^{N} \tau_i \sigma_i. \tag{3.6}$$

Equation (3.6) corresponds to the effective Hamiltonian of the image restoration assuming the smoothness, and then $Z = \text{Tr} e^{-H_{\text{eff}}}$. Regarding the smoothness parameter as inverse temperature, we obtain the following representations:

$$Z = \sum_{\boldsymbol{\sigma}} \exp(-\beta H(\boldsymbol{\sigma})) \tag{3.7}$$

$$H_0(\boldsymbol{\sigma}) = -\sum_{<i,j>} \sigma_i \sigma_j - Th \sum_{i} \sum_{i=1}^{N} \tau_i \sigma_i, \tag{3.8}$$

from which we can easily understand that the image restoration model corresponds to the model with uniform interactions between two spins and with the random field.

We introduce the probability of an original image $\boldsymbol{\xi}$ and noise type for evaluating the restoration performance:

$$P(\boldsymbol{\xi}) \propto \exp\left(\beta_s \sum_{<i,j>} \xi_i \xi_j\right) \tag{3.9}$$

$$P(\boldsymbol{\tau}|\boldsymbol{\xi}) \propto \exp\left\{-\frac{1}{2a_\tau^2} \sum_{i=1}^{N} (\tau_i - \tau_0 \xi_i)^2\right\} \tag{3.10}$$

$$= \exp\left\{-\frac{1}{2a_\tau^2} \sum_{i=1}^{N} (\tau_i^2 + \tau_0^2) + \frac{\tau_0}{a_\tau^2} \sum_{i=1}^{N} \tau_i \xi_i\right\}. \tag{3.11}$$

As we mentioned in Sec. 2.5, $\beta_s$ corresponds to the "true" smoothness, $1/a_\tau^2$ is the "true" variance and $\tau_0$ corresponds to the "true" signal strength.

In the classical system, the optimal performance is achieved at Nishimori temperature, $T = 1/\beta = \frac{\tau_0}{a_\tau^2}$. In order to extend the above formulation to the quantum one with the quantum fluctuation, the transverse field, we reconsider the following Hamiltonian:[1]

$$\hat{H}_{\text{eff}} = \hat{H}_{\text{eff0}} + \hat{H}_{\text{eff1}} \tag{3.12}$$

$$\hat{H}_{\text{eff0}} = -\beta \sum_{<i,j>} \hat{\sigma}_i^z \hat{\sigma}_j^z - h \sum_{i} \tau_i \hat{\sigma}_i^z \tag{3.13}$$

$$\hat{H}_{\text{eff1}} = -\gamma \sum_{i=1}^{N} \hat{\sigma}_i^x, \tag{3.14}$$

[1]We note that the Hamiltonian is effective Hamiltonian in which the spin configuration follows Boltzman distribution $P \propto \exp(-H_{\text{eff}})$.

where the Pauli matrices are defined by

$$\hat{\sigma}_i^z = \begin{pmatrix} 1 & 0 \\ 0 & -1 \end{pmatrix}, \ \hat{\sigma}_i^x = \begin{pmatrix} 0 & 1 \\ 1 & 0 \end{pmatrix}. \tag{3.15}$$

The $\hat{H}_{\text{eff1}}$ is the effective transverse field which induce the tunneling effect between states, and then $\gamma$ is the "effective" strength of the transverse field. We should careful about the treatment of $\gamma$ which should be contained the temperature part. Thus, we have the following relation in the context of our paper,

$$\gamma = \beta\Gamma, \tag{3.16}$$

where $\Gamma$ is the traditional strength of transverse field, which leads to $\hat{H} = \hat{H}_0 - \Gamma \sum_i \hat{\sigma}_i^x$. In order to understand this, we rewrite Eqs. (3.12)-(3.12) as follows:

$$\hat{H} = \hat{H}_0 + \hat{H}_1 \tag{3.17}$$

$$\hat{H}_0 = -\sum_{<i,j>} \hat{\sigma}_i^z \hat{\sigma}_j^z - Th \sum_i \tau_i \hat{\sigma}_i^z \tag{3.18}$$

$$\hat{H}_1 = -\Gamma \sum_{i=1}^{N} \hat{\sigma}_i^x. \tag{3.19}$$

Inoue actually has been formulated the model by means of the effective transverse field $\gamma$, and then the results are slightly different from the case by using $\Gamma$, as we will show below.

In this system incorporating the transverse field, the overlap corresponding to Eq. (2.108) can be represented as

$$M(\beta, h, \Gamma) = \operatorname*{Tr}_{\boldsymbol{\xi}} \int d\boldsymbol{\tau} P(\boldsymbol{\xi}) P(\boldsymbol{\tau}|\boldsymbol{\xi}) \xi_{\text{sgn}} \langle \hat{\sigma}_i^z \rangle_{\beta,h,\Gamma}, \tag{3.20}$$

$$= [\text{sgn} \langle \hat{\sigma}_i^z \rangle_{\beta,h,\Gamma}] \tag{3.21}$$

where the local magnetization $\langle \hat{\sigma}_i^z \rangle_{\beta,h,\Gamma}$ of the system is

$$\langle \hat{\sigma}_i^z \rangle_{\beta,h,\Gamma} \equiv \frac{\text{Tr}_{\boldsymbol{\sigma}} \hat{\sigma}_i^z e^{-\hat{H}_{\text{eff}}}}{\text{Tr}_{\boldsymbol{\sigma}} e^{-\hat{H}_{\text{eff}}}}. \tag{3.22}$$

Under these formulation, we investigate the restoration performance incorporating the transverse field. Note that $[\cdot]$ means the data average, i.e., $[\cdot] = \text{Tr}_{\boldsymbol{\xi}} \int d\boldsymbol{\tau} P(\boldsymbol{\xi}) P(\boldsymbol{\tau}|\boldsymbol{\xi})(\cdot)$.

We here reconfirm the MPM estimate incorporating the quantum fluctuation and call it the quantum MPM (QMPM) estimate. The quantum fluctuation is introduced the restoration process as controlled parameter with temperature, and then we investigate the performance by calculating the overlap (3.21) in terms of statistical mechanical approach (see Fig.3.1).

## 3.3 Analysis for mean-field model

Before we start the analysis, we reformulate the system to the infinite rage (mean-field) model as it is for the classical case:

$$\sum_{<i,j>} \to \frac{1}{2} \sum_{i \neq j}. \tag{3.23}$$

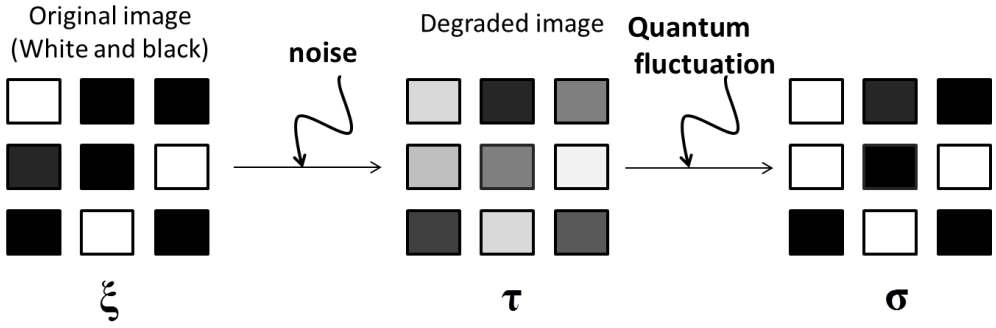


Figure 3.1: Conceptual picture in image restoration via quantum fluctuation. Introducing the transverse field which mean the quantum fluctuation, we consider the QMPM estimate and the CMPM estimate.

In this treatment, a spin (pixel) is connected with all other spins. Although the above condition is slightly different from the real cases, the effective results may be give through a statistical mechanical approach. For deriving the state equations and the explicit expression of the overlap, we need to analyze the quantum system which is described as Pauli matrices. We therefore use the *Suzuki-Trotter* (S-T) decomposition,

$$\exp(\hat{U}+\hat{K}) = \lim_{P\to\infty}\left(e^{\hat{U}/P}e^{\hat{K}/P}\right)^{P}, \tag{3.24}$$

where $\hat{U}$ and $\hat{K}$ are some matrices and $P$ is called the *Trotter number*. To apply this formula to the system, we can derive the corresponding classical system on the space with extra dimension (Trotter axis), because we can operate the trace (see Appendix B). For S-T decomposition, the effective partition function in the image restoration can be obtained as follows,

$$Z = \lim_{P\to\infty}\left(\frac{1}{2}\sinh\frac{2\gamma}{P}\right)^{\frac{NP}{2}} \operatorname*{Tr}_{\boldsymbol{\sigma}} \exp(-H_{\text{eff}}) \tag{3.25}$$

$$H_{\text{eff}} = -\frac{\beta}{2NP}\sum_{i\neq j}\sigma_i(t)\sigma_j(t) - \frac{h}{P}\sum_{t=1}^{P}\sum_{i=1}^{N}\tau_i\sigma_i(t). - \frac{1}{2}\log\left(\coth\frac{\beta\Gamma}{P}\right)\sum_{i=1}^{N}\sum_{t=1}^{P}\sigma_i(t)\sigma_i(t+1), \tag{3.26}$$

where $t$ stands for the Trotter axis, and then the third term in the right hand side of (3.26) represents the interaction on the Trotter axis. Note that $\gamma = \beta\Gamma$. Introducing the order parameter,

$$m_0 = \frac{1}{N}\sum_{i=1}^{N}\xi_i \tag{3.27}$$

$$m(t) = \frac{1}{N}\sum_{i=1}^{N}\sigma_i(t), \tag{3.28}$$

we can derive the following expression of the free energy after performing easy calculations as follows

$$-\beta[f] = -\frac{\beta m^2}{2} + \mathop{\mathrm{Tr}}_{\boldsymbol{\xi}} \int Du \frac{e^{\beta_s m_0 \xi}}{2\cosh \beta_s m_0} \log 2\cosh \sqrt{\Phi^2 + \beta^2 \Gamma^2} \tag{3.29}$$

$$\Phi = \beta m + h a_\tau u + h \tau_0 \xi, \tag{3.30}$$

where $m_0$ and $m$ corresponds to magnetization of the original image and the estimated image, respectively. Here, to derive the above expression, we use the static approximation (SA),

$$m(t) = m. \tag{3.31}$$

The SA suggests that the order parameter is invariant along Trotter axis. The saddle point condition give the state equations as follows (Inoue 2001):

$$m_0 = \tanh \beta_s m_0 \tag{3.32}$$

$$m = \mathop{\mathrm{Tr}}_{\xi} \int Du \frac{e^{\beta_s m_0 \xi}}{2\cosh \beta_s m_0} \frac{\Phi \tanh \Phi}{\Xi} \tag{3.33}$$

$$\Xi = \sqrt{\Phi^2 + \beta^2 \Gamma^2}, \tag{3.34}$$

where $\gamma = \beta\Gamma$. The detailed calculations for deriving the state equations are given in Appendix C1. The overlap defined by Eq. (3.21) can be expressed as follows as the function of $\beta$, $h$ and $\Gamma$, [2]

$$M(\beta, h, \Gamma) = \mathop{\mathrm{Tr}}_{\xi} \int Du \frac{e^{\beta_s m_0 \xi}}{2\cosh \beta_s m_0} \mathrm{sgn}(\Phi). \tag{3.35}$$

This equation can be understand in analogy with classical case (2.123). The mathematical derivation for the overlap is given in Appendix D.

## 3.4 Results

In this section, we give some numerical results by calculating Eqs. (3.32)-(3.35). Although the image restoration previously investigated as we noted earlier, we investigate the restoration by using not $\gamma$ but $\Gamma = \beta\gamma$ because of consideration for fundamental meaning of the transverse field. And then, we show the result which slightly different from the previous work and clarify the improvable region due to the transverse field.

### 3.4.1 Peaked behavior of restoration performance

First of all, we investigate the restoration performance by calculating the overlap $M$ numerically. Figure 3.2(a) shows the dependence the overlap $M$ on the smoothness parameter (temperature) $T$ in the case that $h$ is kept to the optimum value $\frac{T_s \tau_0}{T a_\tau^2}$. In

[2] We use here the trivial relation,

$$\mathrm{sgn}\left(\frac{\Phi \tanh \Phi}{\Xi}\right) = \mathrm{sgn}(\Phi), \quad \text{for } \Xi > 0$$

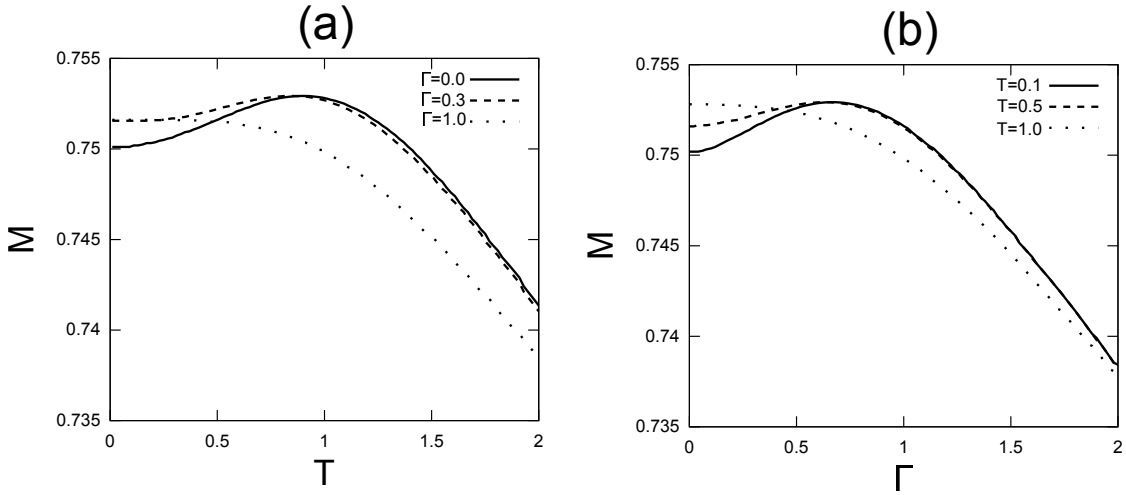


Figure 3.2: Dependence of the overlap $M$ on the smoothness (temperature) $T$ (a) and on the transverse field $\Gamma$ (b) for $T_s = 0.9$ in the case that $h = \frac{T_s \tau_0}{T a_\tau^2} = 0.9$. In (a), each line indicates the cases that $\Gamma = 0.0$, $\Gamma = 0.3$ and $\Gamma = 1.0$. In (b), each line indicates the cases that $T = 0.1$, $T = 0.5$ and $T = 1.0$.

the case that $\Gamma = 0.0$, which corresponds to the classical case, the overlap is peaked at $T = T_s = 0.9$ as we saw in Sec. 2.5. If we introduce the transverse field, we see that the overlap has peak at some temperature which is different value in the classical case. The overlap in the case that $\Gamma = 0.3$ is actually peaked at $T = 0.9$, and then the peaked value approaches to the classical case, i.e., $M_{top} \sim 0.7529$. On the other hand, however, there is no peaked behavior in the case that $\Gamma = 1.0$. Consequently, although the peaked behavior disappear increasing the strength of the transverse field, the optimal restoration performance can achieve it in the classical case by controlling $\Gamma$ appropriately. That result is one of the important results in this work. We give the peaked behavior on the $(\Gamma - T)$ phase in Fig. 3.3, where the gradation indicate the amount of the overlap and the dashed line represents the peaked overlap $M_{top}$. We can see that a point which gives peaked overlap decrease monotonically from $T = 0.9$ without the transverse field to $T = 0.05$ with the finite transverse field ($\Gamma = 0.673$). Note that we cannot gain the numerical solutions of Eqs. (3.32)-(3.35) in the low temperature limit for the numerical accuracy. Focusing on the amount of the overlap, we see that $M_{top} \simeq 0.7529$ at $(\Gamma = 0, T = 0.9)$ and $M_{top} \simeq 0.7529$ at $(\Gamma = 0.673, T = 0.05)$, and thus the peaked overlap incorporating the transverse field can achieve it via thermal fluctuation, conventional estimation.

Let us consider the comparison with the previous work proposed by Inoue, in which the transverse is defined by $\gamma$ instead of $\Gamma$ we use here. Figure 3.4(a) shows the dependence the overlap $M$ on $T$ in the cases that $\gamma = 0.0$, $\gamma = 0.3$ and $\gamma = 1.0$. The case that $\gamma = 0.0$ corresponds to the classical case which give same result as the solid line in Fig. 3.2(a). In the cases that $\gamma = 0.3$ and $\gamma = 1.0$, although the overlap is peaked at some temperature in both cases, it goes to same value in the low temperature limit $T = 0$, i.e., $M \sim 0.7501$. Thus, the overlap presents invariably peaked

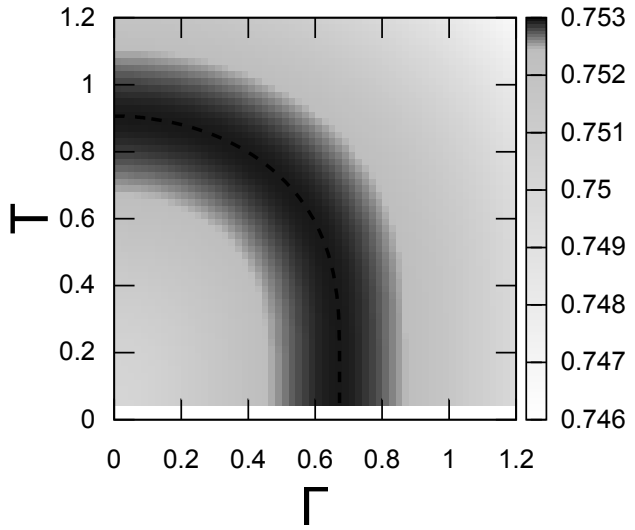


Figure 3.3: Amounts of the overlap (gradation) and peaked overlap $M_{top}$ (dashed line).

behavior even if $\gamma$ increase extremely. Therefore, the behavior of the restoration performance by using $\gamma$-expression slightly different from that by using $\Gamma$-expression as the transverse field. We can easily understand the reason for difference as follows. While $\gamma$ cannot be seen as independent parameter of $\beta = 1/T$ because $\gamma$ is incorporated in the "effective" Hamiltonian, $\Gamma$ can be seen as independent parameter of $\beta$. For this reason, the overlap incorporated $\gamma$ goes to same value in the low temperature limit, i.e., $M(\beta, h, \gamma) \to M(\infty, h, \infty), (\beta \to \infty)$. The peaked behavior on $(\gamma - T)$ phase is shown in Fig.3.4(b). The figure shows that the dashed line corresponding to it in Fig. 3.3 represents asymptotic behavior which mean that $M_{top}$ exists in the condition that $\gamma \to \infty$ and $T = 1/\beta \to 0$. The behavior different from it represented in Fig, 3.3.

### 3.4.2 Improvable behavior of restoration performance

Next, we focus on the *improvable region* where that the restoration performance via the transverse field is better than it in the conventional estimate. In order to understand the region mathematically, we introduce the following quantity,

$$\Delta M(\beta, h, \Gamma) \equiv M(\beta, h, \Gamma) - M(\beta, h, 0). \tag{3.36}$$

If $\Delta M(\beta, h, \Gamma)$ is lager than 0, the parameter set $\{\beta, h, \Gamma\}$ are in the improvable region. On the other hand, if $\Delta M(\beta, h, \Gamma) < 0$ give the *Worsen region*. Figure 3.5(a) is the dependence $\Delta M(\beta, h, \Gamma)$ on $\Gamma$ for $T_s = 1.0$ $h = \frac{T_s \tau_0}{T a_\tau^2}$. The region where $\Delta M > 0$ correspond to the improvable region, while $\Delta M < 0$ correspond to the worsen region. Thus, we can see that the improvable region exists in low temperature region. Figure 3.5(a) shows the improvable region, the worsen region and the peaked overlap $M_{top}$ which corresponds to the dashed line in Fig. 3.3. We can see that the region by means of the transverse field, the quantum fluctuation, exists on a widespread basis.

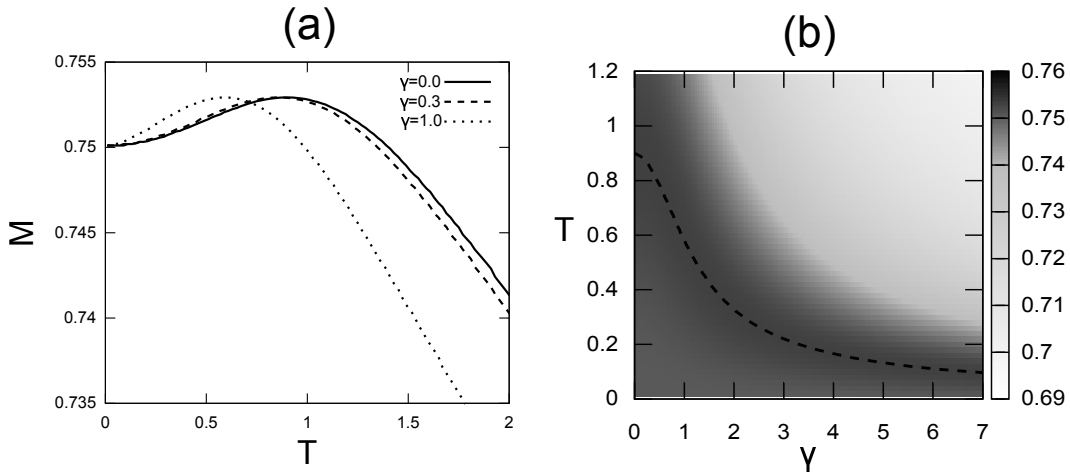


Figure 3.4: Previous results of $M$ vs $T$ for $T_s = 1.0, h = \frac{T_s \tau_0}{T a_\tau^2} = 0.9$. In this case, we use the transverse field as $\gamma = \beta\Gamma$.

## 3.5 Summary and discussion

In this chapter, we investigated the image restoration performance via transverse field by using the statistical mechanical approach. Remaining the classical formulation, by adding the transverse field to the Hamiltonian, we considered the MPM estimate incorporating the quantum fluctuation (the QMPM estimate). The total Hamiltonian formulated here as the quantum Ising spin model with random field. While the transverse field is introduced to "effective" Hamiltonian in the previous study, it is introduced to "pure" Hamiltonian in this work, which means that the transverse field defined by the previous work corresponds to be proportional to the inverse temperature, i.e., $\gamma = \beta\Gamma$. As a result, the behavior given in previous study is slightly different from our results. We then conclude our work as follows:

1. The transverse field allows us to restore an image instead of the thermal fluctuation. The restoration incorporating the transverse field can the original information as with the conventional strategy. In other words, the QMPM estimate works well. And then, the peaked overlap exists in some parameter region.

2. The restoration performance may appropriately same as it via classical algorithm.

3. Comparing with previous work in which the transverse field is used as one incorporating the inverse temperature, the peaked behavior is slightly different from our results.

4. In the lower temperature region where the temperature is lower than Nishimori temperature, the improvable region due to the transverse field exists. Thus, although the optimal performance with the transverse field can not be better than classical one, the transverse field can induce an improvement of the restoration performance in a certain region.

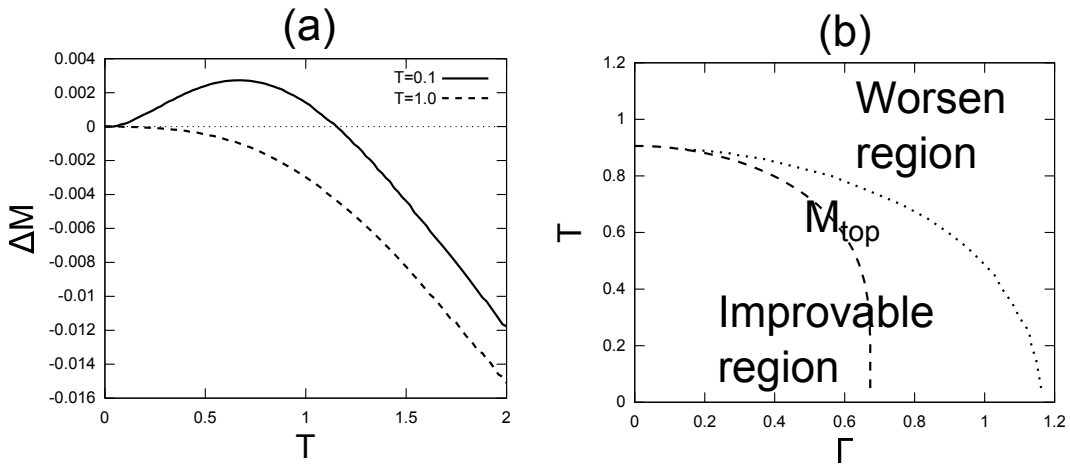


Figure 3.5: (a) Dependence of $\Delta M$ defined in Eq. (3.36) on $\Gamma$ for $T_s = 1.0, h = \frac{T_s \tau_0}{T a_\tau^2} = 0.9$. (b) Improvable region ($\Delta M > 0$) and worsen region ($\Delta M < 0$), and the boundary between them corresponds to $\Delta M = 0$. Dashed line is $M_{top}$ which indicates the same as the dashed line in Fig. 3.3.

The above results are given by the numerical solutions for the self-consistent equations under the static approximations. We may need to the validity of the approximation. Actually, there is a case broken the approximation in the quantum spin glass model (e.g., Obuchi et al. 2007). The problem is the future work. In the context of the image restoration, we can expand the model to the gray scale model. Because the multi state model however give the week effect of the transverse field, it is not easy to perform the expansion. If we can discuss an image restoration which has many tone generally, the information processing via the transverse field will be a rich argument.

# Chapter 4

# Error correcting codes with transverse field

In this chapter, we discuss the decoding performance of error-correcting codes based on a model in which quantum fluctuations are introduced by means of a transverse field. The essential issue in this chapter is whether the quantum fluctuation improves the decoding quality compared with the conventional estimation based on thermal fluctuation, which is the MPM estimate and also is called finite-temperature decoding. The results are illustrated by numerically solving saddle-point equations and performing a Monte Carlo simulation. We also evaluated the upper bound of the overlap between the original sequence and the decoded sequence derived from the equations of state for the order parameters, which is a measure of the decoding performance. [1]

## 4.1 Introduction

As we mentioned in Chap. 2, the error-correcting code is closely related to the mean-field spin glass model, and then we calculate the decoding performance of such the model by using the statistical mechanical approach. In particular, Sourlas has represented error-correcting codes in terms of a mean-field spin glass model that can be considered as a generalization of the Mattis model (Sourlas 1989). Rujan suggested that decoding procedure of the model can be modified so it operates not in the ground state but in a state at a finite temperature (Rujan 1993). The decoding of other error-correcting codes, e.g., low-density parity check code and convolutional code, has also been investigated by means of statistical-mechanical analysis (Kabashima and Saad 1999; Montanari and Srourlas 2000). The detailed illustration is given in Sec. 1.4.

In the field of the solid state physics, the quantum spin glass models have been investigated since the 1980's in order to clarify the microscopic properties of spin glasses. A well-known problem is how the transverse field, which induces the tunneling effect

[1] Preliminary results for the present work also have been published elsewhere:
Otsubo, Y., Inoue, J., Nagata, K., Okada, M. (2012). *Physical Review E*, 86, 051138-1 - 051138-10. Published under licence in *Effect of quantum fluctuation in error-correcting codes* by APS. Publishing Ltd. Content from this work may be used under the terms of the Creative Commons Attribution 3.0 licence. Any further distribution of this work must maintain attribution to the authors and the title of the work, journal citation and DOI.

between states, affects the quantum phase transition (Chalrabarti et al. 1996). The properties of the Sherrington-Kirkpatrick model with a transverse field have been investigated by using the mean-field approximation and the replica method, and it has been found that there is a phase transition from the spin glass phase to the paramagnetic phase depending on the strength of the transverse field (Ishii and Yamamoto 1985; Thirumalai et al. 1989). The replica method has also been used to investigate the random energy model (Goldscmidit 1990). Moreover the the replica symmetry breaking solution when quantum effects are taken into account consideration has been researched (Goldscmidit and Lai 1990; Kim and Kim and Kim 2002).

Although there have been numerous studies on information processing using classical spin glasses as a model and on the properties of quantum spin glasses themselves, the effect of introducing a transverse field, i.e., quantum fluctuation, into an information processing model has not been thoroughly investigated. We expected that quantum fluctuations would induce some changes in decoding quality compared with classical decoding, as inspired by the annealing method. The quantum annealing is an algorithm for finding the global minimum of an objective function for a process analogous to simulated annealing by using quantum fluctuation, and that is known to be useful method in the optimization problems (e.g., Farhi et al. 2001). Inoue has investigated the topic of image restoration by using quantum fluctuations, but that problem corresponds not to a spin glass model, which has random interactions among spins, but to a random field model (Inoue 2001, see Chap. 3). Though the spin glass with the transverse field has been investigated in terms of error correcting (Inoue 2005, 2009), the analytical representation of the decoding measure is not correct and then then our interesting in this thesis is still open.

In this work, we focus on Sourlas code, an error-correcting code that can be described in terms of a mean-field spin glass model. We investigate the decoding performance of Sourlas code on the basis of a model in which a quantum fluctuation is introduced by means of the transverse field.

This chapter is organized as follows. In Sec. 4.2, we present a Bayes formulation of the Sourlas code. In Sec. 4.3, we analyze the model. In Sec. 4.4, we present analytical and simulation results and evaluate the upper bound of the overlap, which is a measure of the decoding performance of Sourlas code. Section 4.5 is a summary and discussion of the results.

## 4.2 Formulation

First, we describe the error-correcting code model and *the maximum a posteriori probability* (MAP) and *the maximizer of the posterior marginals* (MPM) estimates. Next, we extend the model to one with a quantum transverse field, i.e., with quantum fluctuations.

The idea of error-correcting codes is to add redundancy to messages so that receivers can recover the original message from noisy output. Suppose that the original message is represented by a configuration of Ising spins $\boldsymbol{\xi} = \{\xi_1, \cdots, \xi_N\}, (\xi_i = \pm 1, i = 1, .., N)$ that has been generated according to a probability distribution function $P(\boldsymbol{\xi})$. We can formulate the *Sourlas code* as a mean-field model with $p$-body spin interactions (Sourlas 1989). We assume that the sender transmits all possible combinations ${}_N C_p$ of

the products of $p$-components in an $N$-dimensional vector $\boldsymbol{\xi}$ with components $\xi_{i1}\cdots\xi_{ip}$, through a Gaussian channel with mean $J_0 p!\xi_{i1}\cdots\xi_{ip}/N^{p-1}$ and variance $J^2 p!/2N^{p-1}$. That is, the output probability is given by

$$P(J_{i1\ldots ip}|\xi_{i1}\cdots\xi_{ip}) = \left(\frac{N^{p-1}}{J^2\pi p!}\right)^{\frac{1}{2}} \exp\left\{-\frac{N^{p-1}}{J^2 p!}\left(J_{i1\ldots ip} - \frac{J_0 p!\xi_{i1}\cdots\xi_{ip}}{N^{p-1}}\right)^2\right\}, \quad (4.1)$$

where $J$ and $J_0$ are independent of $N$ and $p$, and $J_0/J$ means the signal-to-noise ratio. The expression $P(J_{i1\cdots ip}|\xi_{i1}\cdots\xi_{ip})$ means the conditional probability of the signal $J_{i1\cdots ip}$ given encoded message $\xi_{i1}\cdots\xi_{ip}$. Furthermore, we assume that each bit $\xi_i$ in the original message $\boldsymbol{\xi}$ is generated independently (the so-called memory-less channel), i.e.,

$$P(\boldsymbol{J}|\boldsymbol{\xi}) = \prod_{i=1}^{N} P(J_{i1\cdots ip}|\xi_{i1}\cdots\xi_{ip}) \quad (4.2)$$

and the prior is uniform i.e., $P(\boldsymbol{\xi}) = 2^{-N}$. We can express the posterior probability $P(\boldsymbol{\sigma}|\boldsymbol{J})$ in terms of Eqs. (4.1) and (4.2) by using the Bayes formula

$$P(\boldsymbol{\sigma}|\boldsymbol{J}) = \frac{P(\boldsymbol{J}|\boldsymbol{\sigma})P(\boldsymbol{\sigma})}{\mathrm{Tr}_{\boldsymbol{\sigma}} P(\boldsymbol{J}|\boldsymbol{\sigma})P(\boldsymbol{\sigma})} \quad (4.3)$$

$$\propto \exp(\beta \sum_{i1<\ldots<ip} J_{i1\cdots ip}\sigma_{i1}\cdots\sigma_{ip}), \quad (4.4)$$

where $\beta(\equiv 1/T)$ is the controlled parameter in the signal retrieval algorithm. The optimal retrieval can be achieved if a $\beta$ corresponding to the noise level is chosen as $2J_0/J^2$ in the Gaussian channel (4.1).

We shall write the dynamical variables used for decoding as $\boldsymbol{\sigma} = \{\sigma_1, \cdots, \sigma_N\}$, $(\sigma_i = \pm 1, i = 1, ..., N)$. Equation (4.4) represents the probability distribution of the inferred spin configuration $\boldsymbol{\sigma}$ given the output $\boldsymbol{J}$. We can regard the right hand side of Eq. (4.4) as being a Gibbs-Boltzmann distribution, and hence, we shall call $\beta$ the inverse temperature.

We might choose the spin configuration that maximizes Eq. (4.4) as the decoded sequence. This is the MAP estimate corresponding to finding the ground state of the following Hamiltonian:

$$H = -\sum_{i1<\ldots<ip} J_{i1\cdots ip}\sigma_{i1}\cdots\sigma_{ip}. \quad (4.5)$$

The sum in this Hamiltonian runs over all possible combinations of $p$ spins out of $N$ spins. Therefore, we can see that the problem of the error-correcting code model is closely related to a ground-state search in the mean-field models of spin glasses, e.g., the SK model ($p = 2$) and random energy model ($p \to \infty$) (Derrida 1981).

In the MPM estimate framework, we focus on a single bit $\sigma_i$ and consider the posterior marginal probability:

$$P(\sigma_i|\boldsymbol{J}) = \frac{\mathrm{Tr}_{\boldsymbol{\sigma}(\neq\sigma_i)} \exp(\beta \sum_{i1<\ldots<ip} J_{i1\cdots ip}\sigma_{i1}\cdots\sigma_{ip})}{\mathrm{Tr}_{\boldsymbol{\sigma}} \exp(\beta \sum_{i1<\ldots<ip} J_{i1\cdots ip}\sigma_{i1}\cdots\sigma_{ip})}. \quad (4.6)$$

Let us compare $P(\sigma_i = +1|\boldsymbol{J})$ and $P(\sigma_i = -1|\boldsymbol{J})$. The inferred spin in terms of the MPM estimate is given by

$$\begin{aligned}\hat{\xi}_i &= \mathrm{sgn}\left(P(\sigma_i = +1|\boldsymbol{J}) - P(\sigma_i = -1|\boldsymbol{J})\right) \\ &= \mathrm{sgn}\left(\mathop{\mathrm{Tr}}_{\sigma_i} \sigma_i P(\sigma_i|\boldsymbol{J})\right) \\ &= \mathrm{sgn}\left(\frac{\mathrm{Tr}_{\boldsymbol{\sigma}} \sigma_i \mathrm{e}^{-\beta H}}{\mathrm{Tr}_{\boldsymbol{\sigma}} \mathrm{e}^{-\beta H}}\right) \\ &\equiv \mathrm{sgn}\langle\sigma_i\rangle_\beta, \end{aligned} \tag{4.7}$$

where we have defined the brackets $\langle\cdot\rangle_\beta$ as

$$\langle\cdot\rangle_\beta = \frac{\mathrm{Tr}_{\boldsymbol{\sigma}} (\cdot)\, \mathrm{e}^{-\beta H}}{\mathrm{Tr}_{\boldsymbol{\sigma}} \mathrm{e}^{-\beta H}}. \tag{4.8}$$

Equation (4.7) means calculating the local magnetization at a finite temperature $T(\equiv 1/\beta)$. Hence, the MPM estimate is also called *finite-temperature decoding*. In this work, we call this decoding algorithm the conventional MPM (CMPM) estimate.

Now, let us introduce the overlap $M$, defined as

$$M^{\mathrm{classic}}(\beta) = \mathop{\mathrm{Tr}}_{\boldsymbol{\xi}} \int \prod_{i1<\ldots<ip} dJ_{i1\ldots ip} P(\boldsymbol{J}|\boldsymbol{\xi}) P(\boldsymbol{\xi}) \xi_i \mathrm{sgn}\langle\sigma_i\rangle_\beta \tag{4.9}$$

$$\equiv [\xi_i \mathrm{sgn}\langle\sigma_i\rangle_\beta], \tag{4.10}$$

which is the quality of the retrieved signal. Henceforth, we use the bracket $[\cdot]$ for data-average over the distribution $P(\boldsymbol{J}|\boldsymbol{\xi})P(\boldsymbol{\xi})$ as in (4.9). The larger overlap is, the better the decoding performance will be. It is known that the MPM estimate is better than the MAP estimate, i.e., ground-state decoding, if we choose the temperature appropriately. This temperature is well known as the *Nishimori temperature*, which is $\beta = 2J_0/J^2 \equiv \beta_p$ for Eqs. (4.1) and (4.4).

We can extend the above formulation to the quantum case by adding a *quantum transverse field* term leading to the tunnel effect,

$$\hat{H}_1 \equiv -\Gamma \sum_i \hat{\sigma}_i^x \tag{4.11}$$

to the Hamiltonian (4.5) as a *quantum fluctuation*. The expression $\hat{\sigma}_i^x$ means the $x$ component of the Pauli matrix, and $\Gamma$ controls the quantum fluctuation strength. We still give detailed explanation for the transverse field in Chapter 3. Thus, a quantum Hamiltonian can be obtained by adding a transverse field (4.11) to the classical Hamiltonian (4.5):

$$\hat{H} = \hat{H}_0 + \hat{H}_1 \tag{4.12}$$

$$\hat{H}_0 = -\sum_{i1<\ldots<ip} J_{i1\ldots ip} \hat{\sigma}_{i1}^z \cdots \hat{\sigma}_{ip}^z \tag{4.13}$$

where $\hat{\sigma}_i^z$ is the $z$ component of the Pauli matrix. In the case of $\Gamma = 0$, the system corresponds to a classical system without any quantum effects. In order to understand

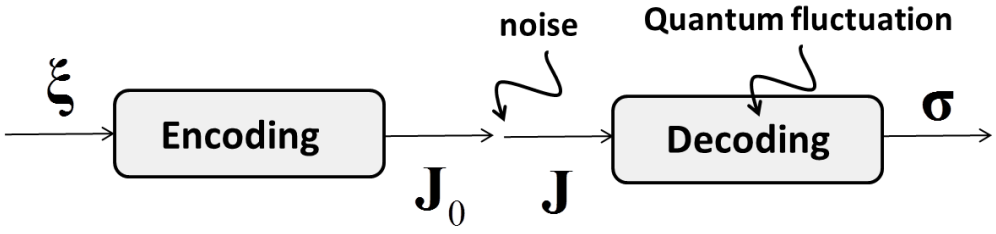


Figure 4.1: Conceptual picture in error correcting code via quantum fluctuation.

the effect of this quantum fluctuation (Eq. (4.11)), let us consider the case of a single-spin system. Denoting the eigen states of $\hat{\sigma}^z$ as $|+\rangle = (1,0)^t$ and $|-\rangle = (0,1)^t$, the $x$ component of the Pauli matrix becomes $\hat{\sigma}^x = |+\rangle\langle -| + |-\rangle\langle +|$. Thus, we find that $\hat{\sigma}^x |\pm\rangle = |\mp\rangle$; that is, the up-state described by $|+\rangle$ transits to the down-state described by $|-\rangle$ by means of the tunnel effect.

The overlap in the case of a quantum system (4.12) is defined as

$$M(\beta,\Gamma) = \mathop{\mathrm{Tr}}_{\boldsymbol{\xi}} \int \prod_{i1<\ldots<ip} dJ_{i1\ldots ip} P(\boldsymbol{J}|\boldsymbol{\xi}) P(\boldsymbol{\xi}) \xi_i \mathrm{sgn}\langle \hat{\sigma_i^z} \rangle_{\beta,\Gamma} \tag{4.14}$$

$$= [\xi_i \mathrm{sgn}\langle \hat{\sigma}_i^z \rangle_{\beta,\Gamma}]. \tag{4.15}$$

The inferred spin in terms of the MPM estimate including a quantum fluctuation corresponding to eq. (4.7) is written as a density matrix: [2] $\hat{\rho} \equiv e^{-\beta \hat{H}(\boldsymbol{\sigma}|\boldsymbol{J})} / \mathrm{Tr} e^{-\beta \hat{H}(\boldsymbol{\sigma}|\boldsymbol{J})}$ (Inoue et al. 2009):

$$\hat{\xi}_i = \mathrm{sgn}\left(\mathrm{Tr}(\hat{\sigma}_i^z \hat{\rho})\right) \tag{4.16}$$

We confirm here our purpose of this chapter. While the conventional decoding process is MPM estimate in which temperature is controlled, our proposition is how the quantum fluctuation affects the decoding performance. In other words, we propose the MPM estimate incorporating the transverse field, the quantum MPM (QMPM) estimate.

## 4.3 Analysis

In order to explicitly calculate the decoding performance of the error-correcting code model with quantum fluctuations, we use the standard replica method to express the overlap equation (Eq. (4.14)) from the saddle point equations that determine the equilibrium state.

First, we apply a *Suzuki-Trotter* (S-T) *decomposition* (Suzuki, 1976, see Appendix B)

$$\exp(\hat{K} + \hat{U}) = \lim_{P\to\infty} \left( e^{\hat{K}/P} e^{\hat{U}/P} \right)^P \tag{4.17}$$

[2] We will actually calculate this quantity in "classical system" by using Suzuki-Trotter formula as we explain in next section.

to the partition function $Z = \mathrm{Tr}\exp(-\beta\hat{H})$ with $\hat{U} = -\sum J_{i1\cdots ip}\hat{\sigma}^z_{i1}\cdots\hat{\sigma}^z_{ip}$, $\hat{K} = -\Gamma\sum_i \hat{\sigma}^x_i$ in order to cast the problem as an equivalent classical spin system. Accordingly, $Z$ and the effective Hamiltonian $H_{\mathrm{eff}}$ are given by

$$
\begin{aligned}
Z &= \lim_{P\to\infty}\left(\frac{1}{2}\sinh\frac{2\beta\Gamma}{P}\right)^{\frac{NP}{2}} \mathrm{Tr}_{\boldsymbol{\sigma}}\exp\left(-H_{\mathrm{eff}}\right) && (4.18)\\
H_{\mathrm{eff}} &= -\frac{\beta}{P}\sum_{t=1}^{P}\sum_{i1<\ldots<ip} J_{i1\ldots ip}\sigma_{i1}(t)\cdots\sigma_{ip}(t) \\
&- \frac{1}{2}\log\left(\coth\frac{\beta\Gamma}{P}\right)\sum_{i=1}^{N}\sum_{t=1}^{P}\sigma_i(t)\sigma_i(t+1), && (4.19)
\end{aligned}
$$

where $P$ is called the Trotter number and $t$ is the Trotter index. We can see that the dimensionality of the corresponding classical system after application of the S-T formula increases by 1. Using the well-known replica method,

$$
[\log\ Z] = \lim_{n\to 0}\frac{[Z^n]-1}{n}, \tag{4.20}
$$

we calculate the free energy density $[\log Z]$ in terms of $[Z^n]$, where

$$
[Z^n] = \mathop{\mathrm{Tr}}_{\boldsymbol{\xi}}\int\prod_{i1<\ldots<ip} d\boldsymbol{J}P(\boldsymbol{\xi})P(\boldsymbol{J}|\boldsymbol{\xi})Z^n. \tag{4.21}
$$

The subsequent application of a gauge transformation $J_{i1\ldots ip}\to J_{i1\ldots ip}\xi_{i1}\cdots\xi_{ip}$ and $\sigma_i\to\sigma_i\xi_i$ in $[Z^n]$ removes $\boldsymbol{\xi}$ from the integrand of the Sourlas code model. Thus, the problem turns to be equivalent to the case of $\xi_i = 1(\forall i)$, i.e., the ferromagnetic gauge. Hence, in thermodynamic limit $N\to\infty$, introducing the following order parameters,

$$
\begin{aligned}
m_\mu(t) &= \frac{1}{N}\sum_i \sigma_i^\mu(t) && (4.22)\\
Q_{\mu\nu}(t,t') &= \frac{1}{N}\sum_i \sigma_i^\mu(t)\sigma_i^\nu(t') && (4.23)\\
Q_{\mu\mu}(t,t') &= \frac{1}{N}\sum_i \sigma_i^\mu(t)\sigma_i^\mu(t'), && (4.24)
\end{aligned}
$$

we can obtain the free energy per spin (bit) and the saddle-point equations of it with

respect to the order parameters: [3]

$$
\begin{aligned}
-\beta[f] &= \frac{\beta^2 J^2}{4}\left(\chi^p - q^p\right) + \frac{1}{2}q\hat{q} - \chi\hat{\chi} - m\hat{m} + \beta J_0 m^p + \\
&\quad \int Dz \log \int Dz 2\cosh\sqrt{\Phi^2 + \Gamma^2} && (4.25)\\
m &= \int Dw \int Dz \frac{\Phi \sinh \Xi}{\Omega \Xi} && (4.26)\\
q &= \int Dw \left( \int Dz \frac{\Phi \sinh \Xi}{\Omega \Xi} \right)^2 && (4.27)\\
\chi &= \int \frac{Dw}{\Omega} \int Dz \left( \frac{\beta^2 \Gamma^2 \sinh \Xi}{\Xi^3} + \frac{\Phi^2 \cosh \Xi}{\Xi^2} \right) && (4.28)\\
\Xi &= \sqrt{\Phi^2 + \beta^2 \Gamma^2} && (4.29)\\
\phi &= \frac{\Phi}{\beta} = pJ_0 m^{p-1} + wJ\sqrt{\frac{pq^{p-1}}{2}} + zJ\sqrt{\frac{p\left(\chi^{p-1} - q^{p-1}\right)}{2}} && (4.30)\\
\Omega &= \int Dz \cosh \Xi. && (4.31)
\end{aligned}
$$

Here, $\int Du(\cdot) = \int_{-\infty}^{\infty} du(\cdot)\mathrm{e}^{-\frac{u^2}{2}}/\sqrt{2\pi}$. Note that the above equations of state for the order parameters (4.26)–(4.31) are obtained under replica symmetry (RS) and the static approximation (SA):

$$
m_\mu(t) = m,\ Q_{\mu\nu}(t,t') = q,\ Q_{\mu\mu}(t,t') = \chi. \tag{4.32}
$$

The detailed illustration for deriving these equations are given in Appendix C2 and the previous work (Obuchi et al. 2007). Although Obuchi et al. derived these equations, the work was not investigated in terms of error correcting but physical interesting, and then the overlap which is decoding measure has not been interesting.

The final goal in this section is to derive the expression of the overlap $M$. The overlap in the quantum case can be obtained in the similar way as is done in the classical system (see Sec. 2.6). The physical meanings of $m$ and $q$ are the magnetization and the spin glass order parameter respectively, and each parameters can be denoted as $m = [\langle\sigma_i\rangle_{\beta,\Gamma}],\ q = [\langle\sigma_i\rangle^2_{\beta,\Gamma}]$. By comparing these expressions and Eqs. (4.26) and (C69), we see that $\int Dz \frac{\Phi \sinh \Xi}{\Omega \Xi}$ is closely related to $\langle\sigma_i\rangle_{\beta,\Gamma}$. We can confirm this by adding $h\sum_i \sigma_i^\mu(t)\sigma_i^\nu(t')$ to $[Z^n]$. The detailed calculations are given in Appendix D. The final form of the overlap $M(\beta,\Gamma)$ is [4]

$$
M(\beta,\Gamma) = \int Dw \mathrm{sgn}\left( \int Dz \frac{\Phi \sinh \Xi}{\Omega \Xi} \right). \tag{4.33}
$$

In the case of a classical system, i.e., $\Gamma = 0$, the overlap $M^{\mathrm{classic}}$ can be derived from

[3] We here omit the explicit expression for the conjugate parameters, $\hat{m}$, $\hat{q}$ and $\hat{\chi}$ by substituting the saddle point conditions of them into the expressions of $m$, $q$ and $\chi$.

[4] Inoue et al. derive the overlap in the case that $T = 0$, pure quantum case (Inoue et al. 2009). However, the analytical results may not be correct because the saddle point approximation for $T = 0$ should be treated rigorously (Inoue, private communication).

Eq. (4.33) for $\int Dz \frac{\Phi \sinh \Xi}{\Omega \Xi} = \tanh \beta \left( wJ \sqrt{\frac{pq^{p-1}}{2}} + pJ_0 m^{p-1} \right)$ as

$$M^{\text{classic}}(\beta) = \int Dw \text{sgn} \left( wJ \sqrt{\frac{pq^{p-1}}{2}} + pJ_0 m^{p-1} \right). \tag{4.34}$$

This form is the same one derived from the previous work (Nishimori, 1999, see Eq. (2.155)).

## 4.4 Results

Below, we numerically solve Eqs. (4.26)–(4.31) and (4.33) and discuss the performance of decoding based on a model with quantum fluctuations. We also show the results of a quantum Monte Carlo simulation and calculate an upper bound of the overlap.

### 4.4.1 Stability of error correction

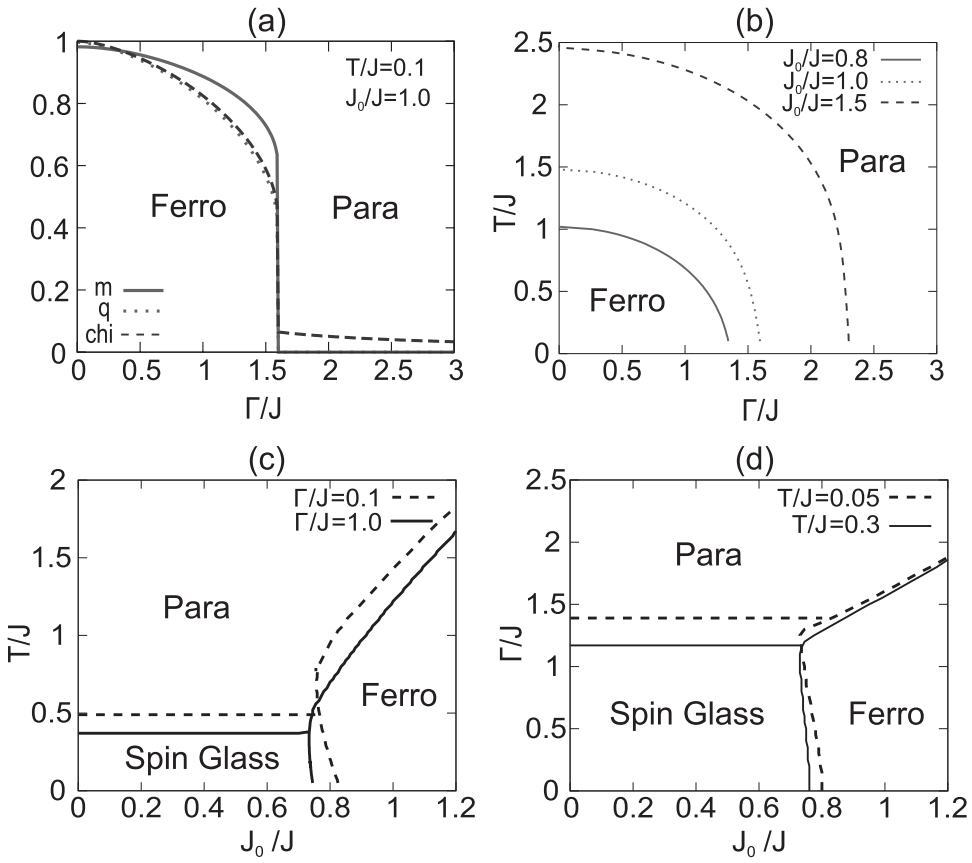


Figure 4.2: (a): Dependence of order parameters $m$, $q$, and $\chi$ on the level of quantum fluctuation $\Gamma/J$ for $p = 3$, $T/J = 0.1$, and $J_0/J = 1.0$. (b)-(d): Phase diagram for each parameter with $p = 3$.

As a preliminary step to calculating the decoding performance, we shall determine whether or not decoding is possible by solving Eqs. (4.26)–(4.31). As we increase the strength of the transverse field $\Gamma/J$, i.e., the quantum fluctuation, we observe a first-order transition at a finite $\Gamma/J$ for $p = 3$, $T/J = 0.1$, and $J_0/J = 1.0$ (see Fig. 4.2(a)). In the ferromagnetic phase (Ferro: $m > 0$, $q > 0$, $\chi > 0$), the overlap $M$ has a finite value, which mean that error correction is possible. On the other hand, the paramagnetic phase (Para: $m = 0$, $q = 0$, $\chi > 0$) is a random guess phase for which error correction is impossible.

The phase diagrams of the model are shown in Fig. 2(b)-(d). As the signal-to-noise (SN) ratio, $J_0/J$ increase, the ferromagnetic phase becomes larger. We can see that the ferromagnetic phase exists in low-temperature region $T \sim 0$. Moreover, the ferromagnetic phase disappears, and then non-retrieval spin glass phase (Spin Glass: $m = 0$, $q > 0$, $\chi > 0$) appears in its place as the SN ratio $J_0/J$ decrease. Note that the phase boundary in the low temperature limit ($T \to 0$) has not been determined.

### 4.4.2 Peaked behavior of decoding performance

We here present the peaked performance of the decoding performance by seeing the overlap. Then we have two approaches. One is the analytical investigation by solving Eqs. (4.26)–(4.33), and the other is the quantum Monte Carlo simulation. The latter is the simulation for the quantum system by using the classical computer (not quantum computer).

#### Analytical results

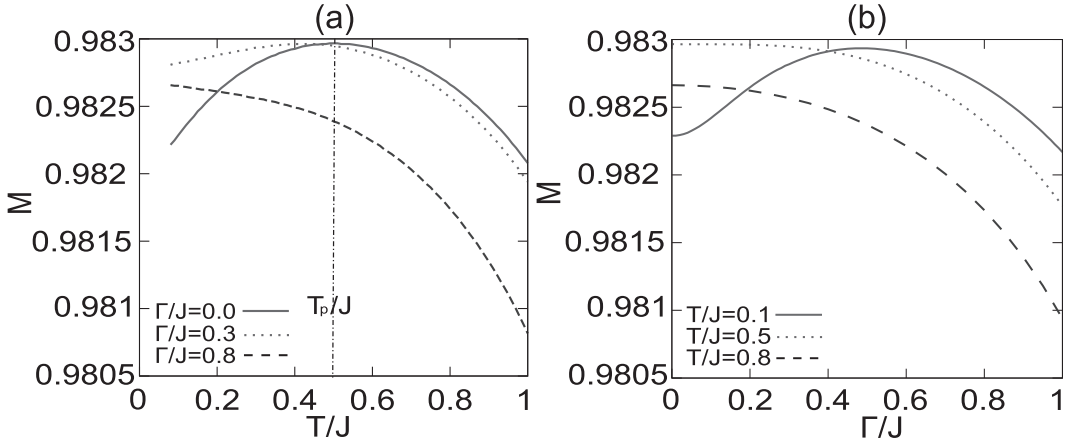


Figure 4.3: (a): Dependence of the overlap $M$ on temperature $T/J$ for $p = 3$ and $J_0/J = 1.0$, where $\Gamma/J$ is fixed to 0.0, 0.3, and 0.8. The solid line corresponds to the line in Fig. 2.13 (b): Dependence of $M$ on level of quantum fluctuation $\Gamma/J$ for $p = 3$ and $J_0/J = 1.0$, where $T/J$ is fixed to 0.1, 0.5, and 0.8. In these cases, the Nishimori temperature corresponds to 0.5.

First, we numerically solved Eqs. (4.26)–(4.33) and plotted the dependence of the overlap $M$ on $T/J$ for $p = 3$ and $J_0/J = 1.0$. Figure 4.3(a) shows that the

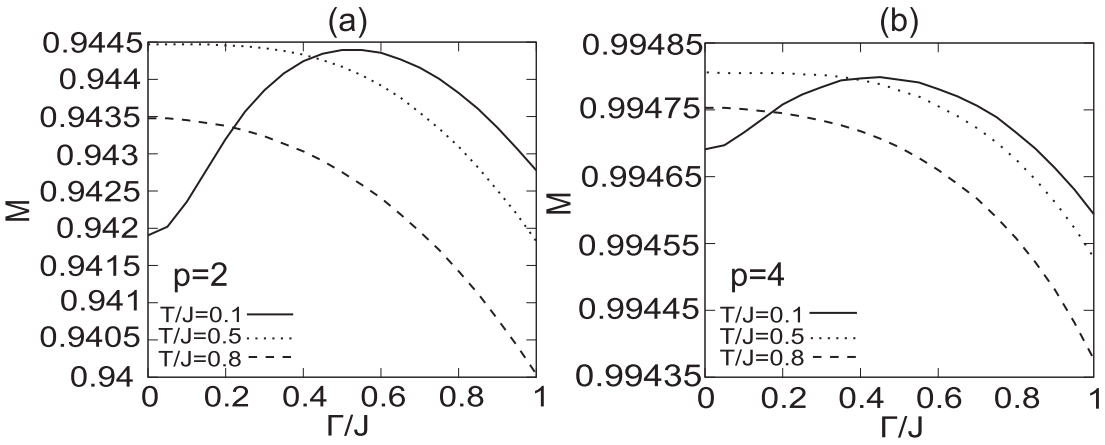


Figure 4.4: Dependence of overlap $M$ on level of quantum fluctuation $\Gamma/J$ for $p = 2$ (a) and $p = 4$ (b) for $J_0/J = 1.0$.

optimal amplitude of temperature $T/J$ at $\Gamma/J = 0.0$ is 0.5, which corresponds to the Nishimori temperature in the case of $J_0/J = 1.0$. The overlap for $\Gamma/J = 0.3$ is at a maximum for a finite $T/J$ smaller than 0.5. The maximum value of $M$ is approximately 0.983, which is roughly equal to the case of $\Gamma = 0.0$. Thus, the MPM estimate with a quantum fluctuation (the QMPM estimate) seems to achieve the same optimal decoding performance as the conventional MPM (CMPM) estimate. Next, let us consider a large quantum fluctuation, $\Gamma/J = 0.8$. In this case, the overlap $M$ monotonically decreases as the temperature $T/J$ increases. In the low temperature region, however, we find that the overlap due to the quantum fluctuation is larger than in the classical case. This means that the quantum fluctuations do make the decoding performance better than a classical estimate based on the thermal fluctuation when the temperature is lower than the Nishimori temperature.

Figure 4.3(b) shows the dependence of the overlap $M$ on $\Gamma/J$. At low temperature, $T/J = 0.1$, there is a quantum fluctuation that maximizes the overlap at the finite amplitude of $\Gamma/J$. The maximum overlap is approximately 0.983, which is equal to the value in the classical case. We see that the overlap in the case of $T/J = 0.5$, which corresponds to the Nishimori temperature, reaches a maximum at $\Gamma = 0.0$. The overlap has a lower value in the case of $T/J = 0.8$.

Figure 4.4 shows the overlap for $p = 2$ and $p = 4$. These overlaps are qualitatively similar to those in Fig. 4.3. We also find that the overlap is large if the number of spin interactions $p$ is large. In the case of the random energy model, $p \to \infty$, we can use Eqs. (4.26)–(4.31) to prove that $M \to 1$ for $\chi \sim q \sim 1, m \sim 1$ (Obuchi et al. 2007)

Figure 4.5 shows the phase diagram for the overlap in $T/J$-$\Gamma/J$ space. The gradation indicates the amount of the overlap, and the solid line represents the maximum overlap 0.983. These results imply that the decoding performance can be made approximately optimal by using quantum fluctuations. Figure 4.6 which is the detail result for optimal overlap, $M_{top}$, dependence of the transverse field $\Gamma$ on the solid line in Fig. 4.5 in detail however shows that $M_{top}$ decreases according with $\Gamma$.

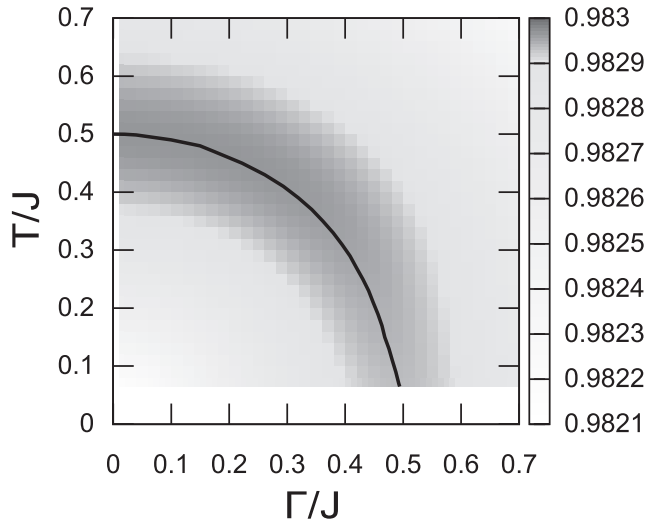


Figure 4.5: Phase diagram for $p = 3$ and $J_0/J = 1.0$. The gradation represents the amount of the overlap. The solid line represents the maximal value of the overlap, i.e., $M_{top} \simeq 0.983$.

### Quantum Monte Carlo results

A $d$-dimensional quantum system can be transformed into a $(d+1)$-dimensional classical system by using the Trotter decomposition, as mentioned in Sec. 4.3. The local field at site $x$ and the Trotter axis $k$ can be written as

$$h_x(k) = -\frac{\beta}{2M} \sum_{i \neq x} J_{ix}\sigma_i(k) - \frac{B}{2}(\sigma_x(k-1) + \sigma_x(k+1)). \tag{4.35}$$

In the Metropolis algorithm, the spin system is updated by the transition probability, $\mathrm{Prob}\left(\sigma_x(k) = -\sigma_x(k)\right) = \exp(-\Delta H_{\mathrm{eff}})$ with $\Delta H_{\mathrm{eff}} = 2h_x(k)\sigma_x(k)$ (Metropolis et al. 1953). Accordingly, we can calculate the expectation $\langle\sigma_i\rangle$ and the overlap $M$ under the ferromagnetic gauge. Figures 4.7(a) and (b) plot the overlap $M$ as a function of $T/J$ in the cases of the classical system and $\Gamma/J = 0.1$ for $p = 2$, $N = 500$, and $P = 20$. We find that the overlap decreases in an overall sense. Figure 4.7(b) is a magnified view of Fig. 4.7(a), and the solid horizontal line is the maximum overlap obtained from the analysis. Here, we can see that each overlap is non-monotonic and is a maximum at a finite temperature $T/J$. The decoding performance in the classical case is optimal at $T/J \sim 0.5$, which corresponds to the Nishimori temperature. On the other hand, the optimal temperature shifts to the low-temperature region in the case of $\Gamma/J = 0.1$, but the maximum overlap, about 0.944, does not change. Figures 4.7(c) and (d) show the overlap $M$ as a function of quantum fluctuation $\Gamma/J$. The overlap reaches a maximum (0.944) at finite $\Gamma/J$. These findings are qualitatively similar to the analytical results presented in the previous subsection.

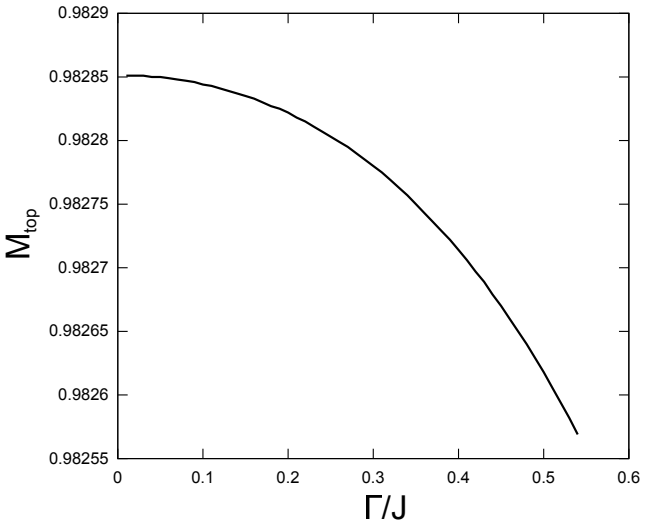


Figure 4.6: The dependence of $M_{top}$ on $\Gamma/J$ for $J_0/J = 1.0$. Here we set the temperature $T/J$ on the optimal value corresponding to a value of $\Gamma$.

### 4.4.3 Improvable behavior of decoding performance

We particularly investigate the decoding performance in low temperature region, where the overlap is larger than classical case, as we see the above subsection. Then, we introduce the following quantity

$$\Delta M(\beta, \Gamma) \equiv M(\beta, \Gamma) - M(\beta, 0), \tag{4.36}$$

which means the difference between the overlap with the transverse field and it in the classical case. The region where $\Delta M > 0$ presents the *improvable region*, and the other indicates the *Worsen region*. Figure 4.8(a) shows the dependence of $\Delta M$ on $\Gamma/J$ in the case that $T/J = 0.1$ and 0.5. We can see that the parameter can be separated into the improvable region ($\Delta M > 0$) and the worsen region ($\Delta M < 0$), depending on $T/J$ and $\Gamma/J$. We then clarify the improvable region and the worsen region on the $\Gamma/J - T/J$ plane (Fig. 4.8(b)). The transverse field can present advancement of the decoding performance in the the temperature lower than Nishimori temperature.

### 4.4.4 Upper bound of the overlap

As we saw the above section, the optimal overlap incorporating the transverse field, $M_{top}$ slightly decrease by increasing $\Gamma$. In this section, we derive the inequality of the overlap and then clarify the upper bound of it. By theoretically estimating the upper bound of the overlap, we can show that the decoding performance in the presence of quantum fluctuations reaches the optimal performance for the classical system, $\Gamma = 0$.

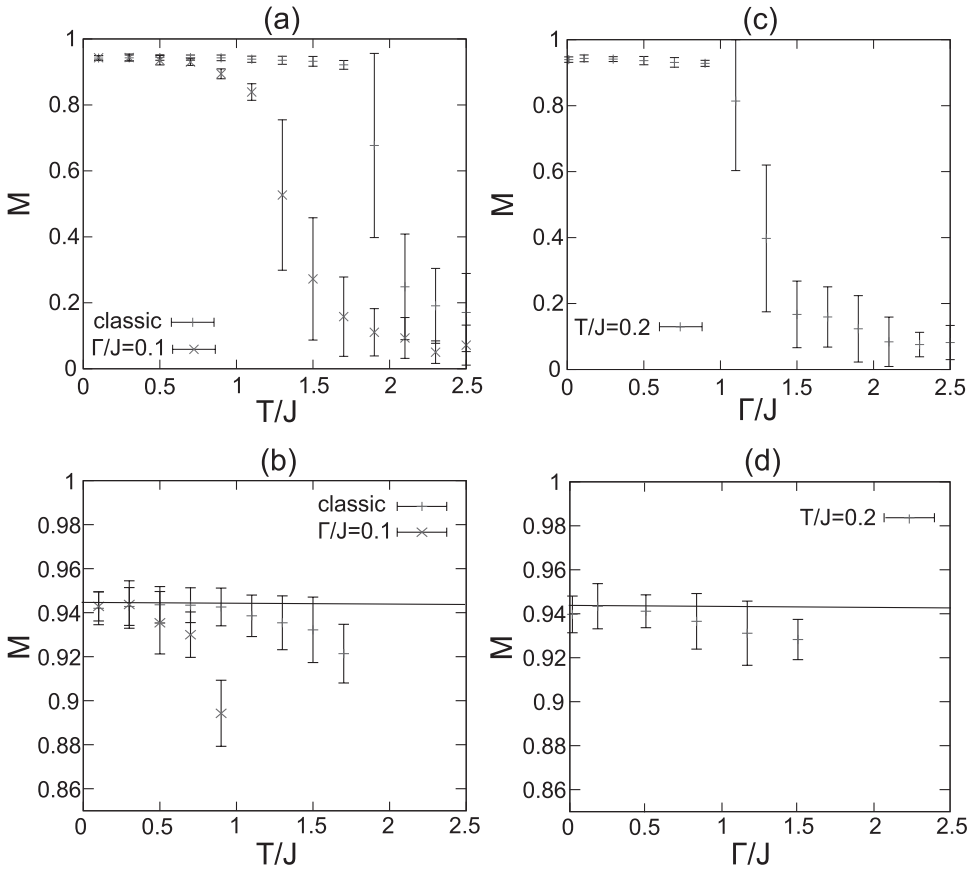


Figure 4.7: (a): Dependence of overlap $M$ on temperature $T/J$ for $p = 2$ and $J_0/J = 1.0$. (b): Magnified view of (a). (c): Dependence of overlap $M$ on quantum fluctuation $\Gamma/J$ for $p = 2$ and $J_0/J = 1.0$. (d): Magnified view of (c). In (b) and (d), the horizontal line is the maximum value, 0.944, obtained by solving Eqs. (4.26)–(4.33) (see Fig. 4.4(a)). The error bars in each figure were calculated by averaging over ten independent runs.

To show this, we rewrite the overlap in the classical case defined by (4.9) as follows:

$$
\begin{aligned}
& M^{\text{classic}}(\beta) \\
= \; & \mathop{\mathrm{Tr}}_{\boldsymbol{\xi}} \int \prod_{i1<\cdots<ip} dJ_{i1\ldots ip} \frac{C_{Np}^{1/2}}{2^N} \mathrm{e}^{f(J_{i1\ldots ip})} \exp\left(\beta_p \sum_{i1<\ldots<ip} J_{i1\ldots ip}\xi_{i1}\cdots\xi_{ip}\right) \xi_i \mathrm{sgn}\left(\frac{\mathrm{Tr}\sigma_i \mathrm{e}^{-\beta H}}{\mathrm{Tr}\mathrm{e}^{-\beta H}}\right) \\
\leq \; & \int \prod_{i1<\cdots<ip} dJ_{i1\ldots ip} \frac{C_{Np}^{1/2}}{2^N} \mathrm{e}^{f(J_{i1\ldots ip})} \left\| \mathop{\mathrm{Tr}}_{\boldsymbol{\xi}} \xi_i \exp\left(\beta_p \sum_{i1<\ldots<ip} J_{i1\ldots ip}\xi_{i1}\cdots\xi_{ip}\right)\right\| \\
& \times \left\| \mathrm{sgn}\left(\frac{\mathrm{Tr}\sigma_i \mathrm{e}^{-\beta \hat{H}}}{\mathrm{Tr}\mathrm{e}^{-\beta \hat{H}}}\right)\right\| \\
\leq \; & \int \prod_{i1<\cdots<ip} dJ_{i1\ldots ip} \frac{C_{Np}^{1/2}}{2^N} \mathrm{e}^{f(J_{i1\ldots ip})} \left\| \mathop{\mathrm{Tr}}_{\boldsymbol{\xi}} \xi_i \exp\left(\beta_p \sum_{i1<\ldots<ip} J_{i1\ldots ip}\xi_{i1}\cdots\xi_{ip}\right)\right\| \\
\equiv \; & M_{\max}^{\text{classic}}.
\end{aligned}
\tag{4.37}
$$

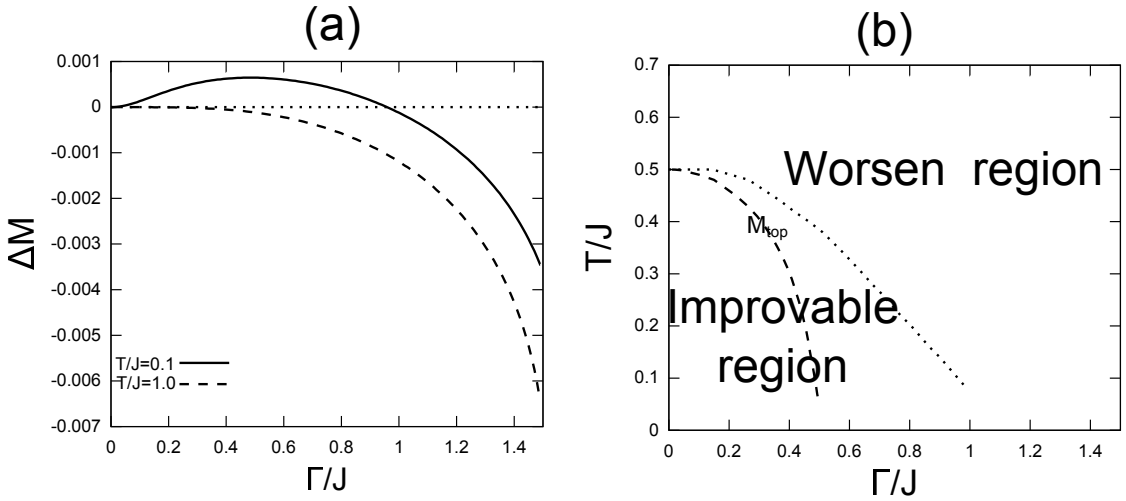


Figure 4.8: (a): $\Delta M$ vs $\Gamma$ for $J_0/J = 1.0$ in the case that $T/J = 0.1$ and $T/J = 0.5$. (b): The improvable region ($\Delta M > 0$) and the worsen region $\Delta M < 0$) and the boundary between them (dotted line) indicates $\Delta M = 0$. The dashed line represents $M_{top}$ corresponding to the solid line in Fig, 4.5.

Here, $C_{Np} = N^{p-1}/J^2\pi p!$, $f(J_{i1\ldots ip}) = -N^{p-1}J^2p!\sum J^2_{i1\ldots ip} - J_0p!_NC_p/J^2N^{p-1}$ for Eq. (4.1) and $M^{\rm classic}_{\rm max}$ means the upper bound in the classical case. For the quantum system, the overlap (4.14) can be rewritten as follows:

$$
\begin{aligned}
& M(\beta,\Gamma) \\
= \; & \mathop{\rm Tr}_{\boldsymbol{\xi}} \int \prod_{i1<\cdots<ip} dJ_{i1\ldots ip} \frac{C_{Np}^{1/2}}{2^N} {\rm e}^{f(J_{i1\ldots ip})} \exp\left(\beta_p \sum_{i1<\ldots<ip} J_{i1\ldots ip}\xi_{i1}\cdots\xi_{ip}\right) \xi_i {\rm sgn}\left(\frac{{\rm Tr}\hat{\sigma}_i^z {\rm e}^{-\beta\hat{H}}}{{\rm Tr}{\rm e}^{-\beta\hat{H}}}\right) \\
\leq \; & \int \prod_{i1<\cdots<ip} dJ_{i1\ldots ip} \frac{C_{Np}^{1/2}}{2^N} {\rm e}^{f(J_{i1\ldots ip})} \left\| \mathop{\rm Tr}_{\boldsymbol{\xi}} \xi_i \exp\left(\beta_p \sum_{i1<\ldots<ip} J_{i1\ldots ip}\xi_{i1}\cdots\xi_{ip}\right)\right\| \left\| {\rm sgn}\left(\frac{{\rm Tr}\hat{\sigma}_i^z {\rm e}^{-\beta\hat{H}}}{{\rm Tr}{\rm e}^{-\beta\hat{H}}}\right)\right\| \\
\leq \; & \int \prod_{i1<\cdots<ip} dJ_{i1\ldots ip} \frac{C_{Np}^{1/2}}{2^N} {\rm e}^{f(J_{i1\ldots ip})} \left\| \mathop{\rm Tr}_{\boldsymbol{\xi}} \xi_i \exp\left(\beta_p \sum_{i1<\ldots<ip} J_{i1\ldots ip}\xi_{i1}\cdots\xi_{ip}\right)\right\| \\
= \; & M^{\rm classic}_{\rm max}. \qquad (4.38)
\end{aligned}
$$

Thus, the optimal decoding performance in the presence of quantum fluctuations is the same as in the case of thermal fluctuation. Here, we can see that the maximum overlap of the classical system corresponds to the overlap at the Nishimori temperature

$\beta_p = 2J_0/J^2$ for Eq. (4.37):

$$
\begin{aligned}
& M_{\max}^{\text{classic}} \\
= & \int \prod_{i1<\cdots<ip} dJ_{i1\ldots ip} \frac{C_{Np}^{1/2}}{2^N} \mathrm{e}^{f(J_{i1\ldots ip})} \frac{\left(\mathrm{Tr}_{\boldsymbol{\xi}} \xi_i \exp\left(\beta_p \sum_{i1<\ldots<ip} J_{i1\ldots ip}\xi_{i1}\cdots\xi_{ip}\right)\right)^2}{\left\|\mathrm{Tr}_{\boldsymbol{\xi}} \xi_i \exp\left(\beta_p \sum_{i1<\ldots<ip} J_{i1\ldots ip}\xi_{i1}\cdots\xi_{ip}\right)\right\|} \\
= & \mathop{\mathrm{Tr}}_{\boldsymbol{\xi}} \int \prod_{i1<\cdots<ip} dJ_{i1\ldots ip} \frac{C_{Np}^{1/2}}{2^N} \exp\left\{-\frac{N^{p-1}}{J^2 N^{p-1}} \sum_{i1<\ldots<ip} \left(J_{i1\ldots ip} - \frac{J_0 p!}{N^{p-1}} \xi_{i1}\cdots\xi_{i1}\right)^2\right\} \xi_i \\
\times & \frac{\mathrm{Tr}_{\boldsymbol{\xi}} \xi_i \exp\left(\beta_p \sum_{i1<\ldots<ip} J_{i1\ldots ip}\xi_{i1}\cdots\xi_{ip}\right)}{\left\|\mathrm{Tr}_{\boldsymbol{\xi}} \xi_i \exp\left(\beta_p \sum_{i1<\ldots<ip} J_{i1\ldots ip}\xi_{i1}\cdots\xi_{ip}\right)\right\|} \\
= & \mathop{\mathrm{Tr}}_{\boldsymbol{\xi}} \int \prod_{i1<\cdots<ip} dJ_{i1\ldots ip} \frac{C_{Np}^{1/2}}{2^N} \exp\left\{-\frac{N^{p-1}}{J^2 N^{p-1}} \sum_{i1<\ldots<ip} \left(J_{i1\ldots ip} - \frac{J_0 p!}{N^{p-1}} \xi_{i1}\cdots\xi_{i1}\right)^2\right\} \xi_i \mathrm{sgn}\langle\xi_i\rangle_{\beta_p} \\
= & M(\beta_p). \qquad (4.39)
\end{aligned}
$$

The inequality shows that the optimal decoding performance incorporating the transverse field can not exceed the optimal one in the classical case and then it is maximized at the case of no transverse field.

### 4.4.5 Shannon bound

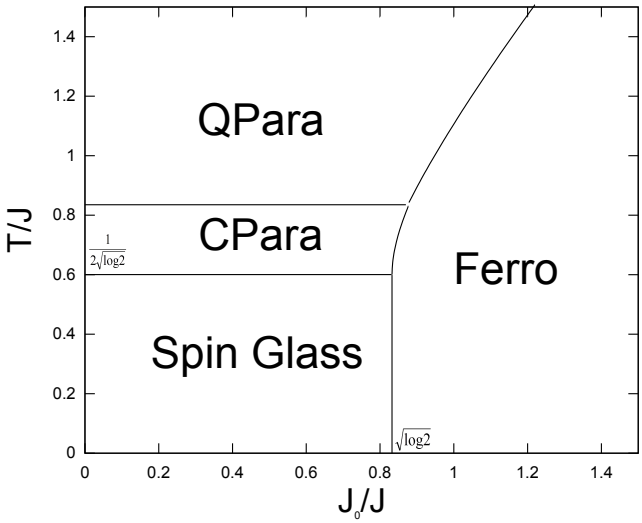


Figure 4.9: Phase diagram in the REM with the transverse field for $\Gamma = 0.75$ (Obuchi et al. 2007). In the Ferro phase, the error-free decoding can be achieved.

In this, subsection, we mention the Shannon bound in the limit $p \to \infty$. In the classical system, the Sourlas code, equivalent to the REM, is capable to the error-free decoding in the ferromagnetic phase (see Sec. 2.6). Considering $0 \leq \ m, q, \chi \leq 1$, the

conjugate variables $\hat{m}, \hat{q}$ and $\chi$ must be 0 or $\infty$ in the limit $p \to \infty$ for Eqs. (C71), (C72) and (C73). We should have the consistent relations among each parameters. Considering the condition that $(\hat{m}, \hat{q}, \hat{\chi}) = (\infty, \infty, \infty)$, we obtain the variables as follows: $(m, q, \hat{\chi}) = (1, 1, 1)$ for Eqs. (4.26)–(4.31). It would appear naturally that the ferromagnetic phase satisfy the conditions. The overlap then goes to one, and then the error-free decoding can be achieved, which mean that the QMPM estimate also allows us to decode perfectly in the limit $p \to \infty$.

Next, we consider the condition that the perfect decoding occurs. The phase transitions of the quantum REM with the ferromagnetic phase was investigated in the previous work (Obuchi et al. 2007; Inoue 2009). Let us consider the phase in which $m = 0$, $\hat{m} = 0$. If $\hat{q} = 0$, there are two situations that $\hat{\chi}$ is 0 or $\infty$. In the case that $(\hat{m}, \hat{q}, \hat{\chi}) = (0, 0, \infty)$, we obtain the variables $(m, q, \chi) = (0, 0, 1)$. On the other hand, in the case that $(\hat{m}, \hat{q}, \hat{\chi}) = (0, 0, 0)$, we obtain $(m, q, \chi) = (0, 0, \tanh \beta\Gamma/\beta\Gamma)$. The former corresponds to the *classical paramagnetic phase*(CPara) in which the quantum effect is not advantage for $\chi = 1$ and the latter is the *quantum paramagnetic phase* (QPara). Next, we consider the condition that $\hat{q} = \infty$ under the condition that $\hat{\chi} = 0$ and $\hat{m} = 0$. In this case, we obtain the variables as follows: $(m, q, \chi) = (0, 1, 1)$ because of finite $q$ and the condition that $q \leq \chi$. The phase corresponds to the spin glass phase.

We summarize these phases:

$$\text{Ferro}: \quad (m, q, \chi) = (1, 1, 1), \tag{4.40}$$

$$\text{Spinglass}: \quad (m, q, \chi) = (0, 1, 1), \tag{4.41}$$

$$\text{CPara}: \quad (m, q, \chi) = (0, 0, 1), \tag{4.42}$$

$$\text{Qpara}: \quad (m, q, \chi) = (0, 0, \frac{\tanh \beta\Gamma}{\beta\Gamma}). \tag{4.43}$$

Although we can consider the other variations, these other solutions which give the consistency between the order parameters and the conjugate variables of it are nothing. Focusing on the Spin glass phase, the Ferro phase and CPara phase, the quantum effect dose not affect the system because $\chi = 1$ and then the cases correspond to the classical case. From the above consideration, the RS condition also may be broken in the quantum REM along with the classical REM. Obuchi et al. investigated the 1RSB solutions along with the classical case in the spin glass phase and then depicted the phase diagrams (see Fig. 4.9).

Our interest is the Shannon bound in the context of the error correcting. As we addressed the conditions of each phase above, the boundary between the Spin glass phase and the Ferro phase does not change, and then the condition which give $R < C$ is same as the classical case. Therefore, we can see that the error-free decoding can be achieved in the following condition for $R < C$:

$$\sqrt{\log 2} < \frac{J_0}{J}, \tag{4.44}$$

which is the same as the classical condition, Eq. (2.161).

## 4.5 Summary and discussion

In this chapter, we focused on decoding of Sourlas code with the transverse field and analyze the overlap which is the average-case decoding measure by using the statistical

mechanics. The Hamiltonian of the Sourlas code model corresponds to the $p$-body interaction spin glass model with the transverse field. From the analysis by using the replica method which is the standard technique of the mean-field mean-field spin glass model in the thermo dynamic limit, we obtain the following conclusions:

1. There is a phase transition from a ferromagnetic phase in which error-correcting can be achieved to a paramagnetic phase which corresponds to a random guess phase, by solving the saddle point equations numerically. A spin glass phase also occurs as the SN ratio decreases. Thus, we must appropriately control the strength of the quantum and thermal fluctuations in order to retrieve the original message.

2. Although the QMPM estimate seems to have roughly same optimal performance as the CMPM estimate, the performance through the QMPM slightly decreases increasing the strength of the transverse field. In other words, the QMPM estimate may be inferior to the CMPM estimate decoding.

3. A quantum Monte Carlo simulation with a finite number of spins was also carried out, and the results roughly support the analysis.

4. In the low temperature region, the improvable region due to the transverse field exists. Thus, although the optimal performance with the transverse field can not be better than classical one, the transverse field can induce improvement of the average-case decoding performance in a certain parameter region.

5. The upper bound of the overlap were evaluated by deriving the inequality of the overlap. The maximum overlap, which is a function of the thermal and quantum fluctuations, corresponds to that of the classical case. This means that the decoding performance with quantum fluctuations cannot exceed the classical case, but it may be possible to approach the optimal performance at the Nishimori temperature for the CMPM estimate.

6. Considering the limit $p \to \infty$, equivalent the quantum REM, the present case capable to the error-free decoding under the condition which corresponds to the classical one.

Several approximations are used in our analysis, including the replica Symmetric approximation (RS) and the Static Approximation (SA). In order to clarify the properties of error correcting code described as spin glass model rigorously, we will need to carefully check the validity of these approximations. The validity of the RS under SA could be checked by calculating the Almeida-Thouless (AT) line. The AT line has been analytically calculated for the SK model. However, the analysis was done under the SA only (Kim and Kim 2002). Ray et al. also attempted to draw the AT line by using Monte Carlo simulations, and they found that it might be possible to conclude that there is no replica symmetry breaking due to the quantum tunneling effects even in the low temperature regime (Ray et al. 1989). On the other hand, the validity of the SA has been shown in the case of random energy model ($p \to \infty$) by using a large-$p$ expansion. However, the SA may be invalid for the case of a finite $p$ (Obuchi et al. 2007). Hence, the limitation of the RS and SA is still an open question in the research

field of spin glasses. Moreover, although we focused on the region of finite thermal and quantum fluctuation in this paper, the decoding performance of a pure quantum system that has no thermal fluctuation remains an open question. An analytical treatment of this question will require one to derive the equations of state for the order parameters and the overlap in the low temperature limit.

# Chapter 5

# CDMA multiuser demodulation with transverse field

We examine the average-case performance of a code-division multiple-access (CDMA) multiuser demodulator in which quantum fluctuations are utilized to demodulate the original message within the context of Bayesian inference. The quantum fluctuations are built into the system as a transverse field in the infinite-range Ising spin glass model. We evaluate the performance measurements by using statistical mechanics. We confirm that the CDMA multiuser modulator using quantum fluctuations achieve roughly same performance as the conventional CDMA multiuser modulator through thermal fluctuations on average. We also find that the relationship between the quality of the original information retrieval and the amplitude of the transverse field is somehow a 'universal feature' in typical probabilistic information processing, viz., in image restoration, error-correcting codes, and CDMA multiuser demodulation.

## 5.1 Introduction

Quantum fluctuations by means of the transverse field have been intensely-investigated within the context of combinatorial optimization problems, which induce tunneling instead of thermal jumps between states (Kadowaki 1998; Farhi 2001; Santoro 2002). The algorithm is called *quantum annealing* (QA) or *quantum adiabatic algorithm*. QA has been applied to various optimization problems by solving the Schrödinger equation or carrying out Quantum Monte Carlo simulations on classical computers. However, what we call a *quantum annealer* with current superconducting devices has been launched by D-wave systems based in British Columbia (Harris et al. 2007; Johnson et al. 2011; Boixo 2013). Taking into account these scientific and technological advances, quantum fluctuations induced by transverse fields could have the potential to provide us with several effective tools for solving combinatorial optimization problems. It is also interesting for us to consider the possible application of the quantum fluctuations to probabilistic information processing with developments in the research field of algorithms by making use of quantum fluctuations. Restoration (decoding) algorithms incorporating transverse fields have recently been investigated in image restoration and Sourlas code, which have both been described with infinite-range spin glass models. The average-case performance of these systems has been analyzed with statistical mechanics in the

thermodynamic limit (Inoue 2001; Otsubo 2012).

Infinite-range spin glass models have received a lot of attentions in recent years in terms of information processing, due to adoption of the framework of Bayesian statistics. For example, the Sherrington-Kirkpatrick (SK) model is closely-linked to error-correcting codes or associative memories in neural networks. The average-case performance of decoding or retrieving has been analytically evaluated using the so-called replica method (Sherrington and Kirkpatrick 1975; Sourlas 1989; Hopfield 1982). The so-called hyper-parameter in these model systems that corresponds to a noise power in the posterior can be regarded as 'temperature' in the Gibbs-Boltzman distribution within the context of statistical physics (Nishimori 2001).

A typical example is the *code-division multiple-access* (CDMA) system that has been recognized as a telecommunication technology that simultaneously enables communication among a huge number of users. It has also been extensively analyzed with the replica method (Tanaka 2001). The basic idea behind the CDMA is to modulate the (original) digital signals of multi-users. The digital signals are modulated by assigning a distinct spreading code for each user. Then, the modulated signals are transmitted through noisy channels. The maximizer of the posterior marginals (MPM) estimate is utilized within the context of Bayesian inference to simultaneously demodulate the original bit sequences of multi-users for a given set of outputs from the noisy channels. It has been well-known that the MPM estimate enables us to construct an optimal demodulator in the sense that the estimate minimizes the bit-error rate on average. Optimal performance is actually achieved by controlling the temperature so that it has the same value as the noise power in the channel. The relationship between the optimal temperature and the corresponding noise amplitude is referred to as the *Nishimori line* (Nishimori 2001). For this reason, the MPM estimate is often called *finite temperature demodulation*.

Quantum-mechanical fluctuations are regarded in the literature on physics, as a counter-part of thermal fluctuations. With this remarkable correspondence in mind, it is naturally expected that the MPM estimate can be extended by means of quantum fluctuations. Namely, the amplitude of quantum fluctuations might be controlled to satisfy a similar relationship to the Nishimori line to achieve the best possible demodulation. In fact, quantum MPM (QMPM) has been proposed thus far and performance has been investigated within the context of image restoration and Sourlas code (Inoue 2001; Otsubo 2012). Obviously, one can consider the 'mixture' of these two distinct fluctuations. Then, the problem that need to be clarified is to explore the best possible mixture to minimize the bit-error rate for decoding on average. More naively, we should answer a question of the following type, viz., "Which fluctuations give us a better average-case performance for typical problems in probabilistic information processing?" Thus far, we have confirmed that the decoding performance of the MPM estimate incorporating the transverse field can roughly achieve the same performance as that of the optimal thermal MPM estimate, at least for image restoration and Sourlas code.

We focus on CDMA multiuser demodulation under thermal and quantum fluctuations as an example to analyze the average-case performance in this research and examine the equivalence between thermal and quantum fluctuations in the literature on the optimal MPM estimate. We then compare performance with that of image restoration and error-correcting codes to clarify the central issue, viz., 'universal fea-

ture' of the equivalence between thermal and quantum fluctuations in Bayesian MPM estimation. We should mention that the demodulating process in the CDMA system is quite similar to so-called *compressed sensing* (CS) (Rangan et al. 2012; Candes et al. 2006; Kabashima et al. 2009). CS and related techniques have been developed to solve various types of modern problems in engineering such as functional magnetic resonance imaging (f-MRI) and photography.

This paper is organized as follows. The next section introduces the CDMA system and quantum-mechanical extension. We then explain how we derive equations of states and the average-case performance measurements by using the replica method in Sec. 5.3. Section 5.4 presents our results. The last section is a summary and contains concluding remarks.

## 5.2 Formulation

Let us consider a demodulation problem for a wireless communication by $N$-users communicating in fully synchronous channels. Then, the received signal at the base station is given by:

$$y^k = \frac{1}{\sqrt{N}} \sum_{i=1}^{N} \eta_i^k \xi_i + \epsilon^k, \tag{5.1}$$

where $\xi_i \in \{-1, 1\}, (i = 1, ..., N)$ is the original information and $\eta_i^k \in \{-1, 1\}, (k = 1, ..., K, i = 1, ..., N)$ is referred to as the spreading code sequences for user $i$. The channel noise, $\epsilon^k$, is inevitably contained in the received signal information (see Fig. 5.1). By using the following notations:

$$\boldsymbol{y} = (y^1, \cdots, y^K)^T, \ \boldsymbol{\xi} = (\xi_1, \cdots, \xi_N)^T, \ \boldsymbol{\epsilon} = (\epsilon^1, \cdots, \epsilon^K)^T, \tag{5.2}$$

$$\mathbf{H} = \begin{pmatrix} \eta_1^1 & \eta_2^1 & \cdots & \eta_N^1 \\ \eta_1^2 & \eta_2^2 & \cdots & \eta_N^2 \\ \cdots & \cdots & \cdots & \cdots \\ \eta_1^K & \xi_2^K & \cdots & \eta_N^K \end{pmatrix}, \tag{5.3}$$

the received signal (5.1) can be rewritten as:

$$\boldsymbol{y} = \frac{1}{\sqrt{N}} \mathbf{H} \boldsymbol{\xi} + \boldsymbol{\epsilon}. \tag{5.4}$$

Here, the problem is to estimate the sequence, $\boldsymbol{\sigma} = (\sigma_1, ..., \sigma_N)$, which yields a satisfactory candidate for the original bit sequence, $\boldsymbol{\xi}$, from the received sequence, $\boldsymbol{y}$. Then, the probability distribution of received information is written as:

$$P(\boldsymbol{y}|\boldsymbol{\sigma}) = \left( \sqrt{\frac{\beta}{2\pi}} \right)^K \exp\left( -\frac{\beta}{2} \left\| \boldsymbol{y} - \frac{\mathbf{H}\boldsymbol{\sigma}}{\sqrt{N}} \right\|^2 \right), \tag{5.5}$$

where $\beta = 1/T$ corresponds to inverse temperature in terms of statistical mechanics assuming that channel noise is generated from an additive white Gaussian. By using the Bayes formula:

$$P(A|B) = \frac{P(B|A)P(A)}{\sum_A P(B|A)P(A)}, \tag{5.6}$$

the posterior is described as a canonical distribution with Hamiltonian $H(\boldsymbol{\sigma})$ as:

$$P(\boldsymbol{\sigma}|\boldsymbol{y}) = \frac{\exp\left(-\beta H(\boldsymbol{\sigma})\right)}{Z}, \tag{5.7}$$

$$Z = \operatorname*{Tr}_{\boldsymbol{\sigma}} \exp(-\beta H(\boldsymbol{\sigma})), \tag{5.8}$$

$$H(\boldsymbol{\sigma}) = \frac{1}{2N}\sum_{i,j}\sum_{k=1}^{K}\eta_i^k\eta_j^k\sigma_i\sigma_j - \frac{1}{\sqrt{N}}\sum_{i=1}^{N}\sum_{k=1}^{K}\eta_i^k y^k\sigma_i \tag{5.9}$$

where we use the condition in Eq. (5.5) and the priors:

$$P(\mathbf{H}) = \frac{1}{2^{NK}} \tag{5.10}$$

$$P(\boldsymbol{\sigma}) = \frac{1}{2^N}, \tag{5.11}$$

which means that both the spreading code and the original information follow uniform distributions. The Hamiltonian (5.9) is exactly the same as the so-called 'anti-Hopfield model' with a random field on each neuron $\sigma_i$ regarding $\boldsymbol{\sigma}$ as a neuronal state. It should be noted that the problem of estimating $\boldsymbol{y}$ from $\boldsymbol{\xi}$ is closely related to that of CS. The problem actually becomes identical to CS with $l_p$ norm by assuming $P(\sigma_i) \propto \exp(-\beta|\sigma_i|^p)$ in the limit of $\beta \to \infty$ instead of Eq. (5.11) as a prior (Kabashima et al. 2001).

We next introduce the maximizer of the posteriori marginal (MPM) estimate, i.e., finite temperature demodulation. We compare the two probabilities that $\sigma_i$ takes, 1 or $-1$, for a given $\boldsymbol{y}$, viz, $P(\sigma_i = \pm 1|\boldsymbol{y})$, to construct the estimate and follow the decision of the 'majority group'. Hence, the MPM estimate for each bit is now given by:

$$\tilde{\sigma}_i = \operatorname{sgn}\left[P(\sigma_i = 1|\boldsymbol{y}) - P(\sigma_i = -1|\boldsymbol{y})\right] \tag{5.12}$$

$$= \operatorname{sgn}\left[\sum_{\sigma_i=\pm 1}\sigma_i P(\sigma_i|\boldsymbol{y})\right] \tag{5.13}$$

$$= \operatorname{sgn}\langle\sigma_i\rangle_\beta, \tag{5.14}$$

where we defined the marginal:

$$P(\sigma_i|\boldsymbol{y}) = \sum_{\boldsymbol{\sigma}\neq\sigma_i} P(\boldsymbol{\sigma}|\boldsymbol{y}), \tag{5.15}$$

where $\langle\cdot\rangle$ indicates the thermal average.

The maximum a posteriori (MAP) estimate, on the other hand, corresponds to searching the ground state of (5.9). Therefore, the MAP estimate can be recovered from the MPM estimate in the zero temperature limit $T = 0$.

We introduce an overlap between original signal $\boldsymbol{\xi}$ and estimated bit $\operatorname{sgn}\langle\sigma_i\rangle_\beta$ to investigate the average-case performance of the demodulation, viz.

$$M(\boldsymbol{y}, \boldsymbol{\xi}|\mathbf{H}) = \frac{1}{N}\sum_i \xi_i \operatorname{sgn}\langle\sigma_i\rangle_\beta. \tag{5.16}$$

The above quantity is expected to be 'self-average' in the limit of $N \to \infty$. This means that observables such as $M(\boldsymbol{y}, \boldsymbol{\xi}|\mathbf{H})$ for a given realization of the data set, $\boldsymbol{y}, \boldsymbol{\xi}$ and $\mathbf{H}$,

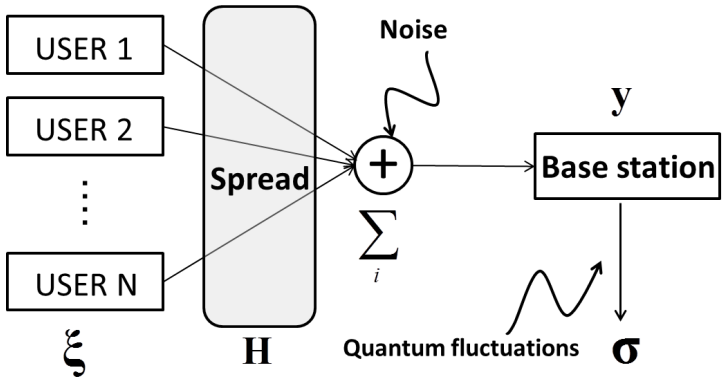


Figure 5.1: CDMA multiuser demodulation with quantum fluctuations.

become identical to the average of itself over the distribution of the Gaussian channel and spreading code, viz.:

$$\begin{aligned} \lim_{N\to\infty} M(\boldsymbol{y},\boldsymbol{\xi}|\mathbf{H}) &= M(\beta) \equiv \sum_{\mathbf{H}} \mathop{\mathrm{Tr}}_{\boldsymbol{\xi}} \int d\boldsymbol{y} P(\mathbf{H}) P(\boldsymbol{\xi}) P(\boldsymbol{y}|\boldsymbol{\xi}) \xi_i \mathrm{sgn}\langle\sigma_i\rangle_\beta \\ &= [\xi_i \mathrm{sgn}\langle\sigma_i\rangle_\beta], \end{aligned} \tag{5.17}$$

where the brackets $[\cdot]$ stands for the average over the data distribution $P(\mathbf{H})P(\boldsymbol{\xi})P(\boldsymbol{y}|\boldsymbol{\xi})$. Hence, $M(\beta)$ is apparently a suitable measurement for the average-case performance of the CDMA system.

We assume that true noise $\boldsymbol{\epsilon}$ in Eq. (5.1) follows an additive Gaussian channel with mean zero and $\sigma_0$ variance to explicitly calculate the above $M$:

$$P(\boldsymbol{\epsilon}) = \left(\frac{1}{\sqrt{2\pi\sigma_0^2}}\right)^2 \exp\left(-\frac{1}{2\sigma_0^2}\|\boldsymbol{\epsilon}\|^2\right) \tag{5.18}$$

$$= \left(\frac{1}{\sqrt{2\pi\sigma_0^2}}\right)^2 \exp\left(-\frac{1}{2\sigma_0^2}\left\|\boldsymbol{y} - \frac{\mathbf{H}\boldsymbol{\xi}}{\sqrt{N}}\right\|^2\right). \tag{5.19}$$

For simplicity, we also assume that the random spreading sequence and information symbols are independent and identically-distributed random variables:

$$P(\boldsymbol{\xi}) = \prod_{i=1}^{N} P(\xi_i) = \frac{1}{2^N}. \tag{5.20}$$

Hence, as the temperature in Eq. (5.5) corresponds to the controlling parameter of the communication channel in the literature on the MPM estimate, optimal performance should be achieved under the condition $\beta = 1/T = \beta_0 = 1/T_0 = 1/\sigma_0^2$, which is nothing but the so-called *Nishimori temperature*.

Although the above formulation is given for the CDMA model based on Bayesian statistics, we will extend it to the quantum-mechanical version by simply adding the

transverse field as:

$$\hat{H} = \hat{H}_0 + \hat{H}_1 \tag{5.21}$$

$$\hat{H}_0 = \frac{1}{2N}\sum_{i,j}\sum_{k=1}^{K}\eta_i^k\eta_j^k\hat{\sigma}_i^z\hat{\sigma}_j^z - \frac{1}{\sqrt{N}}\sum_{i=1}^{N}\sum_{k=1}^{K}\eta_i^k y^k\hat{\sigma}_i^z \tag{5.22}$$

$$\hat{H}_1 = -\Gamma\sum_{i=1}^{N}\hat{\sigma}_i^x, \tag{5.23}$$

where $\hat{\sigma}_i^x$ and $\hat{\sigma}_i^z$ denote the $x$ and $y$ components of the Pauli matrix, and $H_1$ is the transverse field causing quantum tunneling. The strength of the transverse field can be controlled with $\Gamma$.

Let us consider a single-spin system to intuitively figure out the quantum effect in the last equation. Denoting the eigenstates of $\hat{\sigma}^z$ as $|+\rangle = (1,0)^t$ and $|-\rangle = (0,1)^t$, the $x$ component of the Pauli matrix becomes $\hat{\sigma}^x = |+\rangle\langle -| + |-\rangle\langle +|$. Taking into account relation $\hat{\sigma}^x|\pm\rangle = |\mp\rangle$, we find that up-state $|+\rangle$ transits to down-state $|-\rangle$ and vice versa. This means that the transverse field induces the transitions between states by means of tunneling. The Ising spins in the Hamiltonian (5.9) are quantized as Pauli matrices in the framework (5.21). The transverse field is introduced into the Hamiltonian as a non-commutative term. Here, we should bear in mind that the key point of the QMPM estimate is to generate an appropriate ensemble that 'imitates' the actual noise of the Gaussian channel by making use of thermal and quantum fluctuations.

The estimated bit in terms of the QMPM estimate that corresponds to (5.14) can be written as:

$$\tilde{\sigma}_i = \mathrm{sgn}\left(\mathrm{Tr}_s(\hat{\sigma}_i^z\hat{\rho})\right) \tag{5.24}$$

$$= \mathrm{sgn}\left(\langle\hat{\sigma}_i^z\rangle_{\beta,\Gamma}\right), \tag{5.25}$$

where $\hat{\rho} \equiv e^{-\beta\hat{H}}/\mathrm{Tr}e^{-\beta\hat{H}}$. Consequently, the overlap for the case of the quantum system (5.21) is evaluated as:

$$M(\beta,\Gamma) = \sum_{\mathbf{H}}\mathop{\mathrm{Tr}}_{\boldsymbol{\xi}}\int d\boldsymbol{y}P(\mathbf{H})P(\boldsymbol{\xi})P(\boldsymbol{y}|\boldsymbol{\xi})\xi_i\mathrm{sgn}\left(\langle\hat{\sigma}_i^z\rangle_{\beta,\Gamma}\right) \tag{5.26}$$

$$= [\xi_i\mathrm{sgn}\left(\langle\hat{\sigma}_i^z\rangle_{\beta,\Gamma}\right)]. \tag{5.27}$$

Note that the overlap for QMPM depends on the strength of thermal fluctuations controlled by the inverse temperature, $\beta$, and the amplitude of quantum fluctuations determined by the strength of the transverse field, $\Gamma$.

## 5.3 Analysis

We derive saddle point equations that determine the equilibrium state by using the standard replica method to explicitly evaluate performance through the QMPM estimate.

We consider the limit, $N, K \to \infty$, to analyze the multiuser demodulation problem while retaining the ratio:

$$\alpha = \frac{K}{N}, \tag{5.28}$$

of the order 1 object. We apply *Suzuki-Trotter* (ST) *decomposition* (Suzuki 1976):

$$\exp(\hat{H}_0 + \hat{H}_1) = \lim_{P\to\infty} \left(e^{\hat{H}_0/P} e^{\hat{H}_1/P}\right)^P \tag{5.29}$$

to the partition function, $Z = \mathrm{Tr} \exp(-\beta \hat{H})$, with Eq. (5.21) to cast the problem as an equivalent classical spin system to achieve our goal. As a result, the partition function, $Z$, and the effective Hamiltonian, $H_{\text{eff}}$, are given by:

$$Z = \lim_{P\to\infty} \left(\frac{1}{2}\sinh\frac{2\beta\Gamma}{P}\right)^{\frac{NP}{2}} \mathop{\mathrm{Tr}}_{\boldsymbol{\sigma}(t)} \exp\left(-H_{\text{eff}}\right) \tag{5.30}$$

$$\begin{aligned} H_{\text{eff}} &= \frac{\beta}{2NP}\sum_{t=1}^{P}\sum_{i,j}\sum_{k=1}^{K}\eta_i^k\eta_j^k\sigma_i(t)\sigma_j(t) - \frac{\beta}{\sqrt{N}P}\sum_{t=1}^{P}\sum_{i=1}^{N}\sum_{k=1}^{K}\eta_i^k y^k\sigma_i(t) \\ &\quad -\frac{1}{2}\log\frac{\beta\Gamma}{P}\sum_{t=1}^{P}\sum_{i=1}^{N}\sigma_i(t)\sigma_i(t+1), \end{aligned} \tag{5.31}$$

where $P$ is called the Trotter number and $t$ is the Trotter index. We can clearly see that the dimensionality of the corresponding classical system after the ST formula is utilized increases by 1. Using the well-known replica method:

$$[\log\ Z] = \lim_{n\to 0}\frac{[Z^n]-1}{n}, \tag{5.32}$$

we calculate the averaged free energy density, $[\log Z]$, in terms of $[Z^n]$. The replicated partition function is now written as:

$$[Z^n] = \sum_{\mathbf{H}} P(\mathbf{H}) \mathop{\mathrm{Tr}}_{\boldsymbol{\xi}} P(\boldsymbol{\xi}) \int \prod_k dy^k P(y^k|\boldsymbol{\xi}) \mathop{\mathrm{Tr}}_{\{\boldsymbol{\sigma}^\mu(t)\}} \exp\left(-\sum_{\{\boldsymbol{\sigma}^\mu(t)\}} H_{\text{eff}}(\boldsymbol{\sigma}^\mu(t))\right) \tag{5.33}$$

$$\begin{aligned} &= \frac{1}{2^N}\frac{1}{2^{NK}}\sum_{\mathbf{H}}\mathop{\mathrm{Tr}}_{\boldsymbol{\xi}}\int\prod_k dy^k \left(\frac{\beta_0}{2\pi}\right)^{\frac{1}{2}} \exp\left(-\frac{\beta_0}{2}(y^k - \frac{1}{\sqrt{N}}\sum_i \eta_i^k\xi_i)^2\right) \\ &\quad \mathop{\mathrm{Tr}}_{\{\boldsymbol{\sigma}^\mu(t)\}} \exp\left(-\frac{\beta}{2NP}\sum_{t,\mu}\sum_{i,j}\sum_k \eta_i^k\eta_j^k\sigma_i^\mu(t)\sigma_j^\mu(t) + \frac{\beta}{\sqrt{N}P}\sum_{t,\mu}\sum_i\sum_k \eta_i^k y^k\sigma_i^\mu(t)\right. \\ &\quad \left. + B\sum_{t,\mu}\sum_i \sigma_i^\mu(t)\sigma_i^\mu(t+1)\right), \end{aligned} \tag{5.34}$$

where $B \equiv \frac{1}{2}\log\coth\frac{\beta\Gamma}{P}$, $\{\boldsymbol{\sigma}^\mu(t)\} = (\sigma^1(t), ..., \sigma^n(t))$, and $t = 1, ..., P$. The replica

indices are denoted by $\mu$. Introducing the following order parameters:

$$R_\mu(t) = \frac{1}{N}\sum_i \xi_i \sigma_i^\mu(t) \tag{5.35}$$

$$Q_{\mu\nu}(t,t') = \frac{1}{N}\sum_i \sigma_i^\mu(t)\sigma_i^\nu(t') \tag{5.36}$$

$$Q_{\mu\mu}(t,t') = \frac{1}{N}\sum_i \sigma_i^\mu(t)\sigma_i^\mu(t'), \tag{5.37}$$

with $Q_{\mu\mu}(t,t)=1$, free energy density $f$ is given by:

$$\begin{aligned} -\beta f &= \frac{\alpha}{2}\left\{-\log(1-\beta(q-\chi)) + \frac{\beta(1+\beta_0)}{\beta_0} + \frac{\beta(2R-q-(1+\beta_0^{-1}))}{1-\beta(q-\chi)} + \beta(\chi-1)\right\} - \hat{R}R \\ &\quad -\hat{\chi}\chi + \frac{\hat{q}q}{2} + \int Dz \log\left(\int Dw 2\cosh\sqrt{\Phi^2+\beta^2\Gamma^2}\right) \end{aligned} \tag{5.38}$$

$$\Phi = \frac{\phi}{\beta} = z\sqrt{2\hat{\chi}-\hat{q}} + w\sqrt{\hat{q}} + \hat{R}, \tag{5.39}$$

under replica symmetry (RS) and static approximation (SA), viz., $R_\mu(t)=R$, $Q_{\mu\nu}(t,t')=q$, and $Q_{\mu\mu}(t,t')=\chi$ $(t\neq t')$ in the limit of $N\to\infty$. $\hat{R}$, $\hat{q}$ and $\hat{\chi}$ correspond to conjugate Lagrange multipliers of $R$, $q$,, and $\chi$. The saddle-point equations are given by:

$$R = \int Dw \int Dz \frac{\Phi\sinh\Xi}{\Omega\Xi} \tag{5.40}$$

$$q = \int Dw \left(\int Dz \frac{\Phi\sinh\Xi}{\Omega\Xi}\right)^2 \tag{5.41}$$

$$\chi = \int \frac{Dw}{\Omega}\int Dz\left(\frac{\beta^2\Gamma^2\sinh\Xi}{\Xi^3} + \frac{\Phi^2\cosh\Xi}{\Xi^2}\right) \tag{5.42}$$

$$\hat{R} = \frac{\alpha\beta}{1+\beta(\chi-q)} \tag{5.43}$$

$$\hat{q} = \frac{\alpha\beta^2(1+q-2R+\beta_0^{-1})}{(1+\beta(\chi-q))^2} \tag{5.44}$$

$$2\hat{\chi}-\hat{q} = \frac{\alpha\beta^2(\chi-q)}{1+\beta(\chi-q)} \tag{5.45}$$

$$\Xi = \sqrt{\Phi^2+\beta^2\Gamma^2} \tag{5.46}$$

$$\Omega = \int Dz\cosh\Xi, \tag{5.47}$$

where $\int Du(\cdot) = \int_{-\infty}^{\infty} du(\cdot)e^{-\frac{u^2}{2}}/\sqrt{2\pi}$. Considering the classical case of $\Gamma=0$, we easily find that these equations become identical to the classical version with $\chi=1$. The detailed calculations to derive the free energy density (5.38) are given in our Appendix. By comparing these expressions and Eqs. (5.40) and (5.41), we immediately find that $\int Dz\frac{\Phi\sinh\Xi}{\Omega\Xi}$ is closely related to $\langle\hat{\sigma}_i\rangle_{\beta,\Gamma}$. Thus, the final form of the overlap as a performance measurement is easily obtained as (Otsubo et al. 2012):

$$M(\beta,\Gamma) = \int Dw\,\mathrm{sgn}\left(\int Dz\frac{\Phi\sinh\Xi}{\Omega\Xi}\right). \tag{5.48}$$

It should be noted that the overlap for classical MPM is recovered by setting $\Gamma = 0$ in the above expression (5.48).

## 5.4 Results

We evaluate the performance of demodulation with quantum and thermal fluctuations by numerically solving Eqs. (5.40)-(5.48) in the following.

### 5.4.1 Upper bound of overlap

We first derive the inequality for the overlap to clarify the upper bound. The overlap in the classical case defined by Eq. (5.17) can be written as follows:

$$
\begin{aligned}
& M(\beta) \\
= & \operatorname*{Tr}_{\boldsymbol{\xi}} \int \prod_k dy^k C_{NK} \exp\left(-\frac{\beta_0}{2}(y^k)^2\right) \exp\left(-\frac{\beta_0}{2N}\sum_{i,j}\eta_i^k\eta_j^k\xi_i\xi_j + \frac{\beta_0}{\sqrt{N}}\sum_i \xi_i\eta_i y^k\right) \xi_i \mathrm{sgn}\left(\frac{\mathrm{Tr}\sigma_i \mathrm{e}^{-\beta H}}{\mathrm{Tr}\mathrm{e}^{-\beta H}}\right) \\
\leq & \int \prod_k dy^k C_{NK} \exp\left(-\frac{\beta_0}{2}(y^k)^2\right) \left\| \operatorname*{Tr}_{\boldsymbol{\xi}} \xi_i \exp\left(-\frac{\beta_0}{2N}\sum_{i,j}\eta_i^k\eta_j^k\xi_i\xi_j + \frac{\beta_0}{\sqrt{N}}\sum_i \xi_i\eta_i y^k\right)\right\| \\
\times & \left\| \mathrm{sgn}\left(\frac{\mathrm{Tr}\sigma_i \mathrm{e}^{-\beta H}}{\mathrm{Tr}\mathrm{e}^{-\beta H}}\right)\right\| \\
\leq & \int \prod_k dy^k C_{NK} \exp\left(-\frac{\beta_0}{2}(y^k)^2\right) \left\| \operatorname*{Tr}_{\boldsymbol{\xi}} \xi_i \exp\left(-\frac{\beta_0}{2N}\sum_{i,j}\eta_i^k\eta_j^k\xi_i\xi_j + \frac{\beta_0}{\sqrt{N}}\sum_i \xi_i\eta_i y^k\right)\right\| \\
\equiv & M_{\max}^{\mathrm{classic}}.
\end{aligned}
\tag{5.49}
$$

We should notice that factor $C_{NK}$ denotes $2^{-N}2^{-NK}\sqrt{\beta_0/2\pi}$ from Eqs. (5.10) and (5.20). $M_{\max}^{\mathrm{classic}}$ means the upper bound in the classical case. However, the overlap for the quantum case is given by:

$$
\begin{aligned}
& M(\beta,\Gamma) \\
= & \operatorname*{Tr}_{\boldsymbol{\xi}} \int \prod_k dy^k C_{NK} \exp\left(-\frac{\beta_0}{2}(y^k)^2\right) \exp\left(-\frac{\beta_0}{2N}\sum_{i,j}\eta_i^k\eta_j^k\xi_i\xi_j + \frac{\beta_0}{\sqrt{N}}\sum_i \xi_i\eta_i y^k\right) \xi_i \mathrm{sgn}\left(\frac{\mathrm{Tr}\hat{\sigma}_i^z \mathrm{e}^{-\beta \hat{H}}}{\mathrm{Tr}\mathrm{e}^{-\beta \hat{H}}}\right) \\
\leq & \int \prod_k dy^k C_{NK} \exp\left(-\frac{\beta_0}{2}(y^k)^2\right) \left\| \operatorname*{Tr}_{\boldsymbol{\xi}} \xi_i \exp\left(-\frac{\beta_0}{2N}\sum_{i,j}\eta_i^k\eta_j^k\xi_i\xi_j + \frac{\beta_0}{\sqrt{N}}\sum_i \xi_i\eta_i y^k\right)\right\| \\
\times & \left\| \mathrm{sgn}\left(\frac{\mathrm{Tr}\hat{\sigma}_i^z \mathrm{e}^{-\beta \hat{H}}}{\mathrm{Tr}\mathrm{e}^{-\beta \hat{H}}}\right)\right\| \\
\leq & \int \prod_k dy^k C_{NK} \exp\left(-\frac{\beta_0}{2}(y^k)^2\right) \left\| \operatorname*{Tr}_{\boldsymbol{\xi}} \xi_i \exp\left(-\frac{\beta_0}{2N}\sum_{i,j}\eta_i^k\eta_j^k\xi_i\xi_j + \frac{\beta_0}{\sqrt{N}}\sum_i \xi_i\eta_i y^k\right)\right\| \\
\equiv & M_{\max}^{\mathrm{classic}}.
\end{aligned}
\tag{5.50}
$$

Thus, the optimal demodulating performance of the MPM estimate in the presence of quantum fluctuations is the same as that in the thermal fluctuations. We can confirm that overlap is maximum at the Nishimori temperature, $T_0 = 1/\beta_0$, as:

$$\begin{aligned} M_{\max}^{\text{classic}} &= \mathop{\mathrm{Tr}}_{\boldsymbol{\xi}} \int \prod_k dy^k C_{NK} \exp\left(-\frac{\beta_0}{2}(y^k - \frac{1}{\sqrt{N}}\sum_i \eta_i^k \xi_i)^2\right) \xi_i \\ &\times \frac{\mathrm{Tr}_{\boldsymbol{\xi}} \xi_i \exp\left(-\frac{\beta_0}{2N}\sum_{i,j}\eta_i^k\eta_j^k\xi_i\xi_j + \frac{\beta_0}{\sqrt{N}}\sum_i \xi_i\eta_i y^k\right)}{\left\|\mathrm{Tr}_{\boldsymbol{\xi}} \xi_i \exp\left(-\frac{\beta_0}{2N}\sum_{i,j}\eta_i^k\eta_j^k\xi_i\xi_j + \frac{\beta_0}{\sqrt{N}}\sum_i \xi_i\eta_i y^k\right)\right\|} \\ &= \mathop{\mathrm{Tr}}_{\boldsymbol{\xi}} \int \prod_k dy^k C_{NK} \exp\left(-\frac{\beta_0}{2}(y^k - \frac{1}{\sqrt{N}}\sum_i \eta_i^k \xi_i)^2\right) \xi_i \mathrm{sgn}\langle\xi_i\rangle_{\beta_0} \\ &= M(\beta_0). \end{aligned} \tag{5.51}$$

The inequality means that the optimal demodulating performance through the MPM estimate incorporating the transverse field can not exceed the optimal one in the classical case. However, we must mention that as the $\Gamma, T$-dependence of demodulating performance on the QMPM estimate could not be clarified with the above argument, we next need to numerically solve the saddle point equations (5.40)-(5.48) to make the issue clearer.

### 5.4.2 Behavior around peak

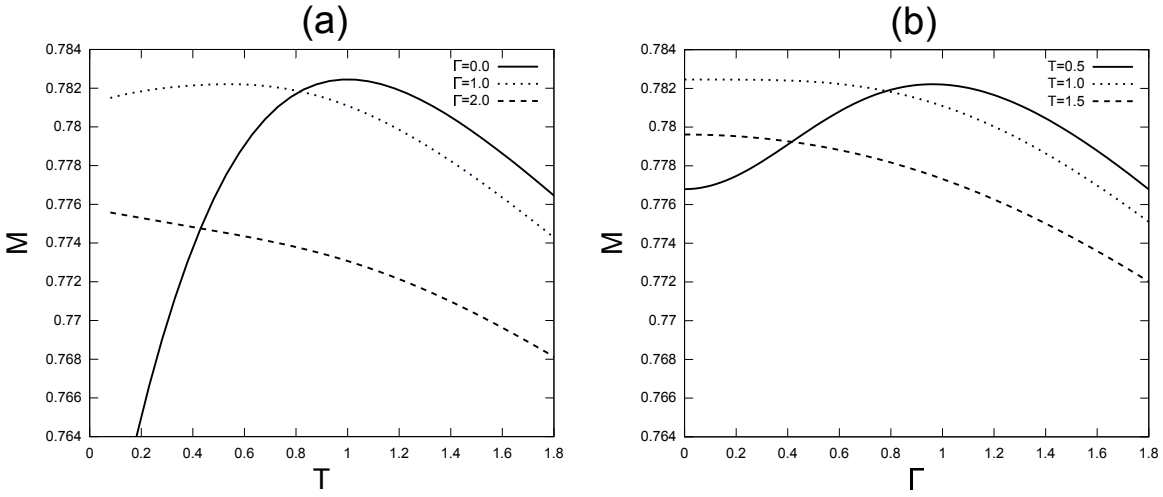


Figure 5.2: (a): Dependence of overlap $M$ on level of thermal fluctuations $T$ for $\alpha = 2.0$ and $T_0 = 1.0$. (b): Dependence of overlap $M$ on level of quantum fluctuations $\Gamma$ for $\alpha = 2.0$ and $T_0 = 1.0$.

Figure 5.2 plots the dependence of overlap $M$ on $T$ and $\Gamma$ for the case of $\alpha = 2.0$ and $T_0 = 1.0$. We find that the overlap has its a single peak at $T = T_0 = 1.0$ for the case without transverse field $\Gamma = 0$ as is well-known (see Fig. 5.2(a)). This means that the optimal performance in demodulation is achieved at some temperature $T = T_0$ that

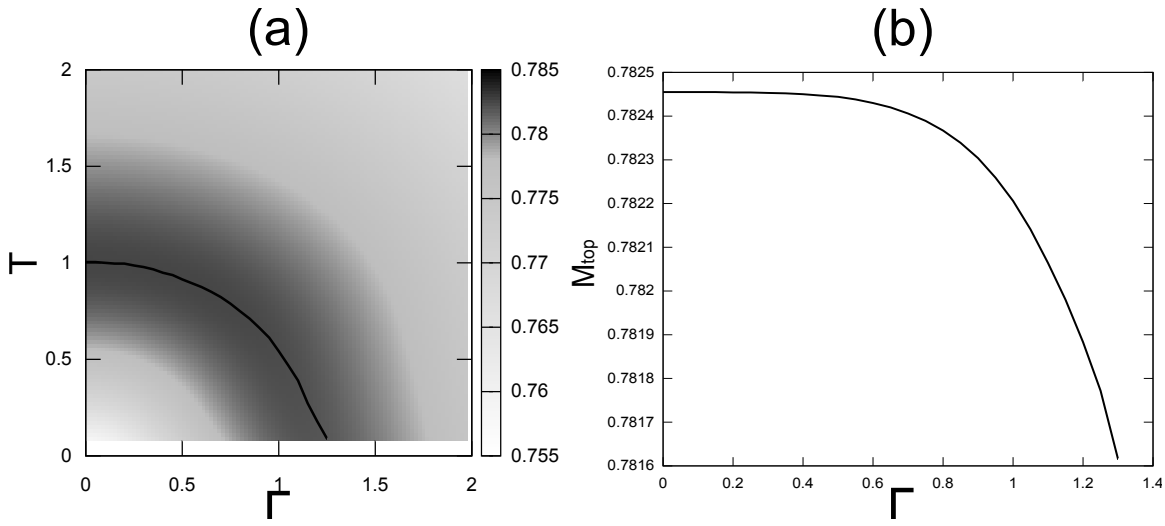


Figure 5.3: (a): Value of overlap on Γ-$T$ plane for $T_0 = 1.0$ and $\alpha = 2.0$. Solid line indicates location of peak in overlap. (b): Dependence of $M_{top}$ on Γ corresponding to solid line in panel (a).

corresponds to the true variance in the Gaussian channel described as Eq. (5.19). Also note that the overlap appropriately exhibits a peak that is obtained by controlling the strength of the quantum fluctuation, Γ. The height of the peak seems to be the same as that of the CMPM estimate. These results are consistent with those in our previous studies (Inoue 2001; Otsubo 2001; see Chap. 3 and Chap. 4).

We next investigate the overlap from the view point of the Γ-$T$ diagram in Fig. 5.3(a). The gradation indicates the values of the overlap and the solid line represents the peaks of the overlap, $M_{top}$. We can observe that $M_{top}$ exists in some range of temperature below the Nishimori temperature $T = T_0$. We should keep in mind that the numerical solution to the overlap in the quite low temperature region ($T < 0.05$) cannot be obtained within reliable precision due to limitations in our computational resources. We can see the dependence of $M_{top}$ on Γ that is indicated by the solid line in Fig. 5.3(b) for $\alpha = 2.0$ and $T_0 = 1.0$. We find that the peak of overlap $M_{top}$ decreases monotonically from 0.7824 to 0.7816. Therefore, we must conclude that quantum fluctuations worsen optimal performance slightly for large Γ. Obviously, the results are consistent with our argument using the inequalities (5.49)-(5.51).

### 5.4.3 Dependence of demodulating performance on chip ratio

The dependence of overlap on $\alpha$ is plotted in Figs. 5.4(a) ( $T_0 = 1.0, T = 1.0$) and (b) ($T_0 = 0.08, T = 0.08$) for various Γ values. As the temperature is set to the Nishimori temperature for both cases, the overlap has a peak at $\Gamma = 0$ as we noted in the previous section. Since parameter $\alpha$ means the chip ratio, we naturally assumed that overlap would increase as $\alpha$ increased. We find that the slope of increase in the overlap for the quantum case is much gentler than that for the classical case.

When the variance of the Gaussian channel $T_0$ is very small, first-order phase tran-

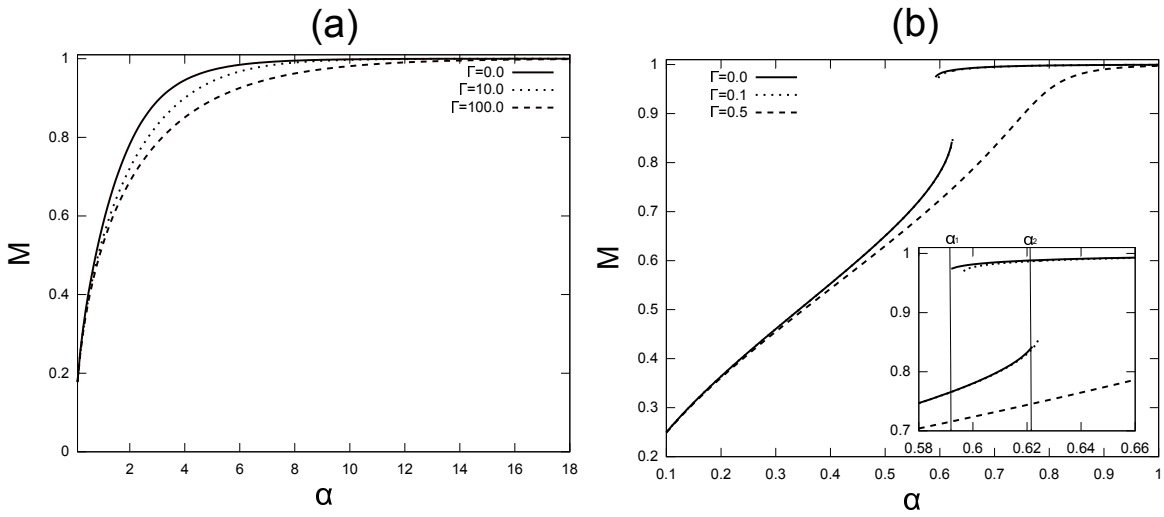


Figure 5.4: Overlap $M$ vs chip ratio $\alpha$. (a): Results for $T_0 = 1.0$ and $T = T_0$. (b): Results for $T_0 = 0.08$ and $T = T_0$. Bi-stable solutions coexist for $\Gamma = 0$ in region $\alpha_1 < \alpha < \alpha_2$.

sition takes place around $\alpha \simeq 0.6$ for $\Gamma = 0$. In contrast, we find that for relatively large quantum fluctuations, $\Gamma = 0.5$, the overlap continuously converges to unity. These results imply that quantum fluctuations never improve the average-case performance of MPM estimate for any choice of the chip ratio, $\alpha$.

We confirm that two possible solutions coexist at low temperature (see the inset of Fig. 5.4 (b)), which lead to a sort of hysteresis phenomenon. Such a bi-stable region obtained under the RS and SA ansatz disappears as $\Gamma$ increases. The spinodal lines in $(\alpha, \Gamma)$-space are plotted in Fig. 5.5. The distinction between the solid and dashed lines comes from the dependence of $\Gamma$ on $\alpha_1$ (solid) or $\alpha_2$(dashed). As can be shown in Fig. 5.5 (a) $T_0 = T = 0.08$, the region of $\alpha$ in which solutions coexist is maximum at $\Gamma = 0$. However, there is also a coexistence region for solutions to $T_0 = 0.08$ and $T = 0.05$ with slightly different shapes from those of $T_0 = T = 0.08$. The coexistence region gradually narrows for the both cases as $\Gamma$ increases, and the region eventually disappears. Similar behavior has been found in $(\alpha, T)$-space when $T_0$ is fixed for the classical case, i.e., $\Gamma = 0$ (Yoshida et al. 2007).

### 5.4.4 Improvable region for demodulating performance

The previous section explained our investigation into the average-case performance of the demodulation by means of the QMPM estimate. We focused on the location of the peak of the overlap. Here, we will discuss the conditions under which the performance of the QMPM estimate is better than that of CMPM. This is a slightly different view point from optimality in the overlap.

To quantify the degree of improvement achieved by quantum fluctuations, we introduce the following quantity:

$$\Delta M(\Gamma, \Omega) = M(\Gamma, \Omega) - M(0, \Omega), \tag{5.52}$$

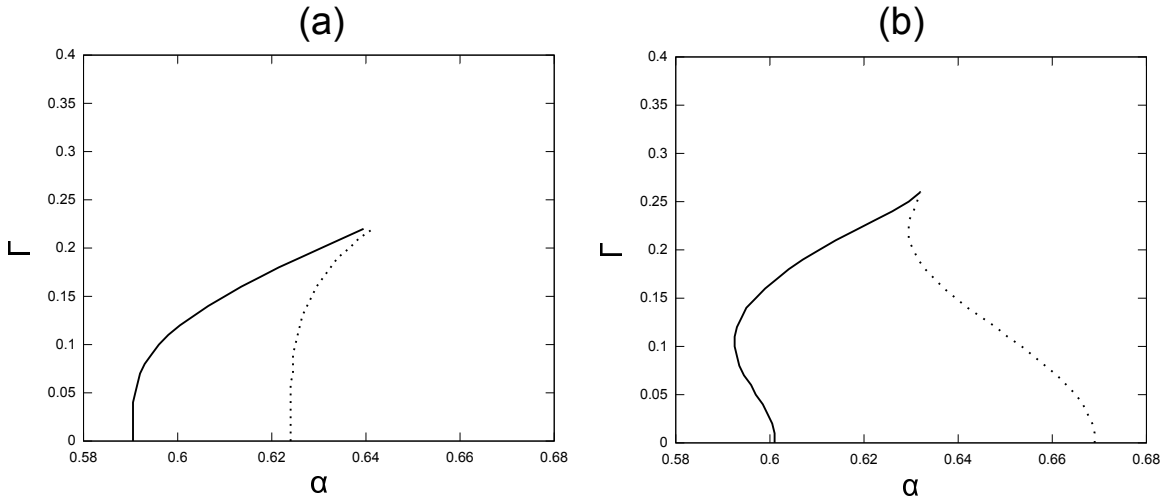


Figure 5.5: (a): Spinodal line at $T_0 = T = 0.08$. (b): Spinodal line at $T_0 = 0.08$ and $T = 0.05$. Solid line represents $\Gamma(\alpha_1)$ and dotted line represents $\Gamma(\alpha_2)$.

i.e., the difference between the overlaps at $\Omega = \{T_0, T, \alpha\} \in \mathcal{R}$ with and without the quantum fluctuations. The quality of quantum demodulation is better than that of classical demodulation for $\Delta M(\Gamma, \Omega) > 0$. It should be noted that the overlap is maximized at $\Gamma = 0$ for $T = T_0$, viz, $\Delta M(\Gamma, \Omega_0) < 0$ for $\Omega_0 = \{T_0, T = T_0, \alpha\} \in \mathcal{R}$ and $\Gamma > 0$. $\Delta M$ is always less than zero for the case of $T > T_0$, as we mentioned in the previous section. For these reasons, we define a region where $\Delta M > 0$ an *improvable region*, whereas the region specified by $\Delta M < 0$ is referred to as a *worsened region* for $T < T_0$.

We have plotted $\Delta M$ as a function of $\Gamma$ for $T_0 = 1.0$ and $T = 0.5$ with various values of $\alpha$ in Fig. 5.6. We find that $\Delta M$ has a peak in some range of $\Gamma$ and it eventually drops to a negative value. Demodulation achieves the best possible performance for a given set of $T$ and $T_0$ at some specific value of $\Gamma$ for which $\Delta M$ has a peak. We should note that $\Delta M = 0$ determines the border of $\Gamma$ between improvable and worsened regions. We have marked the locations in which $\Delta M = 0$ is satisfied for $\alpha = 0.2$, 0.7, 2.0, and 0.5 with respective points labeled A, B, C, and D. The $\Gamma$ for $\Delta M = 0$ is not a monotonic function of $\alpha$ because we clearly find that the inequality $\Gamma_{\rm D} < \Gamma_{\rm C} < \Gamma_{\rm A} < \Gamma_{\rm B}$ holds. This implies the existence of a suitable $\alpha$ to improve demodulating performance. Also note that the peaked value of $\Delta M$ decreases as $\alpha$ increases because both $M(\Gamma, \Omega)$ and $M(0, \Omega)$ converge to unity.

We will next investigate the critical $\Gamma(T)$ at which the improvable and worsened regions are clearly separated. The results are plotted in Figs. 5.7(a) and (b). The dashed lines were obtained under the conditions $\Delta M(\Gamma, \Omega) = 0$. We find that the improvable region is extended up to the low temperature region in Fig. 5.7(a). Interestingly, the critical line (the $\Gamma$-$\alpha$ curve) that separates improvable and worsened regions has a non-monotonic shape with a single maximum at some finite $\alpha$ value. This means that there is a suitable chip ratio, $\alpha$, to improve demodulation performance.

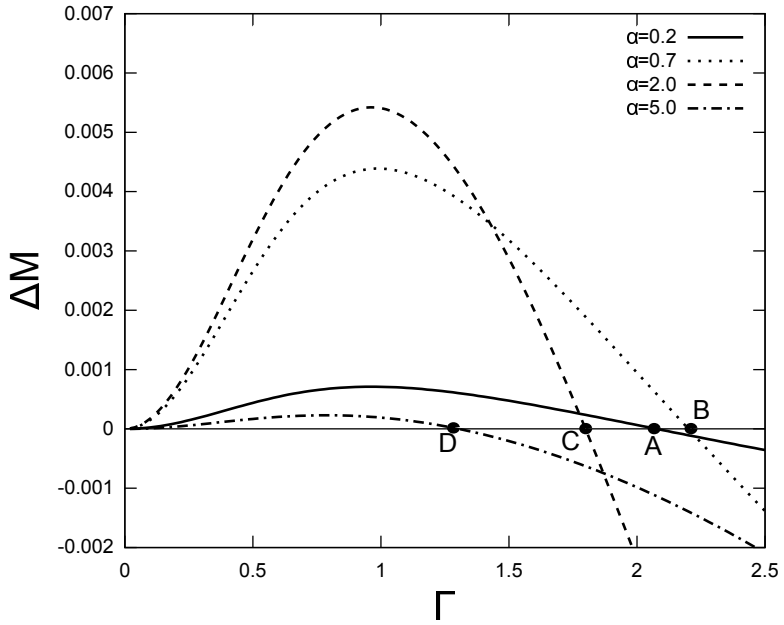


Figure 5.6: Difference between overlaps with and without transverse field for $T_0 = 1.0$ and $T = 0.5$. Closed circles labeled A, B, C, and D denote points at which $\Delta M = 0$ holds.

## 5.5 Summary and discussion

We investigated the average-case performance of a Bayesian CDMA multiuser detector that was extended by means of quantum fluctuations. The following three items summarize what we learned from this study.

1. Quantum fluctuations controlled by the transverse field could not improve the optimal performance of CMPM. To make matters worse, the MPM estimate that incorporated the transverse field (QMPM estimate) never exhibited the same optimal performance as the conventional MPM estimate (CMPM estimate) even within the strictest sense. This conclusion was supported by a mathematically rigorous argument using inequality on the overlap.

2. There was a improvable region below the Nishimori temperature obtained by using the transverse field. Thus, the transverse field actually improved performance for some choices of non-optimal parameters although optimal performance with the transverse field could not be improved.

3. Increasing the chip ratio improved performance. The overlap actually eventually reached unity for both cases with and without the transverse field.

Although we drew the above conclusion from our limited applications of transverse field, there still remain some issues to be resolved. We actually used several approximations, replica symmetry (RS) and static approximation (SA) in our analysis. As

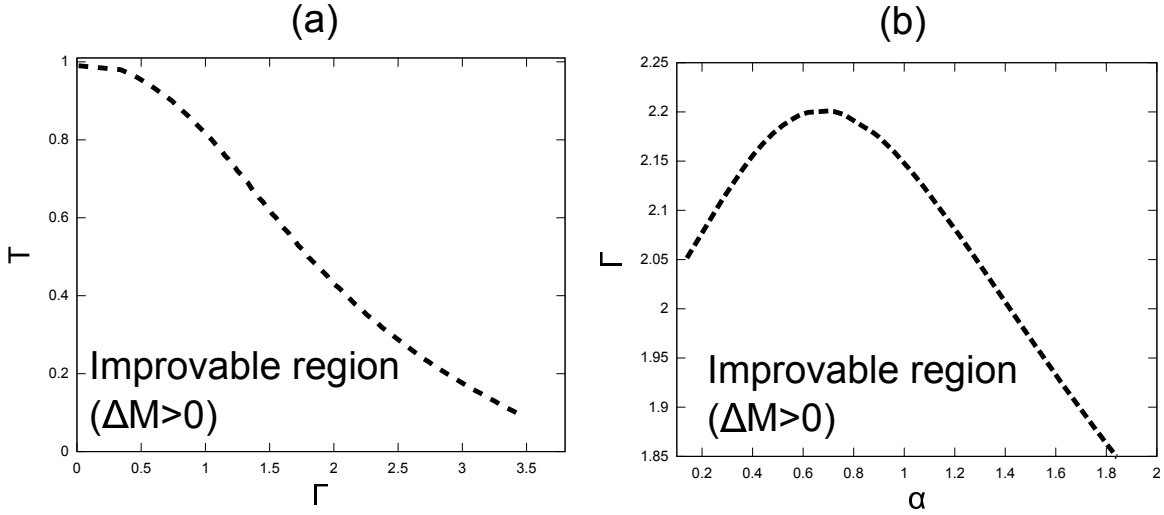


Figure 5.7: Improvable regions in $T$-$\Gamma$ (left) and $\Gamma$-$\alpha$ (right) planes for $T_0 = 1.0$. Dashed lines indicate border at which $\Delta M = 0$ holds for $\alpha = 2.0$ (a) and $T = 0.5$ (b).

it is naturally expected that these approximation may be broken in the low temperature region, we should draw the so-called Almeida-Thouless (AT) line (de Almeida and Thouless 1978), and we also should discuss the validity of the SA. Although the validity of the SA has been investigated partially in the quantum random energy model (Obuchi et al. 2007), has not yet been investigated for Ising spin glass in a transverse field. In general, it is very hard to carry out numerical calculation in very low temperature within reliable numerical accuracy, the pure quantum demodulation which is defined as the QMPM without any thermal fluctuation is also very difficult to be discussed. Besides these perspectives, as we stated in Sec. 5.1, the compressed sensing (CS) is now becoming a hot topic as an effective technique to understand a signal from some observable dates in the various engineering fields. Obviously, our formulation using the transverse field might be applicable to the CS and it should be addressed as our future study.

# Chapter 6

# Summary and concluding remarks

In this thesis, we devoted a detailed examinations of a performance of the probabilistic information processing by means of the transverse field which means the quantum fluctuations from a statistical mechanical point of view by proposing the quantum maximum posterior marginals (QMPM) estimate instead of the conventional MPM (CMPM) estimate. We then addressed three models which are described by mean-field Ising spin models. The average-case performance of the image restoration which can be formulated by the Ising spin model with random field was first in focus. Next, we investigated the average-case decoding performance of the Sourlas code which is one of the typical error-correcting codes and can be formulated by the mean-field spin glass model with $p$-body interactions in which Shannon bound can be saturated in $p \to \infty$. In the last part of our studies, we investigated the CDMA multiuser demodulation which is modern wireless communication system and then can be formulated by the mean-field spin glass model with random field.

In this chapter, the reconfirmation of our purposes and the common thread in these investigations are given in the anterior half. Next half, we summarize the specific discussion of each problem and give the future works to be clarified.

## 6.1 General properties of the QMPM estimate

We conclude the general properties of the QMPM estimate as follows:

**1. QMPM estimate works well.**

Our consecutive motivations in this thesis are simple as discussed in Chap. 2. The most interesting issue is whether the quantum fluctuations can contribute the information processing as with the thermal fluctuations or not. The answer is "yes". In consequence of investigation of the three models, the performances have peaked behavior by controlling the strength of the transverse field. Such a result is interesting despite of introducing the transverse field unrelated to the temperature. We also investigated the peaked behavior on the phase consisted of the strength of the temperature and the transverse field. As a result, increasing the strength of the transverse field, the

temperature which gives the peaked value decreases. It seems that the transverse field can complement the effect of the temperature in the probabilistic information processing. Although our numerical calculations cannot reach the low temperature limit for our computational accuracy, the results sufficiently suggest that the pure QMPM estimate which mean the algorithm for the signal estimation with the transverse field and without the temperature can work well.

**2. QMPM estimate does not provide better performance than it through CMPM estimate in terms of optimal performance.**

Followed by the above results, next interesting goes as follows. What is the amount of the optimal performance achieved with the transverse field as compared to it by using the CMPM estimate? In this question, we need to give an answer carefully. It is seems to that the optimal performance can be roughly same it at Nishimori temperature in all models. However, under scrutiny, it decrease with the transverse field monotonically in the Sourlas code and CDMA system. The decreasing behavior cannot be seen in the image restoration through our numerical results. Such a different behavior may be attribute to numerical accuracy. Thus, the decreasing behavior of the image restoration with the transverse field may not be caught from our computational accuracy. The inequality derived in Chap. 4 and 5 show that the average-case decoding performance with the transverse field generally is less than the optimal performance of the conventional MPM estimate. Such theoretical derivation help the above numerical results.

**3. There is improvable region below Nishimori temperature.**

The transverse field, the quantum fluctuation, actually can improve the average-case performance of the CMPM estimate, although optimal performance with the transverse field cannot be improved. In lower temperature region than Nishimori temperature, the improvable behavior occurs by controlling the strength of the transverse field appropriately. This is natural result because of our first claim that the peaked performance which achieve roughly classical optimal performance can be successfully accomplished at low temperature region.

The above remarks give the quantum annealer which is superconducting device for quantum annealing anew usage. The quantum annealer can be demonstrated in the condition in the sufficiently low temperature condition (about 20 mK). Because the quantum fluctuation enables us to construct a state near the original information instead of the thermal fluctuation, the quantum annealer may be a processor which implements the probabilistic information processing.

## 6.2 Specific properties of the QMPM estimate for each problem

The above properties are major properties of the transverse field in the information processing studied here. Next, the topics on properties of each model through QMPM estimate are summarized.

In the Sourlas code, the quantum fluctuation induces the phase transitions among the ferromagnetic phase, the paramagnetic phase and the spin glass phase. The ferromagnetic phase allows us to decode an original information. Shannon bound which is the condition of perfect decoding can be achieved in a certain limit with or without the transverse field. The Monte Carlo simulation is also performed and it roughly give the results which is consistent with the common properties obtained by the analysis.

In the CDMA multiuser detection, the chip ratio is an important parameter. Increasing the chip ratio improved performance. The overlap, demodulating measure, actually eventually reached unity for both cases with and without the transverse field. The cases that the true noise is small lead to a sort of hysteresis phenomenon. Such a bistable region obtained the RS ans SA ansatz disappears as the strength of the transverse field increases.

## 6.3 Future works

Our approaches are only theoretical focus on solvable models described by mean-field spin models, then quantum channel is less than well thought out. Although our studies might not be investigation about quantum information processing in this mean. However, our works have a potential impacts on the various field as follows.

First, we need to investigate the validity of the approximation we used in this thesis. The replica symmetry (RS) approximation which we use in this studies may be broken in very low temperature region. Because our interest is the average-case performance with the transverse field, we did not discuss the problem. The replica symmetry breaking (RSB) condition can be checked by calculating the Almeida-Thouless (AT) line (de Almeida 1978). The AT line has been studied in quantum SK model, quantum random energy (REM) model and quantum $p$-body spin glass model in the field of quantum statistical physics. Ray et al. also attempted to draw the AT line by using Monte Carlo simulations, and they found that it might be possible to conclude that there is no replica symmetry breaking due to the quantum tunneling effects even in the low-temperature region (Ray et al. 1989). On the other hand, there is no RS ansatz in quantum REM model. For these studies, we need to treat the validity of the replica symmetry carefully. On the other hand, we used the static approximation (SA) that the macroscopic property is invariant with Trotter axis. This treatment is also controversial. The SA is valid in the case of the random energy model ($p \to \infty$) but may be invalid for the case of a finite $p$ (Obuchi et al. 2007). Following the previous perception, we may have to tackle the validity of SA in the models studied here.

The formulation proposed here can be applied to the other information processing problems, although we focused on simple models in this thesis. As an example, a gray-scale image restoration (GSIR) process through the QMPM estimate still remain open, which may be implemented by mapping the set of the pixels onto many-state Potts spins of quantum version (Inoue and Carlucci 2001). The studies of the restoration process in the classical cases have been also investigated by using the mean-field theory. Whether the convergence speed to a solution through the QMPM estimate is faster or not than it through the CMPM estimate is instructive issue. In terms of error correcting code, there are many future studies. As a simple expansion, we can consider the Sourlas code model

with the finite connectivity, which can be analyzed the method developed for diluted spin glass in the classical case (Kabashima and Saad 1998; Wong and Sherrington 1988). The quantum case may be also investigated by similar strategy. The Low-density parity-check code (LDPC) which is also typical error correcting code and saturates Shannon bound get a lot of attention with developing information technology. One of LDPC is formulated by diluted many-body Mattis model in an external field and then the performance of it through QMPM estimate may be analyzed. The dynamics of the error correcting may be analyzed by expanding the *Dynamical Replica Theory* (DRT) which is strong strategy to investigate the dynamics in the disorder spin models to quantum case (Ozeki and Okada 2003). As a simple expanded case of CDMA model, the compressed sensing (CS) has also a more desirable property which is a signal processing technique from relatively few measurements. For example, an application to mobile phone camera sensor allows us to radically reduce battery drain (Schneider 2013). The CS has been also investigated in the field of a medical field and then it may permit speed up a scanning process magnetic resonance imaging (MRI) and CT scanners. If quantum fluctuations can used in these field in a certain means, our theoretical works in this thesis would pay dividends.

We should naturally consider the pure QMPM estimate which means the decoding algorithms with the quantum fluctuations and without the thermal fluctuations. Although we can treat this considering a certain limit $T \to 0$ in the state equations, such a treatment is difficult for integration induced by the transverse field. If we can perform the integration considering the saddle point condition in the limit, we can consider the pure QMPM estimate.

The research fields of the information processing with the transverse field is supposed to expand with developing the device technologies. The quantum computer, quantum annealer, which can demonstrate the algorithm by using the transverse field, was launched and continue remarkable development. With these developments, the researchers in the field of machine learning are interested in such a device technology. At the present stage, the 512-qubit quantum annealer which is called "Vesuvius" is established by D-wave systems. Although a sufficient examination should be done, the computer may trigger a quantum speed up (Rønnow et al. 2013). As mentioned above, our studies and formulation suggest that the quantum annealer may perform probabilistic information processing. We believe that our works may contribute to some mathematical foundation including the quantum annealing, futural information processing with the quantum device.

# Appendix

## A Saddle point approximation

We give the brief description of the saddle point approximation of real function. We consider the following integration and give an assessment of it,

$$I = \int_{-\infty}^{\infty} dx e^{-Nf(x)}. \tag{A1}$$

The key idea of the saddle point approximation is that the above integral goes to the maximum of the integrand in $N \to \infty$ because a negative exponential function decreases rapidly. If $f(x)$ is minimum at $x_0$, it's Taylor expansion around $x_0$ is

$$\begin{aligned} f(x) &= f(x_0) + f'(x_0)(x - x_0) + \frac{1}{2} f"(x_0)(x - x_0)^2 + \cdots & \text{(A2)} \\ &= \sum_{k=0}^{\infty} \frac{1}{k!} f^{(k)}(x - x_0)^k. & \text{(A3)} \end{aligned}$$

Because the integral of the odd function is zero, we consider the following integral instead of Eq. (A1),

$$\begin{aligned} I &= \int_{-\infty}^{\infty} dx \exp\left\{ -Nf(x_0) - \frac{N}{2} f"(x_0)(x - x_0)^2 + O(N(x - x_0)^3) \right\} & \text{(A4)} \\ &= e^{-Nf(x_0)} \int dx \left\{ -\frac{N}{2} f"(x_0)(x - x_0)^2 + O\left( e^{-N(x-x_0)^3} \right) \right\} & \text{(A5)} \\ &\simeq e^{-Nf(x_0)} \sqrt{\frac{2\pi}{Nf"(x_0)}}. & \text{(A6)} \end{aligned}$$

We see that the integral (A1) is influenced on only minimum of integrand $f(x)$ in the thermodynamic limit $N \to \infty$. In this paper, we use $I$ as the partition function $Z$ and then we get the relation that $\beta F = -\log Z \approx -Nf(x_0) + \text{const.}$

## B Suzuki-Trotter formulation

We give detailed calculation of Suzuki-Trotter (S-T) decomposition for a quantum spin glass model (Suzuki 1976). The goal in this section is to obtain the classical Hamiltonian corresponding to the quantum system by using S-T decomposition.

Let us consider the following Hamiltonian incorporating the transverse field:

$$\hat{H} = \hat{H}_0(\hat{\sigma}_i^z) - \Gamma \sum_i \hat{\sigma}_i^x \equiv \hat{U} + \hat{K} \tag{B1}$$

As we see in main text, the $H_0$ is the problem Hamiltonian and $\Gamma$ stands for the strength of the transverse field. The S-T formula is given as

$$\begin{aligned} \left( e^{\hat{U}/P} e^{\hat{K}/P} \right)^P &= \exp\left\{ \hat{U} + \hat{K} + \frac{1}{2P} [\hat{K}, \hat{U}] + O(P^{-3}) \right\} & \text{(B2)} \\ &\to \exp(\hat{U} + \hat{K}),\ (P \to \infty), & \text{(B3)} \end{aligned}$$

where $P$ is the Trotter number and the product of matrices transform to sum of these. By using this formula and inserting complete system $I = \sum_{\boldsymbol{\sigma}(t)} |\boldsymbol{\sigma}(t)\rangle \langle\boldsymbol{\sigma}(t)|$, the partition function $Z = \mathrm{Tr} e^{-\beta \hat{H}}$ can be calculated as follows:

$$\begin{aligned} Z &= \lim_{P\to\infty} \sum_{\{\boldsymbol{\sigma}(1)\}} \langle\boldsymbol{\sigma}(1)| e^{-\frac{\beta\hat{U}}{P}} |\boldsymbol{\sigma}'(1)\rangle \langle\boldsymbol{\sigma}'(1)| e^{-\frac{\beta\hat{K}}{P}} |\boldsymbol{\sigma}(2)\rangle \langle\boldsymbol{\sigma}(2)| \cdots \\ &\quad \cdots |\boldsymbol{\sigma}(M-1)\rangle \langle\boldsymbol{\sigma}(M)| e^{-\frac{\beta\hat{U}}{P}} |\boldsymbol{\sigma}'(M)\rangle \langle\boldsymbol{\sigma}'(M)| e^{-\frac{\beta\hat{K}}{P}} |\boldsymbol{\sigma}(1)\rangle , \end{aligned} \tag{B4}$$

where $|\boldsymbol{\sigma}_i(t)\rangle = |\sigma_1(t)\rangle \otimes \cdots \otimes |\sigma_N(t)\rangle$ and $\hat{\sigma}_i^z |\sigma_i(t)\rangle = \sigma_i(t) |\sigma_i(t)\rangle$. Because $\hat{U}$ corresponds to the potential term $\hat{H}_0$ which depends on only $\hat{\sigma}^z$, we can derive the following relations:

$$\langle\boldsymbol{\sigma}(t)|e^{-\frac{\beta\hat{U}}{P}}|\boldsymbol{\sigma}'(t)\rangle = \exp\left(-\frac{\beta}{P} H_0(\boldsymbol{\sigma}(t))\right). \tag{B5}$$

We can see, here, the potential term transform to classical spin set $\boldsymbol{\sigma}(t)$ on extra dimension (Trotter dimension). The kinetic term $\hat{K}$ which corresponds to the transverse field can be calculated as follows:

$$\begin{aligned} \langle\boldsymbol{\sigma}(t)|e^{-\frac{\beta\hat{K}}{P}}|\boldsymbol{\sigma}'(t+1)\rangle &= \langle\boldsymbol{\sigma}(t)|e^{\frac{\beta\Gamma}{P}\sum_i \hat{\sigma}_i^x}|\boldsymbol{\sigma}'(t+1)\rangle && \text{(B6)} \\ &= \prod_i \langle\boldsymbol{\sigma}(t)|e^{\frac{\beta\Gamma}{P}\hat{\sigma}_i^x}|\boldsymbol{\sigma}'(t+1)\rangle && \text{(B7)} \\ &= \prod_i \langle\boldsymbol{\sigma}(t)|\hat{I}\cosh\frac{\beta\Gamma}{P} + \hat{\sigma}_i^x \sinh\frac{\beta\Gamma}{P}|\boldsymbol{\sigma}'(t+1)\rangle && \text{(B8)} \\ &= \begin{cases} \prod_i \cosh\frac{\beta\Gamma}{P}, & (\sigma_i(t) = \sigma_i(t+1)) \\ \prod_i \sinh\frac{\beta\Gamma}{P}, & (\sigma_i(t) = -\sigma_i(t+1)) \end{cases} && \text{(B9)} \\ &= \begin{cases} \prod_i \left(\frac{1}{2}\sinh\frac{2\beta\Gamma}{P}\right)^{\frac{1}{2}} (\coth\frac{\beta\Gamma}{P})^{\frac{1}{2}}, & (\sigma_i(t) = \sigma_i(t+1)) \\ \prod_i \left(\frac{1}{2}\sinh\frac{2\beta\Gamma}{P}\right)^{\frac{1}{2}} (\tanh\frac{\beta\Gamma}{P})^{\frac{1}{2}}, & (\sigma_i(t) = -\sigma_i(t+1)) \end{cases} && \text{(B10)} \\ &= \prod_i \left(\frac{1}{2}\sinh\frac{2\beta\Gamma}{P}\right)^{\frac{1}{2}} (\coth\frac{\beta\Gamma}{P})^{\frac{\sigma_i(t)\sigma_i(t+1)}{2}} && \text{(B11)} \\ &= \left(\frac{1}{2}\sinh\frac{2\beta\Gamma}{P}\right)^{\frac{N}{2}} \prod_i (\coth\frac{\beta\Gamma}{P})^{\frac{\sigma_i(t)\sigma_i(t+1)}{2}}. && \text{(B12)} \end{aligned}$$

Then the kinetic term can be transformed to the classical system. In summary, we can derive the final form of the partition function of the system with the transverse field as

follows:

$$Z = \lim_{P\to\infty}\left(\frac{1}{2}\sinh\frac{2\beta\Gamma}{P}\right)^{\frac{NP}{2}}\sum_{\{\boldsymbol{\sigma}(t)\}}\left\{\prod_{t=1}^{P}\exp\left(-\frac{\beta}{P}H_0(\boldsymbol{\sigma}(t))\right)\right\}\prod_{t=1}^{P}\prod_{i=1}^{N}(\coth\frac{\beta\Gamma}{P})^{\frac{\sigma_i(t)\sigma_i(t+1)}{2}} \tag{B13}$$

$$= \lim_{P\to\infty}\left(\frac{1}{2}\sinh\frac{2\beta\Gamma}{P}\right)^{\frac{NP}{2}}\operatorname*{Tr}_{\boldsymbol{\sigma}(t)} e^{-H_{\rm eff}(\boldsymbol{\sigma}(t))} \tag{B14}$$

$$H_{\rm eff}(\boldsymbol{\sigma}(t)) = \frac{\beta}{P}\sum_{t=1}^{P}H_0(\boldsymbol{\sigma}(t)) - \frac{1}{2}\log\left(\coth\frac{\beta\Gamma}{P}\right)\sum_{i=1}^{N}\sum_{t=1}^{P}\sigma_i(t)\sigma_i(t+1). \tag{B15}$$

With attention to the above equation, the quantum system with the transverse field is described as the classical system on the space which has extra dimension. The analysis introduced in this paper are performed by using the effective Hamiltonian $H_{\rm eff}$ in various $\hat{H}_0$ which is defined according to the problems, the image restoration, the error correcting code and CDMA.

# C Derivation of free energy

In this section, we give the detailed calculations for derivation of the state equations in information processing system described as mean-field models. Note that these equations are derived under the conditions of replica symmetry (RS) and static approximation (SA), as we denote above.

## C1 Image restoration

For deriving the free energy, $-\beta[F] = [\log Z]$, we calculate the following quantity,

$$Z = \operatorname*{Tr}_{\boldsymbol{\sigma}}\exp\left\{\frac{\beta}{2NP}\sum_{i\neq j}\sigma_i(t)\sigma_j(t) + \frac{h}{P}\sum_{t=1}^{P}\sum_{i=1}^{N}\tau_i\sigma_i(t) + B\sum_{i=1}^{N}\sum_{t=1}^{P}\sigma_i(t)\sigma_i(t+1)\right\}, \tag{C1}$$

where $B = \frac{1}{2}\log\left(\coth\frac{\beta\Gamma}{P}\right)$. Using the Hubbard-Stratonovich transformation,

$$\exp\left\{\frac{\beta}{2PN}\sum_{t=1}^{P}(\sum_{j=1}^{N}\sigma_j(t))^2\right\} = \prod_{t=1}^{P}\left(\frac{N\beta}{2P\pi}\right)^{\frac{1}{2}}\int dm(t)\exp\left\{-\frac{N\beta}{2P}\sum_{t=1}^{P}m^2(t) + \frac{\beta m(t)}{P}\sum_{t=1}^{P}\sum_{i=1}^{N}\sigma_i(t)\right\}, \tag{C2}$$

we can obtain the following expression:

$$Z = \left(\frac{N\beta}{2P\pi}\right)^{\frac{1}{2}}\int dm(t)\exp\left(-\frac{N\beta}{2P}\sum_{t=1}^{P}m^2(t) + N\log\operatorname*{Tr}_{\sigma}e^{L}\right), \tag{C3}$$

$$L = \frac{1}{P}\left(\beta\sum_{t=1}^{P}m(t)\sigma(t) + h\tau\sum_{t=1}^{P}\sigma(t)\right) + B\sum_{t=1}^{P}\sigma(t)\sigma(t+1). \tag{C4}$$

Here, we use the static approximation (SA) as follows,

$$m(t) = m, \tag{C5}$$

which mean that the order parameter does not depend on the Trotter dimension. Then, we can take the spin trace in the limit $M \to \infty$ as

$$\begin{aligned} \operatorname*{Tr}_{\sigma} e^{L} &= \operatorname*{Tr}_{\sigma} \exp\left(\frac{\beta m + h\tau}{P}\sum_{t=1}^{P}\sigma(t) - B\sum_{t=1}^{P}\sigma(t)\sigma(t+1)\right) && \text{(C6)} \\ &= 2\cosh\sqrt{\Phi^2+\gamma^2} && \text{(C7)} \\ \Phi &= \beta m + h\tau, && \text{(C8)} \end{aligned}$$

where we use the "inverse" S-T decomposition. [1] for the above calculations, we obtain the following expression

$$\log Z \simeq -\frac{N\beta}{2}m^2 + N\log 2\cosh\sqrt{\Phi^2+\gamma^2}. \tag{C9}$$

Next, we should consider the average part $[\cdot] = \mathrm{Tr}_{\boldsymbol{\xi}}\int d\boldsymbol{\tau}P(\boldsymbol{\xi})P(\boldsymbol{\tau}|\boldsymbol{\xi})$. In our formulation, the original image $\boldsymbol{\xi}$ and channel remain classic version even in the quantum case. From the above calculation, we can obtain the averaged free energy per spin as follows:

$$\begin{aligned} -\beta[f] &= -\frac{\beta m^2}{2} + \operatorname*{Tr}_{\xi}\int Du\frac{e^{\beta_s m_0\xi}}{2\cosh\beta_s m_0}\log 2\cosh\sqrt{\Phi^2+\gamma^2} && \text{(C10)} \\ \Phi &= \beta m + ha_\tau u + h\tau_0\xi, && \text{(C11)} \end{aligned}$$

where $u = (\tau - \tau_0\xi)/a_\tau$, $\int Du = \frac{1}{2\sqrt{\pi}}\int due^{-\frac{u^2}{2}}$. We can easily see that the free energy goes to the classical one in $\gamma = 0$. The saddle point conditions of the free energy give the following equations (Inoue 2001):

$$\begin{aligned} m_0 &= \tanh\beta_s m_0 && \text{(C12)} \\ m &= \operatorname*{Tr}_{\boldsymbol{\xi}}\int Du\frac{e^{\beta_s m_0\xi}}{2\cosh\beta_s m_0}\frac{\Phi\tanh\Xi}{\Xi} && \text{(C13)} \\ \Xi &= \sqrt{\Phi^2+\gamma^2}. && \text{(C14)} \end{aligned}$$

The derivation for $m_0$ is the trivial calculation, where it is the magnetization of the original image. Note that $\gamma = \beta\Gamma$.

## C2 Sourlas codes

The replica analysis of the $p$-body spin glass model with the Gaussian interaction and ferromagnetic phase has been done by Obuchi et al (Obuchi et al. 2007). We review the analysis in this section.

In Sourlas code, we start the analysis with the following effective partition function,

$$Z = \operatorname*{Tr}_{\boldsymbol{\sigma}}\exp\left(\frac{\beta}{P}\sum_{i1<\ldots<ip}\sum_{t}J_{i1\ldots ip}\sigma_{i1}(t)\cdots\sigma_{ip}(t) + B\sum_{i}\sum_{t}\sigma_i(t)\sigma_i(t+1)\right), \tag{C15}$$

[1] The detailed calculations for this part are given in Eqs. (C54)-(C59) in the next section.

which can be obtained by applying Suzuki-Trotter decomposition to the Hamiltonian of the Sourlas code with transverse field. Following the replica treatment, we calculate the following quantity

$$[Z^n] = \mathop{\mathrm{Tr}}_{\boldsymbol{\xi}} \int \prod_{i1<\ldots<ip} dJ_{i1\ldots ip} \mathrm{P}(J_{i1\ldots ip}|\xi_1 \ldots \xi_p) \mathrm{P}\left(\{\xi_i\}\right) Z^n \tag{C16}$$

$$= \mathop{\mathrm{Tr}}_{\boldsymbol{\xi}} \int \prod_{i1<\ldots<ip} dJ_{i1\ldots ip} \left(\frac{N^{p-1}}{\pi J^2 p!}\right)^{\frac{1}{2}} \exp\left\{-\frac{N^{p-1}}{J^2 p!} \sum_{i1<\ldots<ip} \left(J_{i1\ldots ip} - \frac{J_0 p!}{N^{p-1}} \xi_{i1} \cdots \xi_{ip}\right)^2\right\} \frac{Z^n}{2^N}. \tag{C17}$$

Next, under the gage transformation,

$$J_{i1\ldots ip} \to J_{i1\ldots ip} \xi_{i1} \cdots \xi_{ip}, \tag{C18}$$

$$\sigma_{ik} \to \sigma_{ik} \xi_{ik} \ \ (k = 1, \cdots p), \tag{C19}$$

the Hamiltonian remain invariant as we see in the classical case. By using this transformation and $\mathrm{Tr}_{\boldsymbol{\xi}} = 2^N$, the Eq. (C17) is

$$[Z^n] = \int \prod_{i1<\ldots<ip} dJ_{i1\ldots ip} \left(\frac{N^{p-1}}{\pi J^2 p!}\right)^{\frac{1}{2}} \exp\left\{-\frac{N^{p-1}}{J^2 p!} \sum_{i1<\ldots<ip} \left(J_{i1\ldots ip} - \frac{J_0 p!}{N^{p-1}}\right)^2\right\} Z^n. \tag{C20}$$

For simplicity, we perform the following displacement,

$$k \equiv \frac{N^{p-1}}{J^2 \pi p!}, \ \ l \equiv \frac{N^{p-1}}{J^2 p!}, \ \ m \equiv \frac{J_0 p!}{N^{p-1}} \tag{C21}$$

$$S_i^\mu(t) \equiv \sigma_{i1}^\mu(t) \cdots \sigma_{ip}^\mu(t), \tag{C22}$$

where $\mu$ is the replica index. [2] Under the transformation, we can rewrite Eq. (C20) as follows:

$$[Z^n] = k^{\frac{N_B}{2}} \int \prod_{i1<\ldots<ip} dJ_{i1\ldots ip} \mathrm{Tr}_{\boldsymbol{\sigma}} \exp\left\{-l \sum_{i1<\ldots<ip} (J_{i1\ldots ip} - m)^2 + \frac{\beta}{P} \sum_{i1<\ldots<ip} \sum_t \sum_\mu J_{i1\ldots ip} S_i^\mu(t) + B \sum_i \sum_t \sum_\mu \sigma_i^\mu(t) \sigma_i^\mu(t+1)\right\}. \tag{C23}$$

Here, $N_B$ is ${}_N C_p$. And then, rewriting the first and second term in the right hand side

[2] Note that the replacement parameter $k$ in Eq. (C21) should note be confused with the index $k$ in Eq. (C19).

of the above equation

$$\exp\left\{-l\sum_{i1<\ldots<ip}(J_{i1\ldots ip}-m)^2+\frac{\beta}{M}\sum_{i1<\ldots<ip}\sum_t\sum_\mu J_{i1\ldots ip}S_i^\mu(t)\right\} \tag{C24}$$

$$=\prod_{i1<\ldots<ip}\exp\left[-l\left\{J_{i1\ldots ip}^2-\frac{1}{2l}\left(2lm+\frac{\beta}{P}\sum_{t,\mu}S_i^\mu(t)\right)\right\}^2\right.$$
$$\left.+\frac{\beta^2}{4lP^2}\left(\sum_{t,\mu}S_i^\mu(t)\right)^2+\frac{m\beta}{P}\sum_{t,\mu}S_i^\mu(t)\right], \tag{C25}$$

we perform the Gaussian integral according to $J_{i1\ldots ip}$ as follows:

$$\int\prod_{i1<\ldots<ip}dJ_{i1\ldots ip}\exp\left[-l\left\{J_{i1\ldots ip}^2-\frac{1}{2l}\left(2lm+\frac{\beta}{P}\sum_{t,\mu}S_i^\mu(t)\right)\right\}^2\right.$$
$$\left.+\frac{\beta^2}{4lP^2}\left(\sum_{t,\mu}S_i^\mu(t)\right)^2+\frac{m\beta}{P}\sum_{t,\mu}S_i^\mu(t)\right] \tag{C26}$$

$$=\left(\frac{\pi}{l}\right)^{\frac{N_B}{2}}\prod_{i1<\ldots<ip}\exp\left\{\frac{\beta^2}{4lP^2}\left(\sum_{t,\mu}S_i^\mu(t)\right)^2+\frac{m\beta}{P}\sum_{t,\mu}S_i^\mu(t)\right\}. \tag{C27}$$

Here by using the following relation,

$$\left(\frac{k\pi}{l}\right)^{\frac{N_B}{2}}=\left(\frac{N^{p-1}}{J^2\pi p!}\pi\frac{J^2p!}{N^{p-1}}\right)^{\frac{N_B}{2}}=1, \tag{C28}$$

the partition function can be represented as follows:

$$[Z^n] = \mathop{\mathrm{Tr}}_{\boldsymbol{\sigma}}\exp\left[B\sum_{i,t,\mu}\sigma_i^\mu(t)\sigma_i^\mu(t+1)+\sum_{i1<\ldots<ip}\left\{\frac{\beta^2}{4lP^2}\left(\sum_{t,\mu}S_i^\mu(t)\right)^2+\frac{m\beta}{P}\sum_{t,\mu}S_i^\mu(t)\right\}\right]. \tag{C29}$$

By using the following relations of each sum,

$$\frac{1}{N^{p-1}}\sum_{i1<\ldots<ip}S_i^\alpha(t) \simeq \frac{N}{p!}\left(\frac{1}{N}\sum_i\sigma_i^\alpha(t)\right)^p \tag{C30}$$

$$\frac{1}{N^{p-1}}\sum_{i1<\ldots<ip}S_i^\alpha(t)S_i^\beta(t') \simeq \frac{N}{p!}\left(\frac{1}{N}\sum_i\sigma_i^\alpha(t)\sigma_i^\beta(t')\right)^p, \tag{C31}$$

Eq. (C23) can be rewritten as follows:

$$[Z^n] = \mathop{\mathrm{Tr}}_{\boldsymbol{\sigma}}\exp\left\{B\sum_{i,t,\mu}\sigma_i^\mu(t)\sigma_i^\mu(t+1)+\frac{\beta^2J^2N}{4P^2}\sum_{t,t'}\sum_{\mu,\nu}\left(\frac{1}{N}\sum_i\sigma_i^\mu(t)\sigma_i^\nu(t')\right)^p\right.$$
$$\left.+\frac{J_0N\beta}{P}\sum_{t,\mu}\left(\frac{1}{N}\sum_i\sigma_i^\mu(t)\right)^p\right\}. \tag{C32}$$

We, here, introduce the following order parameters which characterize the macroscopic property of the system.

$$m_\mu(t) = \frac{1}{N}\sum_i \sigma_i^\alpha(t) \tag{C33}$$

$$Q_{\mu\nu}(t,t') = \frac{1}{N}\sum_i \sigma_i^\mu(t)\sigma_i^\nu(t') \tag{C34}$$

$$Q_{\mu\mu}(t,t') = \frac{1}{N}\sum_i \sigma_i^\mu(t)\sigma_i^\mu(t'). \tag{C35}$$

The physical meaning of $m_\mu(t)$ and $Q_{\mu\nu}(t,t)$ corresponds to magnetize and spin glass order parameter respectively. In the quantum spin glass system, $Q_{\mu\mu}(t,t)$ is newly introduced, which mean the order parameter on the Trotter (extra dimension) axis. Representing the second term of the right hand side in the Eq. (C32) as

$$\begin{aligned}
&\sum_{t,t'}\sum_{\mu,\nu}\left(\frac{1}{N}\sum_i \sigma_i^\mu(t)\sigma_i^\nu(t')\right)^p \\
&= \sum_{t,t'}\left\{\sum_\mu\left(\frac{1}{N}\sum_i \sigma_i^\mu(t)\sigma_i^\mu(t')\right)^p + 2\sum_{\mu<\nu}\left(\frac{1}{N}\sum_i \sigma_i^\mu(t)\sigma_i^\nu(t')\right)^p\right\} \qquad \text{(C36)}\\
&= \sum_{t,t'}\left\{\sum_\mu Q_{\mu\mu}(t,t')^p + 2\sum_{\mu<\nu} Q_{\mu\nu}(t,t')^p\right\}, \qquad \text{(C37)}
\end{aligned}$$

we obtain the partition function incorporating the order parameters as follows:

$$\begin{aligned}
[Z^n] &= \mathop{\mathrm{Tr}}_{\boldsymbol{\sigma}}\int\prod_{\mu,t} dm_\mu(t)d\hat{m}_\mu(t)\prod_{\mu,t,t'} dQ_{\mu\mu}(t,t')d\hat{Q}_{\mu\mu}(t,t')\prod_{\mu<\nu,t,t'} dQ_{\mu\nu}(t,t')d\hat{Q}_{\mu\nu}(t,t')\, e^{\Lambda} \\
&\quad \exp\left\{B\sum_{i,t,\mu}\sigma_i^\mu(t)\sigma_i^\mu(t+1) + \frac{\beta^2J^2N}{4P^2}\sum_{t,t'}\left(\sum_\mu Q_{\mu\mu}(t,t')^p + 2\sum_{\mu<\nu} Q_{\mu\nu}(t,t')^p\right)\right. \\
&\quad \left. + \frac{J_0N\beta}{P}\sum_{t,\mu} m_\mu(t)^p\right\} \qquad \text{(C38)}\\
\Lambda &= \frac{1}{P}\sum_{t,\mu}\hat{m}_\mu(t)\left(\sum_i \sigma_i^\mu(t) - Nm_\mu(t)\right) + \frac{1}{P^2}\sum_{t,t',\mu}\hat{Q}_{\mu\mu}(t,t')\left(\sum_i \sigma_i^\mu(t)\right. \\
&\quad \left. - NQ_{\mu\mu}(t,t')\right) + \frac{1}{P^2}\sum_{t,t',\mu<\nu}\hat{Q}_{\mu\nu}(t,t')\left(\sum_i \sigma_i^\mu(t)\sigma_i^\nu(t) - NQ_{\mu\nu}(t,t')\right), \qquad \text{(C39)}
\end{aligned}$$

where $e^\Lambda$ term is generated from the Fourier transform of a Gaussian function and $\hat{A}$ is conjugate Lagrange multiplier of $A$. Now, we calculate the trace over $\boldsymbol{\sigma} = (\{\sigma^1(t)\},...,\{\sigma^n(t)\})$ to have the explicit form of order parameters. By noting the following relation,

$$\mathop{\mathrm{Tr}}_{\boldsymbol{\sigma}}\exp(\sum_i\cdots) = \mathop{\mathrm{Tr}}_{\boldsymbol{\sigma}}\prod_i\exp(\cdots) = \left\{\mathop{\mathrm{Tr}}_{\sigma^1,...,\sigma^n}\exp(\cdots)\right\}^N = \exp\left\{N\log\mathop{\mathrm{Tr}}_{\sigma^1,...,\sigma^n}\exp(\cdots)\right\} \tag{C40}$$

we can do the trace independently with respect to each $i$-th spins in the $m$-th replica. Thus, the spacial index disappear due to this operation. When we write $\mathrm{Tr}_{\sigma^1,\ldots,\sigma^n}$ as $\mathrm{Tr}_{\boldsymbol{\sigma}}$ again, we can derive the following form:

$$
\begin{aligned}
[Z^n] &= \mathrm{Extr}\ \ F_n\left(m_\mu(t), \hat{m}_\mu(t), Q_{\mu\mu}(t,t'), \hat{Q}_{\mu\mu}(t,t'), Q_{\mu\nu}(t,t'), \hat{Q}_{\mu\nu}(t,t')\right) && \text{(C41)}\\
&= \exp(-\beta n N f) && \text{(C42)}\\
-\beta n f &= \sum_{t,\mu}\left(\frac{J_0\beta}{P} m_\mu(t)^p - \frac{1}{P}\hat{m}_\mu(t) m_\mu(t)\right) + \sum_{t,t',\mu}\left(\frac{\beta^2 J^2}{4P^2} Q_{\mu\mu}(t,t')^p - \frac{1}{P^2}\hat{Q}_{\mu\mu}(t,t') Q_{\mu\mu}(t,t')\right)\\
&\quad + \sum_{t,t',\mu<\nu}\left(\frac{\beta^2 J^2}{2P^2} Q_{\mu\nu}(t,t')^p - \frac{1}{P^2}\hat{Q}_{\mu\nu}(t,t') Q_{\mu\nu}(t,t')\right) + \log \mathrm{Tr}_{\boldsymbol{\sigma}}\, e^L && \text{(C43)}\\
L &= \frac{1}{P}\sum_{t,\mu}\hat{m}_\mu(t)\sigma^\mu(t) + \frac{1}{P^2}\sum_{t,t',\mu}\hat{Q}_{\mu\mu}(t,t')\sigma^\mu(t)\sigma^\mu(t') + \frac{1}{P^2}\sum_{t,t',\mu<\nu}\hat{Q}_{\mu\nu}(t,t')\sigma^\mu(t)\sigma^\nu(t)\\
&\quad + B\sum_{t,\mu}\sigma^\mu(t)\sigma^\mu(t+1), && \text{(C44)}
\end{aligned}
$$

where Extr represents extremization with respect to each order parameters, which corresponds to saddle point condition represented in Appendix A.

Taking the replica symmetry and the static approximation as follows,

$$
\begin{aligned}
&m_\mu(t) = m, \qquad \hat{m}_\mu(t) = \hat{m} && \text{(C45)}\\
&Q_{\mu\mu}(t,t') = \chi, \quad \hat{Q}_{\mu\mu}(t,t') = \hat{\chi} && \text{(C46)}\\
&Q_{\mu\nu}(t,t') = q, \quad \hat{Q}_{\mu\nu}(t,t') = \hat{q}, && \text{(C47)}
\end{aligned}
$$

we can calculate $e^L$ as follows:

$$
\begin{aligned}
e^L &= \exp\left(\frac{\hat{m}}{P}\sum_{t,\mu}\sigma^\alpha(t) + B\sum_{t,\mu}\sigma^\mu(t)\sigma^\mu(t+1)\right)\int Dw \exp\left(\frac{\sqrt{\hat{q}}}{M}\sum_{t,\mu}\sigma^\mu(t) w\right)\\
&\quad \prod_\mu \int Dz \exp\left(\frac{\sqrt{2\hat{\chi}-\hat{q}}}{M}\sum_t \sigma^\mu(t) z\right) && \text{(C48)}\\
&= \int Dz \prod_\mu \int Dz \exp\left\{B\sum_t \sigma^\mu(t)\sigma^\mu(t+1) + \frac{\hat{m} + \sqrt{\hat{q}} w + \sqrt{2\hat{\chi}-\hat{q}} z}{P}\sum_t \sigma^\mu(t)\right\}. && \text{(C49)}
\end{aligned}
$$

Here, the integral of the above equation is inspired by using the Hubbard-Stratonovich transformation to perform trace over $\boldsymbol{\sigma}$:

$$
\begin{aligned}
\exp\left\{\frac{\hat{q}}{2P^2}\left(\sum_{t,\mu}\sigma^\mu(t)\right)^2\right\} &= \int Dw \exp\left(\frac{\sqrt{\hat{q}}}{P}\sum_{t,\mu}\sigma^\mu(t) w\right) && \text{(C50)}\\
\exp\left\{\frac{2\hat{\chi}-\hat{q}}{2P^2}\sum_\mu\left(\sum_t \sigma^\mu(t)\right)^2\right\} &= \prod_\mu \int Dz \exp\left(\frac{\sqrt{2\hat{\chi}-\hat{q}}}{P}\sum_t \sigma^\mu(t) z\right). && \text{(C51)}
\end{aligned}
$$

It is the key point to use the "inverse" S-T formula for performing trace over $\boldsymbol{\sigma}$. That is, we obtain the following equations:

$$\operatorname*{Tr}_{\boldsymbol{\sigma}} \exp\left(B\sum_t \sigma^\alpha(t)\sigma^\alpha(t+1) + \frac{\Phi}{M}\sum_t \sigma^\alpha(t)\right) = \operatorname*{Tr}_{\boldsymbol{\sigma}} \exp\left(\Gamma\hat{\sigma}^x + \Phi\hat{\sigma}^z\right) \tag{C52}$$

$$\Phi = \hat{m} + \sqrt{\hat{q}}w + \sqrt{2\hat{\chi} - \hat{q}}z, \tag{C53}$$

which is the equation is described by Pauli matrices. Then, we can calculate the sum with respect to $\hat{\boldsymbol{\sigma}}$ as follows:

$$\begin{aligned}
&\operatorname*{Tr}_{\boldsymbol{\sigma}} \exp\left(B\sum_t \sigma^\alpha(t)\sigma^\alpha(t+1) + \frac{\Phi}{P}\sum_t \sigma^\alpha(t)\right) && \text{(C54)}\\
=\ &\operatorname*{Tr}_{\boldsymbol{\sigma}} \left(1 + \hat{T} + \frac{1}{2!}\hat{T^2} + \frac{1}{3!}\hat{T^3}\cdots\right) && \text{(C55)}\\
=\ &\operatorname*{Tr}_{\boldsymbol{\sigma}} \left\{\hat{I}\left(1 + \frac{C}{2!} + \frac{C^2}{4!} + \cdots\right) + \hat{T}\left(1 + \frac{C}{3!} + \frac{C^2}{5!} + \cdots\right)\right\} && \text{(C56)}\\
=\ &1 + \frac{C}{2!} + \frac{C^2}{4!} + \cdots && \text{(C57)}\\
=\ &2\cosh\sqrt{C} && \text{(C58)}\\
=\ &2\cosh\sqrt{\Phi^2 + \Gamma^2}, && \text{(C59)}
\end{aligned}$$

where $\hat{T} = \Gamma\hat{\sigma}^x + \Phi\hat{\sigma}^z$ and then $\hat{T}^2 = (\Phi^2 + \Gamma^2)\hat{I} \equiv C\hat{I}$. And we also use the relation, $\mathrm{Tr}\hat{T} = 0$, $\cosh x = \sum_{l=0}^{\infty} \frac{x^{2l}}{(2l)!}$. Therefore, Eq. (C41) under RS and SA can be written as follows:

$$\begin{aligned}
F_n\left(m, \hat{m}, \chi, \hat{\chi}, q, \hat{q}\right) = \exp N\Bigg\{&n\beta J m^p - nm\hat{m} + \frac{n\beta^2 J^2}{4}\chi^p - n\chi\hat{\chi} + \frac{n(n-1)\beta^2 J^2}{4}q^p \\
&- \frac{n(n-1)}{2}q\hat{q} + \log\int Dw\left(\int Dz 2\cosh\sqrt{\Phi^2 + \Gamma^2}\right)^n\Bigg\}. \qquad \text{(C60)}
\end{aligned}$$

In accordance the replica treatment,

$$[\log Z] = \lim_{n\to 0}\frac{[Z]^n - 1}{n} \tag{C61}$$

we can obtain the following expressions for $f = -\frac{[\log Z]}{\beta}$, $\exp(Nx) \simeq 1 + Nx$:

$$\begin{aligned}
F_n\left(m, \hat{m}, \chi, \hat{\chi}, q, \hat{q}\right) &= \exp\left\{-N\beta n f_n\left(m, \hat{m}, \chi, \hat{\chi}, q, \hat{q}\right)\right\} && \text{(C62)}\\
f\left(m, \hat{m}, \chi, \hat{\chi}, q, \hat{q}\right) &= \lim_{n\to 0} f_n\left(m, \hat{m}, \chi, \hat{\chi}, q, \hat{q}\right). && \text{(C63)}
\end{aligned}$$

And then, the free energy of the Sourlas model under RS and SA is

$$\begin{aligned}
-\beta f^{RS}\left(m, \hat{m}, \chi, \hat{\chi}, q, \hat{q}\right) = &\frac{\beta^2 J^2}{4}\left(\chi^p - q^p\right) + \frac{1}{2}q\hat{q} - \chi\hat{\chi} - m\hat{m} + \beta J_0 m^p + \\
&\int Dz \log\int Dz 2\cosh\sqrt{\Phi^2 + \Gamma^2}. \qquad \text{(C64)}
\end{aligned}$$

Note that we, here, use the following relations under $n \to 0$ for deriving the free energy:

$$\begin{aligned}
& \log \int Dw \left( \int Dz 2\cosh \sqrt{\Phi^2 + \Gamma^2} \right)^n \\
= \; & \log \int Dw \exp \left\{ n \log \left( \int Dz 2\cosh \sqrt{\Phi^2 + \Gamma^2} \right) \right\} && \text{(C65)} \\
\simeq \; & \log \int Dw \left\{ 1 + n \log \left( \int Dz 2\cosh \sqrt{\Phi^2 + \Gamma^2} \right) \right\} && \text{(C66)} \\
\simeq \; & n \int Dw \log \left( \int Dz 2\cosh \sqrt{\Phi^2 + \Gamma^2} \right). && \text{(C67)}
\end{aligned}$$

The saddle point conditions that the free energy is extremized with respect to the variables are

$$\begin{aligned}
m &= \int Dw \int Dz \frac{\Phi \sinh \Xi}{\Omega \Xi} && \text{(C68)} \\
q &= \int Dw \left( \int Dz \frac{\Phi \sinh \Xi}{\Omega \Xi} \right)^2 && \text{(C69)} \\
\chi &= \int \frac{Dw}{\Omega} \int Dz \left( \frac{\beta^2 \Gamma^2 \sinh \Xi}{\Xi^3} + \frac{\Phi^2 \cosh \Xi}{\Xi^2} \right) && \text{(C70)} \\
\hat{m} &= \beta p J_0 m^{p-1} && \text{(C71)} \\
\hat{q} &= \frac{\beta^2 J^2 p}{2} q^{p-1} && \text{(C72)} \\
\hat{\chi} &= \frac{\beta^2 J^2 p}{4} \chi^{p-1} && \text{(C73)} \\
\Xi &= \sqrt{\Phi^2 + \beta^2 \Gamma^2} && \text{(C74)} \\
\Phi &= \hat{m} + \sqrt{\hat{q}} w + \sqrt{2\hat{\chi} - \hat{q}} z && \text{(C75)} \\
\Omega &\equiv \int Dz \cosh \Xi. && \text{(C76)}
\end{aligned}$$

For $\Gamma = 0$, these equations reduce to the state equations for the classical case corresponding that (4.26)-(4.31). In the classical case that $\Gamma = 1$, we can see that $\chi = 1$.

## C3 CDMA multiuser demodulation

We derive the explicit expression for free energy (5.38) in this appendix.

We first introduce the following transformation,

$$u_0^k = \frac{1}{\sqrt{N}} \sum_{i=1}^{N} \eta_i^k \xi_i, \quad u_\mu^k(t) = \frac{1}{\sqrt{N}} \sum_{i=1}^{N} \eta_i^k \sigma_i^\mu(t), \tag{C77}$$

where $k$ stands for the spreading code index, $\mu$ denotes the replica index, $t$ represents the Trotter index and $i$ is the spatial index. Then, we write the partition function

(5.34) in terms of the Fourier transform as:

$$
\begin{aligned}
[Z^n] = & \frac{1}{2^N}\frac{1}{2^{NK}}\sum_{\mathbf{H}}\sum_{\{\boldsymbol{\sigma}^k(s)\}}\mathop{\mathrm{Tr}}_{\boldsymbol{\xi}}\mathop{\mathrm{Tr}}_{\{\boldsymbol{\sigma}^\mu(t)\}}\int\prod_k\frac{du_0^k d\hat{u}_0^k}{2\pi}\exp\left(i\hat{u}_0^k(u_0^k-\frac{1}{\sqrt{N}}\sum_i\eta_i^k\xi_i)\right) \\
& \prod_k\prod_{\mu,t}\frac{du_\mu^k(t)d\hat{u}_\mu^k(t)}{2\pi}\exp\left(i\hat{u}_\mu^k(t)(u_\mu^k(t)-\frac{1}{\sqrt{N}}\sum_i\eta_i^k\sigma_i^\mu(t))\right)\prod_k dy^k\left(\frac{\beta_0}{2\pi}\right)^{\frac{1}{2}}\exp\left(-\frac{\beta_0}{2}(y^k-u_0^k)^2\right) \\
\times \quad & \exp\left(-\frac{\beta}{P}\sum_{\mu,t}\sum_k(\frac{1}{2}(u_\mu^k(t))^2-y^k u_\mu^k(t))\right)\exp\left(B\sum_{\mu,t}\sum_i\sigma_i^\mu(t)\sigma_i^\mu(t+1)\right). \qquad \text{(C78)}
\end{aligned}
$$

Here, we carry out the sum of $\mathbf{H}$ in the above expression as:

$$
\begin{aligned}
L_\xi \equiv & \frac{1}{2^{NK}}\sum_{\mathbf{H}}\prod_k\exp\left(-\frac{i\hat{u}_0^k}{\sqrt{N}}\sum_i\eta_i^k\xi_i\right)\prod_{\mu,t}\prod_k\exp\left(-\frac{i\hat{u}_\mu^k(t)}{\sqrt{N}}\sum_i\eta_i^k\sigma_i^\mu(t)\right) \qquad \text{(C79)} \\
= & \prod_{i,k}\frac{1}{2}\sum_{\eta_i^k}\exp\left\{-\frac{i\eta_i^k}{\sqrt{N}}\left(\hat{u}_0^k\xi_i+\sum_{\mu,t}\hat{u}_\mu^k(t)\sigma_i^\mu(t)\right)\right\} \qquad \text{(C80)} \\
= & \prod_{i,k}\cos\left\{\frac{1}{\sqrt{N}}\left(\hat{u}_0^k\xi_i+\sum_{\mu,t}\hat{u}_\mu^k(t)\sigma_i^\mu(t)\right)\right\} \qquad \text{(C81)} \\
\simeq & \prod_{i,k}\exp\left\{-\frac{1}{2N}\left(\hat{u}_0^k\xi_i+\sum_{\mu,t}\hat{u}_\mu^k(t)\sigma_i^\mu(t)\right)^2\right\} \qquad \text{(C82)} \\
= & \prod_{i,k}\exp\left\{-\frac{1}{2N}(\hat{u}_0^k)^2-\frac{1}{2N}\sum_\mu\left(\sum_t\hat{u}_\mu^k(t)\sigma_i^\mu(t)\right)^2\right. \\
& \left.-\frac{1}{N}\sum_{\mu<\nu}\sum_{t,t'}\hat{u}_\mu^k(t)\hat{u}_\nu^k(t')\sigma_i^\mu(t)\sigma_i^\nu(t')-\frac{1}{N}\hat{u}_0^k\xi_i\sum_{\mu,t}\hat{u}_\mu^k(t)\sigma_i^\mu(t)\right\}. \qquad \text{(C83)}
\end{aligned}
$$

By introducing the order parameters defined by (5.35)-(5.37), we have:

$$
\begin{aligned}
L_\xi = & \int\prod_{\mu,t}dR_\mu(t)\delta\left(R_\mu(t)-\frac{1}{N}\sum_i\xi_i\sigma_i^\mu(t)\right)\prod_{\mu,t,t'}dQ_{\mu\mu}(t,t')\delta\left(Q_{\mu\mu}(t,t')-\frac{1}{N}\sum_i\sigma_i^\mu(t)\sigma_i^\mu(t')\right) \\
\times & \prod_{\mu<\nu,t,t'}dQ_{\mu\nu}(t,t')\delta\left(Q_{\mu\nu}(t,t')-\frac{1}{N}\sum_i\sigma_i^\mu(t)\sigma_i^\nu(t')\right)\exp\left\{-\frac{1}{2}\sum_k(\hat{u}_0^k)^2\right. \\
- & \left.\frac{1}{2}\sum_{\mu,k}\sum_{t,t'}\hat{u}_\mu^k(t)\hat{u}_\mu^k(t')Q_{\mu\mu}(t,t')-\sum_{\mu<\nu}\sum_{t,t',k}\hat{u}_\mu^k(t)\hat{u}_\nu^k(t')Q_{\mu\nu}(t,t')-\sum_k\hat{u}_0^k\sum_{\mu,t}\hat{u}_\mu^k(t)R_\mu(t)\right\}. \qquad \text{(C84)}
\end{aligned}
$$

From the above calculations, we rewrite the partition function (C78) as:

$$
\begin{aligned}
[Z^n] &= \int \left(\prod_{\mu,t} \frac{Nid\hat{R}_\mu(t)dR_\mu(t)}{2\pi}\right)\left(\prod_{\mu,t,t'} \frac{Nid\hat{Q}_{\mu\mu}(t,t')dQ_{\mu\mu}(t,t')}{2\pi}\right) \\
&\quad \times \left(\prod_{\mu<\nu,t,t'} \frac{Nid\hat{Q}_{\mu\nu}(t,t')dQ_{\mu\nu}(t,t')}{2\pi}\right) e^{N(g_1+g_2+g_3)} \qquad \text{(C85)} \\
e^{Ng_1} &= \int \left(\prod_k \frac{du_0^k d\hat{u}_0^k}{2\pi}\right)\left(\prod_{k,\mu,t} \frac{du_\mu^k(t)d\hat{u}_\mu^k(t)}{2\pi}\right)\left(\prod_k dy^k \left(\frac{\beta_0}{2\pi}\right)^{\frac{1}{2}}\right) \exp\left\{-\frac{\beta_0}{2}\sum_k (y^k-u_0^k)^2\right. \\
&\quad -\sum_k \hat{u}_0^k \sum_{\mu,t} \hat{u}_\mu^k(t)R_\mu(t) - \frac{1}{2}\sum_{\mu,k}\sum_{t,t'} \hat{u}_\mu^k(t)\hat{u}_\mu^k(t')Q_{\mu\mu}(t,t') - \sum_{\mu<\nu}\sum_{t,t',k} \hat{u}_\mu^k(t)\hat{u}_\nu^k(t')Q_{\mu\nu}(t,t') \\
&\quad \left.-\frac{1}{2}\sum_k (\hat{u}_0^k)^2 + i\sum_k u_0^k\hat{u}_0^k + i\sum_{k,\mu,t} u_\mu^k(t)\hat{u}_\mu^k(t) - \frac{\beta}{2P}\sum_{\mu,t,k}((u_\mu^k(t))^2 - 2u_\mu^k(t)y^k)\right\} \qquad \text{(C86)} \\
e^{Ng_2} &= \mathop{\mathrm{Tr}}_{\boldsymbol{\xi}} P(\boldsymbol{\xi}) \mathop{\mathrm{Tr}}_{\{\boldsymbol{\sigma}^\mu(t)\}} \exp\left\{\frac{1}{P}\sum_{\mu,t}\hat{R}_\mu(t)\sum_i \xi_i\sigma_i^\mu(t) + \frac{1}{P^2}\sum_{\mu,t,t'}\hat{Q}_{\mu\mu}(t,t')\sum_i \sigma_i^\mu(t)\sigma_i^\mu(t') + \right. \\
&\quad \left. \frac{1}{P^2}\sum_{\mu<\nu,t,t'}\hat{Q}_{\mu\nu}(t,t')\sum_i \sigma_i^\mu(t)\sigma_i^\nu(t') + B\sum_{t,\mu}\sum_i \sigma_i^\mu(t)\sigma_i^\mu(t+1)\right\} \qquad \text{(C87)} \\
e^{Ng_3} &= \exp\left\{-\frac{N}{P}\sum_{\mu,t}\hat{R}_\mu(t)R_\mu(t) - \frac{N}{P^2}\sum_{\mu,t,t'}\hat{Q}_{\mu\mu}(t,t')Q_{\mu\mu}(t,t') - \frac{N}{P^2}\sum_{\mu<\nu,t,t'}\hat{Q}_{\mu\nu}(t,t')Q_{\mu\nu}(t,t')\right\}. \qquad \text{(C88)}
\end{aligned}
$$

In the following, we calculate $e^{Ng_1}, e^{Ng_2}$ and $e^{Ng_3}$, and then derive the free energy of the CDMA model with the transverse field.

By integrating $u_0^k$ and $\hat{u}_0^k$ in Eq. (C86), $e^{Ng_1}$ can be expressed as:

$$
\begin{aligned}
e^{Ng_1} &= \int \left(\prod_{k,\mu,t} \frac{du_\mu^k(t)d\hat{u}_\mu^k(t)}{2\pi}\right)\left(\prod_k dy^k \frac{1}{2\pi}\sqrt{\frac{2\beta_0\pi}{1+\beta_0}}\right) \exp\left\{-\frac{1}{2}\sum_{\mu,k}\sum_{t,t'} \hat{u}_\mu^k(t)\hat{u}_\mu^k(t')Q_{\mu\mu}(t,t')\right. \\
&\quad -\sum_{\mu<\nu}\sum_{t,t',k} \hat{u}_\mu^k(t)\hat{u}_\nu^k(t')Q_{\mu\nu}(t,t') + i\sum_{k,\mu,t} u_\mu^k(t)\hat{u}_\mu^k(t) - \frac{\beta}{2P}\sum_{\mu,t,k}((u_\mu^k(t))^2 - 2u_\mu^k(t)y^k) \\
&\quad \left.-\frac{\beta_0}{2(1+\beta_0)}\sum_k (y^k)^2 - \frac{i\beta_0}{1+\beta_0}\sum_k y^k \sum_{\mu,t}\hat{u}_\mu^k(t)R_\mu(t) + \frac{\beta_0}{2(1+\beta_0)}\sum_k\left(\sum_{\mu,t}\hat{u}_\mu^k(t)R_\mu(t)\right)^2\right\}. \qquad \text{(C89)}
\end{aligned}
$$

The integration over $y^k$ in the above equation can be carried out as:

$$\int \left(\prod_k dy^k\right) \exp\left(\frac{\beta}{P}\sum_{\mu,k,t} u_\mu^k(t) y^k - \frac{\beta_0}{2(1+\beta_0)}\sum_k (y^k)^2 - \frac{i\beta_0}{1+\beta_0}\sum_k y^k \sum_{\mu,t} \hat{u}_\mu^k(t) R_\mu(t)\right)$$

$$= \int \prod_k dy^k \exp\left(-\frac{\beta_0}{2(1+\beta_0)}(y^k)^2 + \left(\frac{\beta}{P}\sum_{\mu,t} u_\mu^k(t) - \frac{i\beta_0}{1+\beta_0}\sum_{\mu,t}\hat{u}_\mu^k(t) R_\mu(t)\right) y^k\right) \tag{C90}$$

$$= \prod_k \sqrt{\frac{2(1+\beta_0)\pi}{\beta_0}} \exp\left(\frac{1+\beta_0}{2\beta_0}\left(\frac{\beta}{P}\sum_{\mu,t} u_\mu^k(t) - \frac{i\beta_0}{1+\beta_0}\sum_{\mu,t}\hat{u}_\mu^k(t) R_\mu(t)\right)^2\right) \tag{C91}$$

$$= \prod_k \sqrt{\frac{2(1+\beta_0)\pi}{\beta_0}} \exp\left\{\frac{\beta^2(1+\beta_0)}{2\beta_0 P^2}\left(\sum_{\mu,t} u_\mu^k(t)\right)^2 - \frac{i\beta}{P}\left(\sum_{\mu,t} u_\mu^k(t)\right)\left(\sum_{\mu,t}\hat{u}_\mu^k(t) R_\mu(t)\right)\right.$$
$$\left. -\frac{\beta_0}{2(1+\beta_0)}\left(\sum_{\mu,t}\hat{u}_\mu^k(t) R_\mu(t)\right)^2\right\}. \tag{C92}$$

The integration over $u_\mu^k(t)$ can be carried out independently for each $k$ as:

$$\prod_k \int \left(\prod_{\mu,t} du_\mu^k(t)\right) \exp\left\{i\sum_{\mu,t} u_\mu^k(t)\hat{u}_\mu^k(t) - \frac{\beta}{2P}\sum_{\mu,t}(u_\mu^k(t))^2 + \frac{\beta^2(1+\beta_0)}{2\beta_0 P^2}\left(\sum_{\mu,t} u_\mu^k(t)\right)^2\right.$$
$$\left. -\frac{i\beta}{P}\left(\sum_{\mu,t} u_\mu^k(t)\right)\left(\sum_{\mu,t}\hat{u}_\mu^k(t) R_\mu(t)\right)\right\} \tag{C93}$$

$$= \prod_k \int Da \left(\prod_{\mu,t} du_\mu^k(t)\right) \exp\left\{\frac{a\beta}{P}\sqrt{\frac{1+\beta_0}{\beta_0}}\sum_{\mu,t} u_\mu^k(t) + i\sum_{\mu,t} u_\mu^k(t)\hat{u}_\mu^k(t) - \frac{\beta}{2P}\sum_{\mu,t}(u_\mu^k(t))^2\right.$$
$$\left. -\frac{i\beta}{P}\left(\sum_{\mu,t} u_\mu^k(t)\right)\left(\sum_{\mu,t}\hat{u}_\mu^k(t) R_\mu(t)\right)\right\} \tag{C94}$$

$$= \prod_k \int Da \prod_{\mu,t} \sqrt{\frac{2P\pi}{\beta}} \exp\left\{\frac{P}{2\beta}\left(\frac{a\beta}{P}\sqrt{\frac{1+\beta_0}{\beta_0}} + i\hat{u}_\mu^k(t) - \frac{i\beta}{P}\sum_{\nu,t'}\hat{u}_\nu^k(t') R_\nu(t')\right)^2\right\} \tag{C95}$$

$$= \prod_k \int Da \prod_{\mu,t} \sqrt{\frac{2P\pi}{\beta}} \exp\left\{\frac{a^2\beta(1+\beta_0)}{2P\beta_0} - \frac{P}{2\beta}(\hat{u}_\mu^k(t))^2 - \frac{\beta}{2P}\left(\sum_{\nu,t'}\hat{u}_\nu^k(t') R_\nu(t')\right)^2\right.$$
$$\left. +ia\sqrt{\frac{1+\beta_0}{\beta_0}}\hat{u}_\mu^k(t) + \left(\sum_{\nu,t'}\hat{u}_\nu^k(t') R_\nu(t')\right)\hat{u}_\mu^k(t) - \frac{ia\beta}{P}\sqrt{\frac{1+\beta_0}{\beta_0}}\left(\sum_{\nu,t'}\hat{u}_\nu^k(t') R_\nu(t')\right)\right\}, \tag{C96}$$

when we apply Hubbard-Stratonovich transformation:

$$\exp\left(\frac{x^2}{2}\right) = \int Da e^{ax}, \quad \left(Da = \frac{da e^{-a^2/2}}{\sqrt{2\pi}}\right), \tag{C97}$$

to term $(u_\mu^k(t))^2$ in Eq. (C93).

Here, we assume replica symmetry (RS) and static approximation (SA) (Bray and Moore 1980):

$$R_\mu(t) = R, \;\; Q_{\mu\nu}(t,t') = q, \;\; Q_{\mu\mu}(t,t') = \chi \; (t \neq t') \tag{C98}$$

$$\hat{R}_\mu(t) = \hat{R}, \;\; \hat{Q}_{\mu\nu}(t,t') = \hat{q}, \;\; \hat{Q}_{\mu\mu}(t,t') = \hat{\chi}. \tag{C99}$$

Note that the following relation exits for $Q_{\mu\mu}(t,t) = 1$ under RS and SA:

$$\sum_{k,\mu}\sum_{t,t'} \hat{u}_\mu^k(t)\hat{u}_\mu^k(t')Q_{\mu\mu}(t,t') \to \chi \sum_{k,\mu}\sum_{t,t'} \hat{u}_\mu^k(t)\hat{u}_\mu^k(t') - (\chi-1)\sum_{k,\mu,t}(\hat{u}_\mu^k(t))^2. \tag{C100}$$

By using the Hubbard-Stratonovich transformation on $(\sum_\mu \sum_t)^2$ and $\sum_\mu(\sum_t)^2$ and bearing in mind the order of the product of indices, $k$, $\mu$, and $t$, we have:

$$\begin{aligned} e^{Ng_1} &= \prod_k \int Da \int Db \prod_\mu \int Dc \prod_t \frac{d\hat{u}_\mu^k(t)}{2\pi}\sqrt{\frac{2P\pi}{\beta}} \exp\left[\frac{a^2\beta(1+\beta_0)}{2P\beta_0} - \frac{P-\beta(\chi-1)}{2\beta}(\hat{u}_\mu^k(t))^2\right. \\ &\quad \left. + \left\{ai\sqrt{\frac{1+\beta_0}{\beta_0}}(1-n\beta R) + b\sqrt{2R-q-n\beta R^2} + c\sqrt{q-\chi}\right\}\hat{u}_\mu^k(t)\right] \qquad \text{(C101)} \\ &= \prod_k \int Da \int Db \exp\left(\frac{na^2\beta(1+\beta_0)}{2\beta_0}\right) \prod_\mu \int Dc \prod_t \frac{1}{2\pi}\sqrt{\frac{2P\pi}{\beta}}\sqrt{\frac{2\beta\pi}{P-\beta(\chi-1)}} \\ &\times \exp\left\{\frac{\beta}{2P}\left(ai\sqrt{\frac{1+\beta_0}{\beta_0}}(1-n\beta R) + b\sqrt{2R-q-n\beta R^2} + c\sqrt{q-\chi}\right)^2\right\}. \qquad \text{(C102)} \end{aligned}$$

Here, we introduce the following replacements to simplify the above equation:

$$A \equiv i\sqrt{\frac{1+\beta_0}{\beta_0}}(1-n\beta R) \tag{C103}$$

$$B \equiv \sqrt{2R-q-n\beta R^2} \tag{C104}$$

$$C \equiv \sqrt{q-\chi} \tag{C105}$$

$$X_{ab} \equiv Aa + Bb. \tag{C106}$$

The coefficient under the condition that $P \to \infty$ can be transformed as:

$$\begin{aligned} \prod_t \sqrt{\frac{P}{P-\beta(\chi-1)}} &\simeq \prod_t \left\{1 + \frac{\beta}{2P}(\chi-1)\right\} \qquad \text{(C107)} \\ &\simeq \prod_t \exp\log\left\{1 + \frac{\beta}{2P}(\chi-1)\right\} \qquad \text{(C108)} \\ &\simeq \exp\left(\frac{\beta}{2}(\chi-1)\right). \qquad \text{(C109)} \end{aligned}$$

Then, we carry out integrations over $a$, $b$, and $c$ as:

$$\begin{aligned}
e^{Ng_1} &= \prod_k \int Da \int Db \exp\left(\frac{na^2\beta(1+\beta_0)}{2\beta_0} + \frac{n\beta}{2}(\chi-1)\right) \prod_\mu \int Dc \exp\left(\frac{\beta}{2}(X_{ab}+Cc)^2\right) \\
&= \prod_k \exp\left(\frac{n\beta}{2}(\chi-1)\right)\left(\frac{1}{1-\beta C^2}\right)^{\frac{n}{2}} \int Da \int Db \exp\left\{\frac{n\beta}{2}\left(\frac{1+\beta_0}{\beta_0}a^2 + \frac{X_{ab}^2}{1-\beta C^2}\right)\right\} \\
&\simeq \prod_k \exp\left(\frac{n\beta}{2}(\chi-1)\right)\left(\frac{1}{1-\beta C^2}\right)^{\frac{n}{2}} \int Da \int Db \left\{1 + \frac{n\beta}{2}\left(\frac{1+\beta_0}{\beta_0}a^2 + \frac{X_{ab}^2}{1-\beta C^2}\right)\right\} \\
&= \prod_k \exp\left(\frac{n\beta}{2}(\chi-1)\right)\left(\frac{1}{1-\beta C^2}\right)^{\frac{n}{2}} \left\{1 + \frac{\beta n}{2}\left(\frac{1+\beta_0}{\beta_0} + \frac{A^2+B^2}{1-\beta C^2}\right)\right\} \\
&= \prod_k \exp\left(\frac{n\beta}{2}(\chi-1)\right)\left(\frac{1}{1-\beta C^2}\right)^{\frac{n}{2}} \left\{1 + \frac{\beta n}{2}\left(\frac{1+\beta_0}{\beta_0} + \frac{2R-q-(1+\beta_0^{-1})}{1-\beta(q-\chi)}\right) + O(n^2)\right\} \\
&\simeq \prod_k \exp\left[\frac{n}{2}\left\{-\log(1-\beta(q-\chi)) + \frac{\beta(1+\beta_0)}{\beta_0} + \frac{\beta(2R-q-(1+\beta_0^{-1}))}{1-\beta(q-\chi)} + \beta(\chi-1)\right\}\right].
\end{aligned}$$

For $\alpha \equiv K/N$, we derive the final expression of $g_1$ as:

$$\frac{g_1}{n} \simeq \frac{\alpha}{2}\left\{-\log(1-\beta(q-\chi)) + \frac{\beta(1+\beta_0)}{\beta_0} + \frac{\beta(2R-q-(1+\beta_0^{-1}))}{1-\beta(q-\chi)} + \beta(\chi-1)\right\}. \tag{C110}$$

We next calculate $e^{Ng_2}$ under RS and SA conditions as:

$$\begin{aligned}
& e^{Ng_2} \\
&= \mathop{\mathrm{Tr}}_{\boldsymbol{\xi}} P(\boldsymbol{\xi}) \mathop{\mathrm{Tr}}_{\{\boldsymbol{\sigma}^\mu(t)\}} \exp\left\{\frac{\hat{R}}{P}\sum_{\mu,t}\sum_i \xi_i\sigma_i^\mu(t) + \frac{\hat{\chi}}{P^2}\sum_{\mu,t,t'}\sum_i \sigma_i^\mu(t)\sigma_i^\mu(t') + \right. \\
&\left. \frac{\hat{q}}{2P^2}\sum_i\left(\sum_{\mu,t}\sigma_i^\mu(t)\right)^2 - \frac{\hat{q}}{2P^2}\sum_i\sum_\mu\left(\sum_t \sigma_i^\mu(t)\right)^2 + B\sum_{t,\mu}\sum_i \sigma_i^\mu(t)\sigma_i^\mu(t+1)\right\} \qquad \text{(C111)} \\
&= \frac{1}{2^N}\mathop{\mathrm{Tr}}_{\boldsymbol{\xi}}\mathop{\mathrm{Tr}}_{\{\boldsymbol{\sigma}^\mu(t)\}}\prod_i\int Dw \exp\left(\frac{w\sqrt{\hat{q}}}{P}\sum_{\mu,t}\sigma_i^\mu(t)\right)\prod_\mu\int Dz\exp\left(\frac{z\sqrt{2\hat{\chi}-\hat{q}}}{P}\sum_t\sigma_i^\mu(t)\right) \\
&\exp\left\{\frac{\hat{R}}{P}\sum_t\sum_i\xi_i\sigma_i^\mu(t) + B\sum_t\sigma_i^\mu(t)\sigma_i^\mu(t+1)\right\} \qquad \text{(C112)} \\
&= \prod_i\frac{1}{2}\mathop{\mathrm{Tr}}_{\xi_i}\int Dw\exp\left(\frac{w\sqrt{\hat{q}}}{P}\sum_{\mu,t}\sigma_i^\mu(t)\right)\prod_\mu\int Dz\exp\left(\frac{z\sqrt{2\hat{\chi}-\hat{q}}}{P}\sum_t\sigma_i^\mu(t)\right) \\
&\mathop{\mathrm{Tr}}_{\sigma_i^\mu(t)}\exp\left\{\frac{\hat{R}}{P}\sum_t\sum_i\xi_i\sigma_i^\mu(t) + B\sum_t\sigma_i^\mu(t)\sigma_i^\mu(t+1)\right\} \qquad \text{(C113)} \\
&= \prod_i\frac{1}{2}\mathop{\mathrm{Tr}}_{\xi_i}\int Dw\prod_\mu\int Dz\mathop{\mathrm{Tr}}_{\sigma_i^\mu(t)}\exp\left\{\frac{z\sqrt{2\hat{\chi}-\hat{q}}+w\sqrt{\hat{q}}+\hat{R}\xi_i}{P}\sum_t\sigma_i^\mu(t) + B\sum_t\sigma_i^\mu(t)\sigma_i^\mu(t+1)\right\}. \qquad \text{(C114)}
\end{aligned}$$

By applying ST decomposition to the above equation, we can take a spin trace as:

$$e^{Ng_2} \rightarrow \prod_i \frac{1}{2}\mathop{\mathrm{Tr}}_{\xi_i} \int Dw \prod_\mu \int Dz \mathrm{Tr} \exp\left\{(z\sqrt{2\hat{\chi}-\hat{q}} + w\sqrt{\hat{q}} + \hat{R}\xi_i)\hat{\sigma}_i^z + \beta\Gamma\hat{\sigma}_i^x\right\} \tag{C115}$$

$$= \prod_i \frac{1}{2}\mathop{\mathrm{Tr}}_{\xi_i} \int Dw \prod_\mu \int Dz 2\cosh\sqrt{\Phi(\xi_i)^2+\beta^2\Gamma^2} \tag{C116}$$

$$= \prod_i \frac{1}{2}\mathop{\mathrm{Tr}}_{\xi_i} \int Dw \left(\int Dz 2\cosh\sqrt{\Phi(\xi_i)^2+\beta^2\Gamma^2}\right)^n \tag{C117}$$

$$\simeq \prod_i \int Dw \left(\int Dz 2\cosh\sqrt{\Phi^2+\beta^2\Gamma^2}\right)^n \tag{C118}$$

$$\simeq \exp N\log\left\{1 + n\int Dz \log\left(\int Dw 2\cosh\sqrt{\Phi^2+\beta^2\Gamma^2}\right)\right\} \tag{C119}$$

$$= \exp Nn\int Dz \log\left(\int Dw 2\cosh\sqrt{\Phi^2+\beta^2\Gamma^2}\right), \tag{C120}$$

where

$$\Phi(\xi_i) = z\sqrt{2\hat{\chi}-\hat{q}} + w\sqrt{\hat{q}} + \hat{R}\xi_i. \tag{C121}$$

Therefore, we obtain:

$$\frac{g_2}{n} \simeq \int Dz \log\left(\int Dw 2\cosh\sqrt{\Phi^2+\beta^2\Gamma^2}\right) \tag{C122}$$

$$\Phi = w\sqrt{2\hat{\chi}-\hat{q}} + z\sqrt{\hat{q}} + \hat{R}. \tag{C123}$$

We finally calculate $e^{Ng_3}$ under RS and SA conditions as:

$$e^{Ng_3} \simeq \exp\left\{nN\left(-\hat{R}R - \hat{\chi}\chi + \frac{\hat{q}q}{2}\right)\right\}.$$

Thus, we obtain the following form:

$$\frac{g_3}{n} \simeq -\hat{R}R - \hat{\chi}\chi + \frac{\hat{q}q}{2}. \tag{C124}$$

From Eqs. (C110), (C122), and (C124), we obtain the free energy density as:

$$-\beta f = \frac{g_1}{n} + \frac{g_2}{n} + \frac{g_3}{n} \tag{C125}$$

$$= \frac{\alpha}{2}\left\{-\log(1-\beta(q-\chi)) + \frac{\beta(1+\beta_0)}{\beta_0} + \frac{\beta(2R-q-(1+\beta_0^{-1}))}{1-\beta(q-\chi)} + \beta(\chi-1)\right\} - \hat{R}R$$
$$-\hat{\chi}\chi + \frac{\hat{q}q}{2} + \int Dz\log\left(\int Dw 2\cosh\sqrt{\Phi^2+\beta^2\Gamma^2}\right) \tag{C126}$$

$$\Phi = \frac{\phi}{\beta} = w\sqrt{2\hat{\chi}-\hat{q}} + z\sqrt{\hat{q}} + \hat{R}. \tag{C127}$$

Considering the classical limits $\Gamma = 0$ and $\chi = 1$, the classical free energy is recovered.

# D Derivation of the Overlap

In this section, we derive the explicit expression for the overlap $M$ of information processing models with the transverse field generally in a similar way to the classical case (Nishimori 2001). Adding the external term $h\sum_i \sigma_i^\mu(t)\sigma_i^\nu(t')$ to the partition function $[Z^n]$, we obtain

$$[Z^n]_{\mu\nu}(t,t') = \mathop{\mathrm{Tr}}_{\boldsymbol{\xi}} P(\boldsymbol{\xi}) \int d\boldsymbol{y} P(\boldsymbol{y}|\boldsymbol{\xi}) \exp\left\{ -\frac{\beta}{P}\sum_{t,\mu} H(\boldsymbol{\sigma}^\mu(t)) + B\sum_{\mu,t,i}\sigma_i^\mu(t)\sigma_i^\mu(t+1) + h\sum_i \sigma_i^\mu(t)\sigma_i^\nu(t') \right\}, \tag{D1}$$

where $B = \log\left(\coth\frac{\beta\Gamma}{P}\right)/2$, and $\boldsymbol{\sigma} = (\boldsymbol{\sigma}^1, ..., \boldsymbol{\sigma}^n), \boldsymbol{\sigma}^k = (\sigma_1^k(t), ...\sigma_N^k(t)), t = 1, ..., P$. The expression $\mu$ and $\nu$ represent the replica indices and $t$ represents the Trotter index. Note that $\boldsymbol{y}$ which corresponds to $\boldsymbol{\tau}$ in the image restoration or $\boldsymbol{J}$ in the error correcting code respectively represents the received information sequence. As we saw the above appendices, after introducing the following variables, [3]

$$m_\mu(t) = \frac{1}{N}\sum_i \sigma_i^\mu(t) \tag{D2}$$

$$Q_{\mu\nu}(t,t') = \frac{1}{N}\sum_i \sigma_i^\mu(t)\sigma_i^\nu(t') \tag{D3}$$

$$Q_{\mu\mu}(t,t') = \frac{1}{N}\sum_i \sigma_i^\mu(t)\sigma_i^\mu(t'), \tag{D4}$$

we can rewrite Eq. (D1) in thermodynamic limit $N\to\infty$ as

$$[Z^n] \simeq \exp(-\beta n N f) \tag{D5}$$

$$-\beta n f = L_0(m_\mu(t), \hat{m}_\mu(t), Q_{\mu\nu}(t,t'), \hat{Q}_{\mu\nu}(t,t'), Q_{\mu\mu}(t,t'), \hat{Q}_{\mu\mu}(t,t')) + \log \mathop{\mathrm{Tr}}_{\boldsymbol{\sigma}} e^L \tag{D6}$$

$$L = \frac{l_m}{P}\sum_{t,\mu}\hat{m}_\mu(t)\sigma^\mu(t) + \frac{l_\chi}{P^2}\sum_{t,t',\mu}\hat{Q}_{\mu\mu}(t,t')\sigma^\mu(t)\sigma_\mu(t') + \frac{l_q}{P^2}\sum_{t,t',\mu<\nu}\hat{Q}_{\mu\nu}(t,t')\sigma^\mu(t)\sigma^\nu(t) + B\sum_{t,\mu}\sigma^\mu(t)\sigma^\mu(t+1) + h\sigma^\mu(t)\sigma^\nu(t'), \tag{D7}$$

where $\hat{(\cdot)}$ means the Fourier-transformed expressions and $L_0$ is the function of order parameters which has various form according with the problems. The coefficients, $l_m$, $l_\chi$, $l_q$, are also variables which change according with the problems. The above equations contain an additional field $h\sigma^\mu(t)\sigma^\nu(t')$, which is a simple extension of the previous researches.

We here differentiate $-\beta n f$ with respect to $h$ as follows

$$\frac{\partial(-\beta n f)}{\partial h} = \frac{\mathrm{Tr}_{\boldsymbol{\sigma}}\sigma^\mu(t)\sigma^\nu(t')e^L}{\mathrm{Tr}_{\boldsymbol{\sigma}}\, e^L}, \tag{D8}$$

[3] In the case of CDMA multiuser detectors, we should read $R$ instead of $m$. In the case of the image restoration, the system can be described by only $m$ because it is not spin glass model.

where we see that $\sigma^\mu(t')\sigma^\nu(t')$ is outside the exponent $e^L$. Our goal is to calculate Eq. (D8) in the limit of $n \to 0$, $h \to 0$ and to prove the expression (3.35), (4.33) and (5.48) in the same sense as in the previous study (Nishimori 2001).

The replica symmetry (RS) and static approximation (SA) lead to

$$\sum_\mu \sum_{t,t'} \sigma^\mu(t)\sigma^\mu(t') = \sum_\mu \left( \sum_t \sigma^\mu(t) \right)^2 \tag{D9}$$

$$\sum_{\mu<\nu} \sum_{t,t'} \sigma^\mu(t)\sigma^\nu(t') = \frac{1}{2} \left\{ \left( \sum_\mu \sum_{t,t'} \sigma^\mu(t) \right)^2 - \sum_\mu \left( \sum_t \sigma^\mu(t) \right)^2 \right\}. \tag{D10}$$

By using the Hubbard-Stratonovich transformation,

$$\exp\left(\frac{x^2}{2}\right) = \int \frac{dz}{\sqrt{2}} \exp\left(-\frac{z^2}{2} + xz\right) = \int Dz \exp(xz), \quad \left(Dz \equiv \frac{dz}{\sqrt{2\pi}}\right), \tag{D11}$$

we can calculate the exponent in (D6) as follows:

$$\begin{aligned} e^L = & \int Dw \prod_{\gamma \neq \mu,\nu} \int Dz \exp\left( B \sum_t \sigma^\gamma(t)\sigma^\gamma(t+1) + \frac{\hat{m} + \sqrt{\hat{q}}w + \sqrt{2\hat{\chi} - \hat{q}}z}{P} \sum_t \sigma^\gamma(t) \right) \\ & \times \int Dz \exp\left( B \sum_{t,\gamma=\mu,\nu} \sigma^\gamma(t)\sigma^\gamma(t+1) + \frac{\hat{m} + \sqrt{\hat{q}}w + \sqrt{2\hat{\chi} - \hat{q}}z}{P} \sum_{t,\gamma=\mu,\nu} \sigma^\gamma(t) + h\sigma^\mu(t)\sigma^\nu(t') \right), \end{aligned} \tag{D12}$$

where $\Phi$ can be seen as it in Eqs. (3.30), (4.30) and (5.39) in each model. Using the Trotter formula, we can take the spin trace in the limit $P \to \infty$ as,

$$\begin{aligned} \operatorname*{Tr}_{\boldsymbol{\sigma}} \exp\left( B \sum_t \sigma^\mu(t)\sigma^\mu(t+1) + \frac{\Phi}{P} \sum_t \sigma^\mu(t) \right) &= \operatorname*{Tr}_{\boldsymbol{\sigma}} \exp\left(\Gamma\hat{\sigma}^x + \Phi\hat{\sigma}^z\right) \\ &= 2\cosh\sqrt{\Phi^2 + \Gamma^2} \\ &= 2\cosh\Xi, \end{aligned} \tag{D13}$$

where $\Xi \equiv \sqrt{\Phi^2 + \beta^2\Gamma^2}$. Therefore, we obtain the final form of $\mathrm{Tr}_{\boldsymbol{\sigma}} e^L$ and $\mathrm{Tr}_{\boldsymbol{\sigma}} \sigma^\mu(t)\sigma^\nu(t') e^L$ in the limit $h \to 0$, respectively. The results are given by

$$\operatorname*{Tr}_{\boldsymbol{\sigma}} e^L = \int Dw \left( \int Dz \ \cosh\Xi \right)^n \tag{D14}$$

$$\begin{aligned} \operatorname*{Tr}_{\boldsymbol{\sigma}} \sigma^\mu(t)\sigma^\nu(t)\, e^L = & \int Dw \left( \int Dz \ 2\cosh\Xi \right)^{n-2} \\ & \times \operatorname*{Tr}_{\boldsymbol{\sigma}^\mu} \int Dz \sigma^\mu(t) \exp\left( B \sum_t \sigma^\mu(t)\sigma^\mu(t+1) + \frac{\Phi}{P} \sum_t \sigma^\mu(t) \right) \\ & \times \operatorname*{Tr}_{\boldsymbol{\sigma}^\nu} \int Dz \sigma^\nu(t) \exp\left( B \sum_t \sigma^\nu(t)\sigma^\nu(t+1) + \frac{\Phi}{P} \sum_t \sigma^\nu(t) \right). \end{aligned} \tag{D15}$$

Equation (D14) corresponds to the denominator of Eq. (D8), which is equal to 1 in the limit of $n \to 0$.

In order to calculate the right hand side of Eq. (D15), we differentiate both sides of the Trotter formula (D13) with respect to $\Phi$, then, we have

$$\mathop{\mathrm{Tr}}_{\boldsymbol{\sigma}} \frac{1}{P} \sum_t \sigma^\mu(t) \exp\left( B \sum_t \sigma^\mu(t)\sigma^\mu(t+1) + \frac{\Phi}{P} \sum_t \sigma^\mu(t) \right) = \frac{2\Phi}{\sqrt{\Phi^2+\Gamma^2}} \sinh \sqrt{\Phi^2+\Gamma^2}. \tag{D16}$$

Thus, we obtain the following equation

$$\begin{aligned} \mathop{\mathrm{Tr}}_{\boldsymbol{\sigma}} \sigma^\mu(t)\sigma^\nu(t)\ e^L &= \int Dw \left( \int Dz\ 2\cosh \Xi \right)^n \frac{\left( \int Dz\ \frac{\Phi}{\Xi} 2\sinh \Xi \right)^2}{\left( \int Dz\ 2\cosh \Xi \right)^2} \\ &\to \int Dw \left( \frac{\int Dz\ \frac{\Phi}{\Xi} \sinh \Xi}{\int Dz\ \cosh \Xi} \right)^2 \quad (n \to 0) \end{aligned} \tag{D17}$$

for

$$\mathop{\mathrm{Tr}}_{\boldsymbol{\sigma^\nu}} \int Dz \sigma^\nu(t) \exp\left( B \sum_t \sigma^\nu(t)\sigma^\nu(t+1) + \frac{\Phi}{P} \sum_t \sigma^\nu(t) \right) = \int Dz\ \frac{\Phi}{\Xi} 2\sinh \Xi \tag{D18}$$

under the RS and SA. We can extend the above methods to the case of an external field with the product of $k$ spins, $h \sum_i \sigma_i^\mu(t)\sigma_i^\nu(t') \cdots$. In such case, we get

$$[\langle \sigma \rangle_{\beta,\Gamma}^k] = \int Dw \left( \frac{\int Dz\ \frac{\Phi}{\Xi} \sinh \Xi}{\int Dz\ \cosh \Xi} \right)^k. \tag{D19}$$

For an arbitrary function $F(x)$ that can be expanded around $x = 0$, the above equation can be expanded to

$$[F(\langle \sigma \rangle_{\beta,\Gamma})] = \int Dw F \left( \frac{\int Dz\ \frac{\Phi}{\Xi} \sinh \Xi}{\int Dz\ \cosh \Xi} \right). \tag{D20}$$

If we take $F(x)$ to be a function $\mathrm{sgn}(x)$ (e.g. $\tanh(ax)$ with $a \to \infty$), we obtain the overlap $M$ in the form:

$$M(\beta,\Gamma) = [\mathrm{sgn}(\langle \sigma \rangle_{\beta,\Gamma})] = \int Dw \mathrm{sgn} \left( \frac{\int Dz\ \frac{\Phi}{\Xi} \sinh \Xi}{\int Dz\ \cosh \Xi} \right). \tag{D21}$$

# Bibliography


[1] de Almeida, J. R. L. and Thouless, D. J. (1978). Stability of the Sherrington-Kirkpatrick solution of a spin glass model, *Journal of Physics A: Mathematical and General*, 11, 983.

[2] Battaglia, D. A., Santoro, G. E., and Tosatti, E. (2005). Optimization by quantum annealing: Lessons from hard satisfiability problem, *Physical Review E*, 71, 066707.

[3] Benioff, P. (1980). The computer as a physical system: A microscopic quantum mechanical Hamiltonian model of computers as represented by Turing machines, *Journal of Statistical Physics*, 22, 5, 563.

[4] Berns, D. M., Rudner, M. S., Valenzuela, S. O., Berggren, K. K., Oliver, W. D., Levitov, L. S., and Orlando, T. P. (2008). Amplitude spectroscopy of a solid-state artificial atom, *Nature*, 455, 51.

[5] Boixo, S., Albash, T., Spedalieri, F. M., Chancellor, N. and Lidar, D.A. (2013). Experimental signature of programmable quantum annealing. *arXiv*: 1212.1739v1.

[6] Born, M. and Fock, V. A. (1928). Beweis des Adiabatensatzes, *Zeitschrift for Physik A*, 51,165 (In German).

[7] Bray, A. J. and Moore, M. A. (1980). Replica theory of quantum spin glasses, *Journal of Physics C: Solid State Physics* , 13, L655.

[8] Candes, E. J., Romberg, J., and Tao, T. (2006). Robust uncertainty principles: exact signal reconstruction from highly incomplete frequency information. *IEEE Transactions on Information Theory*, 52 489.

[9] Derrida, B. (1981). Random-energy model: An exactly solvable model of disordered systems, *Physical Review B* , 24, 2613.

[10] D-Wave Systems Inc., http:j//www.dwavesys.com/.

[11] Edwards, S. F. and Anderson, P. W. (1975). Theory of spin glasses. *Journal of Physics F*, 5, 965.

[12] Farhi, E., Goldstone, J., Gutmann, S. and Sipser, M. (2000). Quantum Computation by Adiabatic Evolution. arXiv:quant-ph/0001106.

[13] Farhi, E., Goldstone, J., Gutmann, S., Lapan, J.,Lundgren, A., and Preda, D. (2001). A Quantum Adiabatic Evolution Algorithm Applied to Random Instances of an NP-Complete Problem. *Science*, 292, 472.

[14] Finnila, a. B., Gomez, M. A., Sebenik, C., Stenson, C., and Doll, J. D. (1994). Quantum annealing: a new method for minimizing multidimensional functions. *Chemical Physics Letters*, 219, 343.

[15] Geman, S. and Geman, D. (1984). Stochastic Relaxation, Gibbs Distributions, and the Bayesian Restoration of Images. *IEEE Transactions on Pattern Analysis and Machine Intelligence*, 6, 721.

[16] Goldschmidt, Y. Y. (1990). Solvable model of the quantum spin glass in a transverse field. *Physical Review B*, 41, 4858.

[17] Goldschmidt, Y. Y. and Lai, P-L. (1990). Ising spin glass in a transverse field: Replica-symmetry-breaking solution. *Physical Review Letters*, 64, 2467.

[18] Harris, R., Berkley, A.J., Johnson, M.W.,Bunyk, P.,Govorkov, S., Thom, M.C., Uchaikin, S., Wilson, A.B., Chung,, J., Holtham, E., Biamonte, J.D., Smirnov, A. Yu, Amin, M. H. S., and Alec Maassen van den Brink. (2007). Sign- and Magnitude-Tunable Coupler for Superconducting Flux Qubits. *Physical Review Letters*, 98, 177001.

[19] Harris, R., Johansson, J., Berkley, A. J., Johnson, M. W., Lanting, T., Han, S., Bunyk, P., Ladizinsky, E., Oh, T., Perminov, I., Tolkacheva, E., Uchaikin, S., Chapple, E. M., Enderud, C., Rich, C., Thom, M., Wang, J., Wilson, B., and Rose, G. (2010). Experimental demonstration of a robust and scalable flux qubit. *Physical Review B*, 81,134510.

[20] Hopfield, J. J. (1982). Neural networks and physical systems with emergent collective computational abilities. *Proceedings of the National Academy of Sciences of the United States of America*, 79, 2554.

[21] Hogg, T. (2003). Adiabatic quantum computing for random satisfiability problems. *Physical Review A*, 67, 022314.

[22] Huse, D. A. and Fisher, D. S. (1986). Residual Energies after Slow Cooling of Disordered Systems. *Physical Review Letters*, 57, 2203.

[23] Inoue, J. and Carlucci, D. M. (2001). Image restoration using the Q-Ising spin glass. *Physical Review E*, 64, 036121.

[24] Inoue, J. (2001). Application of the quantum spin glass theory to image restoration. *Physical Review E*, 63, 046114.

[25] Inoue, J. (2005). Quantum Spin Glasses, Quantum Annealing and Probabilistic Information Processing. *Quantum Annealing and Other Optimization Methods (Lecture Notes in Physics)* , 2005, 259.

[26] Inoue, J., Saika, Y., and Okada, M. (2009). Quantum mean-field decoding algorithm for error-correcting codes. *Journal of Physics: Conference Series* , 143, 012019.

[27] Ishii, H. and Yamamoto, T. (1985). Effect of a transverse field on the spin glass freezing in the Sherrington-Kirkpatrick model. *Journal of Physics C: Solid State Physics* , 18, 6225.

[28] Johnson, M. W., Amin, M. H. S., Gildert, S., Lanting, T., Hamze, F., Dickson, N., Harris, R., Berkley, A. J., Johansson, J., Bunyk, P., et al. (2011). Quantum annealing with manufactured spins. *Nature*, 473, 194.

[29] Josephson, B.D. (1962). Possible new effects in superconductive tunnelling, *Physics Letters*, 1, 251.

[30] Kabashima, Y. and Saad, D. (1998). Belief propagation vs. TAP for decoding corrupted messages. *Europhysics Letters*, 44, 668.

[31] Kabashima, Y., Murayama, Y., and Saad, D. (2000). Statistical physics of regular low-density parity-check error-correcting codes. *Physical Review E*, 84, 1355.

[32] Kabashima, Y. and Saad, D. (2001). in Advanced mean field methods-theory and practice. *MIT press*, Cambridge, Massachusetts.

[33] Kabashima, Y., Wadayama, T., and Tanaka, T. (2009). A typical reconstruction limit for compressed sensing based on Lp-norm minimization. *Journal of Statistical Mechanics: Theory and Experiment*, L09003.

[34] Kadowaki, T. and Nishimori, H. (1998). Quantum annealing in the transverse Ising model. *Physical Review E*, 58, 5355.

[35] Kadowaki, T. (1998). Study of Optimization Problems by Quantum Annealing (Thesis). *arXiv:quant-ph/0205020v1.*

[36] Kirkpatric, S., Gelatt, C. D., and Vecchi, M.. P. (1983). Optimization by Simulated Annealing. *Science*, 220, 671.

[37] Kim, D. H. and Kim, J. J. (2002). Infinite-range Ising spin glass with a transverse field under the static approximation. *Physical Review B*, 66, 054432.

[38] Lupascu, A., Saito, S., Picot, T., de Groot, P. C., Harmans, C. J. P. M., and Mooij, J. E. (2007). Quantum non-demolition measurement of a superconducting two-level system. *Nature Physics*, 3,119.

[39] Martonak, R., Santoro, G. E. and Tosatti, E. (2002). Quantum annealing by the path-integral Monte Carlo method: The two-dimensional random Ising model, *Physical Review B* 66, 094203.

[40] Martonak, R., Sanroro, G. E., and Tosatti, E. (2004). Quantum annealing of the traveling-salesman problem, *Physical Review E* 70, 057701.

[41] Mattis, D. C. (1976). Solvable spin systems with random interactions, *Physics Letters A*, 56, 421.

[42] Messiah, A. (1962). Quantum Mechanics, Vol. 2, North Holland Publishing Company, Amsterdam.

[43] Metropolis, N., Rosenbluth A.W., Rosenbluth, M.N., Teller, A.H., and Teller, E. (1953). Equation of State Calculations by Fast Computing Machines. *Journal of Chemical Physics*, 21, 1087.

[44] Mézard, M. and Montanari, A. (2008). Information, Physics, and Computation. *Oxford graduate texts*, Oxford university press.

[45] Monasson, R. and Zecchina, R. (1997). Statistical mechanics of the random K-satisfiability model. *Physical Review E* , 56, 1357.

[46] Montanari, A. and Sourlas, N. (2000). The statistical mechanics of turbo codes. *The European Physical Journal B - Condensed Matter and Complex Systems* , 18, 107.

[47] Morita, S. and Nishimori, H. (2008). Mathematical foundation of quantum annealing. *Journal of Mathematical Physics*, 49, 125210.

[48] Neven, H., Denchev, V. S., Drew-Brook, M., Zhang, J., Macready, W. G., Rose, G. (2009). Binary Classification using Hardware Implementation of Quantum Annealing. *Advances in Neural Information Processing Systems (NIPS) 2009.*

[49] Nishimori, H. and Wong, M. (1999). Statistical mechanics of image restoration and error-correcting codes. *Physical Review E*, 60, 132.

[50] Nishimori, H. (2001). Statistical Physics of Spin Glasses and Information Processing. *Oxford science publications.*

[51] Nokura, K. (1998). Spin glass states of the anti-Hopfield model. *Journal of Physics A: Mathematical and General*, 31, 7447.

[52] Obuchi, T., Nishimori, H., and Sherrington, D. (2007). Phase Diagram of the p-Spin-Interacting Spin Glass with Ferromagnetic Bias and a Transverse Field in the Infinite- p Limit. *Journal of Physical Society of Japan*, 76, 054002.

[53] Otsubo, Y. Inoue, J., Nagata, K., and Okada, M. (2012). Effect of quantum fluctuation in error-correcting codes. *Physical Review E*, 86, 05113.

[54] Ozeki, T., Okada, M. (2003). Non-monotonic behaviour in relaxation dynamics of image restoration. *Journal of Physics A: Mathematical and General*, 36, 11011.

[55] Perdomo-Ortiz, A., Dickson, N., Drew-Brook, M., Rose, G., and Aspuru-Guzik, A. (2012). Finding low-energy conformations of lattice protein models by quantum annealing. *Scientific Reports*, 2, 571.

[56] Rangan S., Fletcher, A. K., and Goyal, V. K. (2012). Asymptotic Analysis of MAP Estimation via the Replica Method and Applications to Compressed Sensing. *IEEE Transactions on Information Theory*, 58, 1902.

[57] Rønnow, F., Isakov, S., Wecker, D, Boixo, S., and Troyer, M. (2013). Computational performance and scaling of adiabatic quantum annealing processors. *APS March Meeting 2013* , A27, 00007.

[58] Rujan, P. (1993). Finite temperature error-correcting codes. *Physical Review Letters*, 70, 2968.

[59] Santoro, G.E., Martonak, R., and E. Tosatti, Car, R. (2002). Theory of Quantum Annealing of an Ising Spin Glass. *Science*, 295, 5564.

[60] Schneider, D. (2013). New camera Chip captures only what it needs. *IEEE spectrum*, March, 13.

[61] Schuch, N., Wolf, M. M., Verstraete, F., and Cirac, J. I. (2008). Simulation of Quantum Many-Body Systems with Strings of Operators and Monte Carlo Tensor Contractions. *Physical Review Letters*, 100, 040501.

[62] Seung, H. S., Sompolinsky, H., and Tishby, N. (1992). Statistical mechanics of learning from examples. *Physical Review A*, 45, 6056.

[63] Sherrington, D. and Kirkpatrick, S. (1975). Solvable Model of a Spin-Glass. *Physical Review Letter*, 35, 1792.

[64] Shor, P. W. (1994). Algorithms for Quantum Computation: Discrete Logarithms and Factoring. *Proceeding of 35th IEEE Symposium on Foundation of Computer Science*, 124.

[65] Simon, M. K., Omura, J. K., Scholotz, R. A., and Levitt, B. K. (1994). Spread spectrum communications handbook. *McGrew-Hill*, New York.

[66] Sourlas, N. (1989). Spin-glass models as error-correcting codes. *Nature*, 339, 693.

[67] Suzuki, M. (1976). Relationship between d-Dimensional Quanta! Spin Systems and (d+ I) -Dimensional Ising Systems. *Progress of Theoretical.Physics* , 56, 2454.

[68] Suzuki, S. and Okada, M. (2005). Residual Energies after Slow Quantum Annealing. *Journal of the Physical Society if Japan*, 74,1649.

[69] Talagrand, M. (2003). Spin Glasses: A Challenge for Mathematicians. *Springer*.

[70] Tanaka, K. (2002). Statistical-mechanical approach to image processing. *Journal of Physics A: Mathematical and General* , 35, R81.

[71] Tanaka, T. (2001). Statistical mechanics of CDMA multiuser demodulation. *Europhysics Letters*, 54, 540.

[72] Tanaka, T. (2002). A statistical-mechanics approach to large-system analysis of CDMA multiuser detectors. *IEEE Transactions on information theory* 48, 11, 2888.

[73] Tanaka, T. and Okada, M. (2005). Approximate belief propagation, density evolution, and statistical neurodynamics for CDMA multiuser detection. *IEEE Transaction on information theory*, 51, 700.

[74] Tanaka, T. (2007). *RIMS Kôkyûroku*, 1532, 118 (in Japanese).

[75] Thirumalait, D., Lis, Q., and Kirkpatrick, T.R. (1989). Infinite-range Ising spin glass in a transverse field. *Journal of Physics A: Mathematical and General* , 22, 3339.

[76] Thouless, D. J., Anderson, P. W., and Palmer, R. G. (1997). Solution of'solvable model of a spin glass. *Physiological Magagine*, 35, 593.

[77] Verstraete, F., Wolf, M. M., Perez-Garcia, D., and Cirac, J. I. (2006). Criticality, the Area Law, and the Computational Power of Projected Entangled Pair States. *Physical Review Letters*, 96, 220601.

[78] Vandersypen LMK, Steffen M, Breyta G, Yannoni CS, Sherwood MH, Chuang IL (2001). Experimental realization of Shor's quantum factoring algorithm using nuclear magnetic resonance. *Nature*, 414 (6866), 883.

[79] Vicente, R., Saad, D., and Kabashima, Y. (1999). Finite-connectivity systems as error-correcting codes. *Physical Review E*, 60, 5352.

[80] Wang, Z., Job, J., RØnnow, T. F., Troyer, M., Lidar, D. A. (2014). Performance of quantum annealing on random Ising problems implemented using the D-Wave Two. *APS March Meeting 2014*, 59, 1.

[81] Wong, K. Y. M. and Sherrignton, D. (1988). Intensively connected spin glasses: towards a replica-symmetry-breaking solution of the ground state. *Journal of Physics A: Mathematica and General*, 21, L 459.

[82] White, S. R. (1992). Density matrix formulation for quantum renormalization groups. *Physical Review Letters*, 69, 2863.

[83] Yoshida, M., Uezu, T., Tanaka, T., and Okada, M. (2007). Statistical Mechanical Study of Code-Division Multiple-Access Multiuser Detectors -Analysis of Replica Symmetric and One-Step Replica Symmetry Breaking Solutions-. *Journal of the Physical Society of Japan*, 76, 054003.

[84] Young, A. P., Knysh, S., and Smelyanskiy, V. N. (2010). First-Order Phase Transition in the Quantum Adiabatic Algorithm. *Physical Review Letters*, 104, 020502.

[85] Young, A. P., Knysh, S., and Smelyanskiy, V. N. (2008). Size Dependence of the Minimum Excitation Gap in the Quantum Adiabatic Algorithm. *Physical Review Letters*, 101, 170503.